FINITE ELEMENT ANALYSIS OF RESIDUAL STRESS GENERATION DURING SPOT WELDING AND ITS AFFECT ON FATIGUE BEHAVIOR OF SPOT WELDED JOINT

A Dissertation

Presented to

The Faculty of the Graduate School

University of Missouri- Columbia

In Partial Fulfillment

of the Requirements for the Degree

Doctor of Philosophy

By

XIN LONG

Dr. Sanjeev K. Khanna, Dissertation Supervisor

DECEMBER 2005

The undersigned, appointed by the Dean of the Graduate School, have examined the dissertation entitled

FINITE ELEMENT ANALYSIS OF RESIDUAL STRESS GENERATION DURING SPOT WELDING AND ITS EFFECTS ON FATIGUE BEHAVIOR OF SPOT WELDED JOINTS

Presented by Xin Long

A candidate for the degree of Doctor of Philosophy

And hereby certify that in their opinion it is worthy of acceptance

Sanjeev K. Khanna

Robert A. Winholtz

A. Sherif El-Gizawy

Stephen J. Lombardo

Hani A. Salim

P. Frank Pai

ACKNOWLEDGMENTS

I would like to express my sincere gratitude to my advisor: Dr. Sanjeev K. Khanna, for his guidance and friendship in my research work and graduate study. His knowledge, kindness, enthusiasm, patience and support made all the difference in my academic career.

I would like to thank my wife, Xiaonan, for her love, support and encouragement.

I also would like to thank my parents and my parents-in-law for their love, encouragement and help during my study.

I also wish to thank my Ph.D. program committee members: Dr. Robert A. Winholtz, Dr. Stephen J. Lombardo, Dr. Sherif El-Gizawy, Dr. Hani A. Salim and Dr. Frank Pai for their comments and suggestions.

I am grateful to the staff of Engineering Technical Services (ETS) for assistance in the running and repairing equipments and sample machining. I am also grateful to the staff of the Department of Mechanical Engineering for their help. Also, the finical support from NSF for doing those researches is greatly appreciated.

TABLE OF CONTENTS

LIST OF TABLES

LIST OF FIGURES

FINITE ELEMENT ANALYSIS OF RESIDUAL STRESS GENERATION DURING SPOT WELDING AND ITS AFFECT ON FATIGUE BEHAVIOR OF SPOT WELDED JOINT

Xin Long

Dr. Sanjeev K. Khanna, Dissertation Supervisor

ABSTRACT

This dissertation presents the finite element based prediction of residual stress generation in a spot welded joint during the spot welding process and the effects of residual stress on fatigue behavior of a spot welded joint. Finite element analysis was conducted using ANSYS commercial code. This methodology was applied to predict residual stress fields in mild steel and new generation aluminum alloy spot welds. Thermo-physical and thermo-mechanical properties of two kinds of aluminum alloys, 5754 and 6111, were experimentally measured while standard literature data was used for AISI 1020 steel for finite element analysis. It was found that a two dimensional axisymmetric incremental and thermal-electro-mechanical coupled finite element model with temperature dependent materials properties can be used for simulating the residual stress distribution and the spot nugget size in a spot welded steel and aluminum alloy welds. The simulated results show good qualitative agreement with experimental results. It has been found that in the spot nugget, the highest tensile residual stress occurs at the center of the nugget and the residual stress decreases significantly at the edge of the nugget. It was found that two aluminum alloys have similar thermo-physical properties, while the thermo-mechanical properties were quite different. 6111 aluminum alloy has a

higher yield strength and elastic modulus than that of 5754 alloy for all temperatures. Furthermore, spot welded advanced high strength steels, namely dual phase DP600 GI and transformation induced plasticity TRIP600 steels were investigated for their fatigue life, microstructure changes and fatigue fracture mechanisms to develop design data for possible application in future light weight and more fuel efficiency automobiles. The investigation of the microstructure evolution and residual stress as well as their relation to fatigue behavior of spot welded steel sheets suggests that under high fatigue load, dislocation density in spot nugget edge is much higher than that in nugget center area, which indicates significant plastic deformation occurred in the edge of spot nugget during fatigue testing. Under low fatigue load, dislocation density is low in both edge and center area of the spot nugget. The effect of post-heating on the microstructure (mainly dislocation morphology) is that more dislocations are generated during fatigue testing for both high and low loads. Post-heating results in strength decrease of spot welded joint while it releases the residual stress in it, which makes the fatigue life of welded sheet decrease under low fatigue loading condition.

CHAPTER 1
INTRODUCTION AND OBJECTIVES

1.1 Introduction

Spot welding involves the joining of two or more pieces of sheet metal in localized areas where melting and coalescence of a small volume of material occurs from heating caused by resistance to the passage of an electric current. This process is typically used to obtain a lap joint of sheet metal parts. A common example is the mass production of automobiles, where a typical automobile may contain more than 5000 spot welds [1].

When the current is turned off, this volume of molten metal cools down and solidifies, beginning at its outer edges. The volume of metal from the work pieces that has undergone heating, melting, fusion, and resolidification is called the weld nugget. The grain structure in the nugget is considerably coarser than the parent metal. Evidently a spot weld cools down to room temperature non-uniformly. The large temperature gradients created by the intense local heating during the welding process followed by rapid cooling, and also phase changes in the solidifying metal, induce heterogeneous deformations in the metal resulting in the development of internal stresses. These internal or remaining stresses are known as residual stresses.

Generally, we can distinguish three main kinds of residual stress according to the distance over which they can be observed [2]. The first kind of residual stress, termed macroscopic, is long-range in nature, extending over at least several grains of the material. The second kind, often called structural micro stress, covers a distance of one grain or a part of the grain. It can occur between different phases and have different

physical characteristics, or between embedded particles, such as inclusions and the matrix. The third kind of residual stress ranges over several atomic distances within the grain, and is equilibrated over a small part of the grain. In this study we are only concerned with the first kind of residual stress or the macroscopic residual stress field.

In order to increase the reliability of products, study on the mechanical properties of the spot welded joint has been attracting a lot of interest [3-8]. It is known that the mechanical properties of a welded joint are not only determined by the microstructure of weld zone metal, but also by the residual stresses introduced by the heterogeneous thermal cycle during welding. Residual stresses play an important role in influencing the fatigue life and other mechanical properties of the spot welded structure. For instance, when the interaction between residual stresses and future loads occurs, the local area that has the highest residual stresses is a potential source for crack initiation and growth in the weld or heat affected zone (HAZ).

There are several methods to measure residual stresses, but most of them are not suitable for a spot welded joint because the spot nugget has a small size (for example, the diameter of spot nugget in the present study is about 5 mm) and it is not easy to be reached (spot nugget exists between the two workpieces). Recently, high sensitivity moiré interferometry [1] and X-ray techniques [9-10] have been successfully used in the measurement of residual stresses in spot welds, which make it possible to determine the average residual stress distribution in the spot weld.

With advances in computer hardware and finite element method (FEM) software, numerical simulation now plays an important role in study of manufacturing processes. Since experiments alone cannot easily study the spot welding process, numerical

simulation is a potential way to aid in the quantitative study of spot weld residual stress generation. Since 1980s, coupled spot welding models have been developed by many researchers to focus on different aspects of the spot welding process, such as temperature distribution, nugget growth, electrode design, welding parameters optimization, etc. [11-17].

1.2 Objectives

This research has focused on residual stress prediction in spot welded metal sheets of mild steel and aluminum alloys, using the ANSYS finite element code. Since the spot welding process involves thermal, electrical and mechanical phenomena, it is very difficulty to simulate the residual stress generation in spot welding.

A metal's fatigue process is usually associated with microstructure changes, such as dislocations motion, during the initiation period of fatigue crack. For example, numerous sub-grains form in parent grains in metal during cyclic stressing [21]. The boundaries of those sub-grains are made up with heavily jogged, scalloped and tangled dislocations. The density of dislocations within the boundaries tends to change as the fatigue test proceeds. It can be hypothesized that the fatigue behavior, residual stress and microstructure in spot welded sheet are closely related. And the relationship between dislocation density, fatigue loading parameters, residual stress and location in the spot weld has been investigated. In addition to the fatigue behavior, which included fatigue life and failure mechanisms, of advanced high strength steels (AHSS) was investigated. The AHSS steels were so investigated for the following reasons. Due to increased fuel efficiency standards, new materials are needed for decreasing automobile weight. Aluminum alloys and advanced high strength steels (AHSS) are under consideration by

the automotive industry for substituting currently used low-carbon steels and high strength low alloy (HSLA) steels. The advantages of aluminum alloy are that they are light weight (only one-third of steel), satisfy new recycling standards and good corrosion resistance. The main disadvantage is the cost, which includes materials cost and fabrication cost. In addition, lower stiffness than that of steel is also a disadvantage. Thus from an economic point of view, with similar cost as HSLA steels, AHSSs have also attracted a lot of interest in making lighter-weight vehicles. AHSSs, such as dual-phase steel DP600 and transformation induced plasticity steel TRIP600, have yield strength over 550 MPa, compared to that of conventional high strength steels within the range of 210-550 MPa. Therefore, thinner AHSS sheets, which decrease the weight of automobile, can be used without losing any strength. Another advantage of AHSS is that it has higher yield to tensile ratio than that of HSLA steels at the same class, which results in a high level of crash energy absorption and a good formability in stamping.

Spot welding still remains the primary joining method in automobile manufacturing. In the past, fatigue behavior was not a major concern when relatively thick mild steel sheets were used in automobiles. For AHSS steels, however, it was found that significant fatigue damage occurred which is possibley related to the reduction in sheet thickness [18]. Previous studies also show that fatigue strength of high strength spot welded steel joint is not higher than that of mild steels [19-20]. Therefore, it is a major concern to investigate the performance of spot welded joint in AHSSs for improving fatigue design.

Therefore, the objectives of the present study can be summarized as:

(1) Create finite element models for studying residual stress in a spot welded metal sheet joint suing the commercial ANSYS finite element code.

(2) Use the finite element model to simulate the residual stress in a spot welded joint for currently used materials (AISI 1020 steel) and future materials (5754 and 6111 aluminum alloys) in the automotive industry.

(3) Experimentally determine thermo-physical and thermo-mechanical properties of metals for the finite element modeling.

(4) Study sub-microscopic deformation mechanisms in spot welds subjected to fatigue loads and under different residual stress conditions.

(5) Investigate the fracture behavior in spot welded joints subjected to fatigue load.

1.3 Layout of study

The present study has been organized into four general parts:

- Part I contains introductory materials, including introduction, objectives and project schedule.
- Part II deals with numerical simulation of residual stress in a spot welded joint and materials properties measurement for using in simulation, which includes Chapter 2 “Simulation on residual stress in a spot welded steel sheet”, Chapter 3 “Experimental measurement of mechanical and physical properties of aluminum”, and Chapter 4 “Simulation of residual stress in a spot welded aluminum sheet’.
- Part III addresses fatigue and fracture behavior of spot welded advanced high strength steel sheet, which includes Chapter 5.
- Part IV focus on the effect of fatigue loading on sub-microscopic deformation mechanisms in a spot welded joint, which discussed the relation among residuals stress, microstructure, and fatigue properties in Chapter 6.

1.4 References:

[1] Khanna, Sanjeev K; He, Canlong and Agrawal, Hari N., Residual Stress Measurement in Spot Welds and the Effect of Fatigue Loading on Redistribution of Stresses Using High Sensitivity Moiré Interferometry, *ASME Journal of Engineering Materials and Technology*, vol. 123, 2001, pp.132-138.

[2] Lu, J., ed., 1995, *Handbook of Measurement of Residual Stresses*, The Fairmont Press, Georgia.

[3] Darwish, S. M., and Al-Dekhial, S. D., 1999, "Micro-Hardness of Spot Welded Commercial Aluminium as Correlated With Welding Variables and Strength Attributes," *Journal of Materials Processing Technology*, **91,** No. 1, pp. 43-51.

[4] Anastassiou, M., Babbit, M., and Lebrun, J L., 1990, "Residual Stresses and Microstructure Distribution in Spot-Welded Steel Sheets, Relation With Fatigue Behavior," *Materials Science & Engineering A: Structural Materials: Properties, Microstructure & Processing*, **125**, No. 2, pp. 141-156.

[5] Tricoteaux, A., Fardoun, F., Degallaix, S., and Sauvage, F., 1995, "Fatigue Crack Initiation Life Prediction in High Strength Structural Steel Welded Joints," *Fatigue & Fracture of Engineering Materials & Structures*, **18**, No. 2, pp.189-200.

[6] Radaj, D., 1990, "Local Fatigue Strength Characteristic Values for Spot Welded Joints," *Engineering Facture Mechanics*, **37**, No. 1, pp. 245-250.

[7] Radaj, D., 1989, "Stress Singularity, Notch Stress and Structural Stress at Spot-Welded Joints," *Engineering Facture Mechanics*, **34**, No. 2, pp. 495-506.

[8] Satoh, T., Abe, H., Nishikawa, K and Morita, M., 1991, "On Three-Dimensional Elastic-Plastic Stress Analysis of Spot-Welded Joint under Tensile Shear Load," *Transaction of the Japan Welding Society*, **22**, No. 1, pp. 46-51.

[9] Henrysson, H. F.; Abdulwahab, F.; Josefson, B. L. and Fermer, M., 1998, "Residual Stress in Resistance Spot Welds: Finite Element Simulations, X-Ray Measurements and Influence on Fatigue Behavior," *IIS/IIW-1442-98 (ex. doc.XV-1002-98) Class A.*

[10] Anastass, W., and Babbit, H., 1990, "Residual Stresses and Microstructure Distribution in Spot-Welded Steel Sheets: Relation with Fatigue Behavior", *Materials Sciences and Engineering*, A**125**, pp.141-156.

[11] Nied, H. A., 1984, "The Finite Element Modeling of The Resistance Spot Welding Process," *Welding Journal*, **63**, pp.s123-s132.

[12] Tsai, C. L., Jammal, O. A., and Papritan, J. C., 1992, "Modeling of Resistance Spot Weld Nugget Growth," *Welding Journal*, **71**, pp. s47-s54.

[13] Browne, D. J., Chandler H. W., Evans J. T., and Wen J., 1995, "Computer Simulation of Resistance Spot Welding in Aluminum: Part I," *Welding Journal*, **74**, No.10, pp.s339-s344.

[14] Feng, Z., Babu, S.S., Santella, M. L., Riemer, B. W., and Gould, J. E., 1998, "An Incrementally Coupled Electrical-Thermal-Mechanical Model For Resistance Spot Welding," *5th International Conference on Trends in Welding Research, Pine, Mountain, GA*, pp.1-5.

[15] Gupta, O. P., and De, Amitava, 1998, "An Improved Numerical Modeling For Resistance Spot Welding Process and Its Experimental Verification," *Journal of Manufacturing Science and Engineering*, **120**, No. 2, pp.246-251.

[16] Xu, L., and Khan, J. A., 1999, "Nugget Growth Model For Aluminum Alloys During Resistance Spot Welding," *Welding Journal*, **78**, No. 11, pp. s367-s372.

[17] Sun, X., and Dong, P., 2000, "Analysis of Aluminum Resistance Spot Welding Processes Using Coupled Finite Element Procedures," *Welding Journal*, **79**, No.8, pp. s215-s221.

[18] Garbatov, Y. and Guedes Soares C., "Influence of steel strength on the fatigue reliability of welded structural components", Vol.26, No.7, July 2004, pp. 753-762.

[19] El-Sayed, M. E., Stawiarski, T. and Frutiger, R., Fatigue Analysis of Spot-Welded Joints under Variable Amplitude Load History, Engineering Fracture Mechanics, Vol.55, No.3, pp.363-369, 1996.

[20] Stephens, R. I., Fatemi, A., Stephens, R.R. and Fuchs, H. O., Metal Fatigue in Engineering, second edition, A Wiley-Interscience Publication, John Wiley & Sons, Inc., 2001.

[21] Frost N. E.; Marsh K. J. and Pook, L. P. (eds), Metal Fatigue, Oxford University Press, 1974, pp6-35.

CHAPTER 2

NUMERICAL SIMULATION OF RESIDUAL STRESSES IN A SPOT WELDED JOINT

Abstract

An incremental and thermal-electro-mechanical coupled finite element model has been presented in this study for predicting residual stress distribution in a spot welded steel joint. Approximate temperature dependent material properties, including physical and mechanical properties, have been considered. The spot nugget shape and the residual stress distribution were obtained by simulation. The results obtained have been compared with experimental measurements, and good agreement is observed. The highest tensile residual stress occurs at the center of the nugget and the residual stress decreases towards the edge of the nugget.

2.1. Introduction

Spot welding, or resistance spot welding, involves the joining of two or more pieces of sheet metal in localized areas or spots where melting and coalescence of a small volume of material occurs from heating caused by resistance to the passage of an electric current. This process is typically used to obtain a lap joint of sheet metal parts of thickness 0.125 in. (3 mm) or less, using a series of spot welds, in situations where an airtight assembly is not required. A common example is the mass production of automobiles, where a typical automobile may contain more than 5000 spot welds.

When the current is turned off, this volume of molten metal cools down and solidifies, beginning at its outer edges. The volume of metal from the workpieces that have undergone heating, melting, fusion, and resolidification is called the weld nugget. The grain structure in the nugget is considerably coarser than the parent metal. Evidently a spot weld cools down to room temperature non-uniformly. The large temperature gradients created by the intense local heating during the welding process followed by rapid cooling, and also phase changes in the solidifying metal, induce heterogeneous deformations in the metal resulting in the development of internal stresses. These internal or remaining stresses are known as residual stresses.

In order to increase the reliability of products, study on the mechanical properties of the spot welded joint has been attracting a lot of interest [1-6]. It is known that the mechanical properties of a welded joint are not only determined by the microstructure of weld zone metal, but also by the residual stresses introduced by the heterogeneous thermal cycle during welding. Residual stresses play an important role in influencing the fatigue life and other mechanical properties of the spot welded structure. For instance,

when the interaction between residual stresses and future loads occurs, the local area that has the highest residual stresses is a potential source for crack initiation and growth in the weld or heat affected zone (HAZ).

There are several methods to measure residual stresses, but most of them are not suitable for a spot welded joint because the spot nugget has a small size (for example, the diameter of spot nugget in the present study is about 5 mm) and it is not easy to be reached (spot nugget exists between the two workpieces). Recently, high sensitivity moiré interferometry [7] and X-ray techniques [8] have been successfully used in the measurement of residual stresses in spot welds, which make it possible to determine the average residual stress distribution in the spot weld. With moiré methods in conjunction with hole drilling, the average through thickness residual stresses are obtained, while the X-ray method gives the residual stresses in the surface layers of the weld, though etching techniques have been used for through thickness stress measurement using X-rays.

With advances in computer hardware and finite element method (FEM) software, numerical simulation now plays an important role in study of manufacturing processes. Since experiments alone cannot easily study the spot welding process, numerical simulation is a potential way to aid in the quantitative study of spot weld residual stress generation. But because of the complexity of the spot welding process, early efforts mainly focused on the heat transfer problem or surface phenomena by mathematical analysis. In 1984, a thermal-electro-mechanical coupled model was introduced by Nied [9]. Temperature dependent materials properties were used in this model. The results in this work show the mechanical deformation of electrodes and workpieces, and an elliptic shaped weld nugget. Since then, coupled spot welding models have been developed by

many researchers to focus on different aspects of the spot welding process, such as temperature distribution, nugget growth, electrode design, welding parameters optimization, etc. [10-14]. Since spot welding is a strongly coupled model that cannot be solved directly by the commercial software, some of them used sequentially coupled finite element models [9,10]. A sequentially coupled model simulates the temperature field and stress field in the spot weld in a sequential order. Under this condition, the contact radii between the electrode/workpiece and workpiece/workpiece faying interface are assumed to remain constant during the whole welding process. This is not actually true because contact radii are the result of competition between thermal expansion and electrode squeezing force, thus they vary during the welding process. Some authors used an incrementally coupled thermal-electro-mechanical model [11-14]. That means, with a predetermined small time increment, the contact radii from thermal-mechanical analysis is input to the electrical-thermal analysis as electrical and thermal boundary conditions. Then the temperature distribution from electrical-thermal analysis is input to the thermal-mechanical analysis as a body load. This iterative procedure is applied during the whole welding cycle. The incrementally coupled models were used to simulate the squeezing cycle, welding cycle and sometimes holding cycle during the whole welding cycle. However, to accurately study residual stress formation, the whole welding process, which includes squeezing cycle, welding (heating) cycle, holding cycle, and cooling cycle, should be considered in the model. In ref. [15], a whole welding process was simulated using a coupled incremental method, and the residual stress distribution in an aluminum spot welded joint was obtained. But, unfortunately, no experimental data was offered for verification.

In this study, an incrementally coupled finite element model has been developed to study the whole spot welding process, and used to investigate residual stress generation and distribution in a spot welded steel joint. The residual stress results obtained using the finite element model have been compared to the experimental results obtained previously [7] by employing high sensitivity moiré interferometry. The growth of the spot weld nugget has also been obtained using the finite element method. The nugget size was compared with the nugget in an actual spot welded specimen by cutting and etching the nugget cross-section.

2.2. Numerical Model

The spot welding process involves a complex coupling among thermal, electrical, physical, and chemical processes, which makes it difficult to be modeled. The residual stress simulation of the whole welding process, including squeezing, welding, holding and cooling cycles, has been included in the model presented here. Commercial finite element code ANSYS and the APDL (ANSYS Parametric Design Language) were used to model the coupling between electrical and thermal phenomenon and between the thermal and mechanical phenomenon. The electrode contact and electrode separation problems have also been considered because the electrodes will be removed from the workpiece after the holding cycle.

2.2.1 Basic Theory

A spot welding model involves electrical field, temperature field, and stress and strain field equations. Due to the axisymmetric nature of the electrode and the workpeice, a

quarter of the physical model for two-dimensional analysis is created and is shown in Figure 2.1.

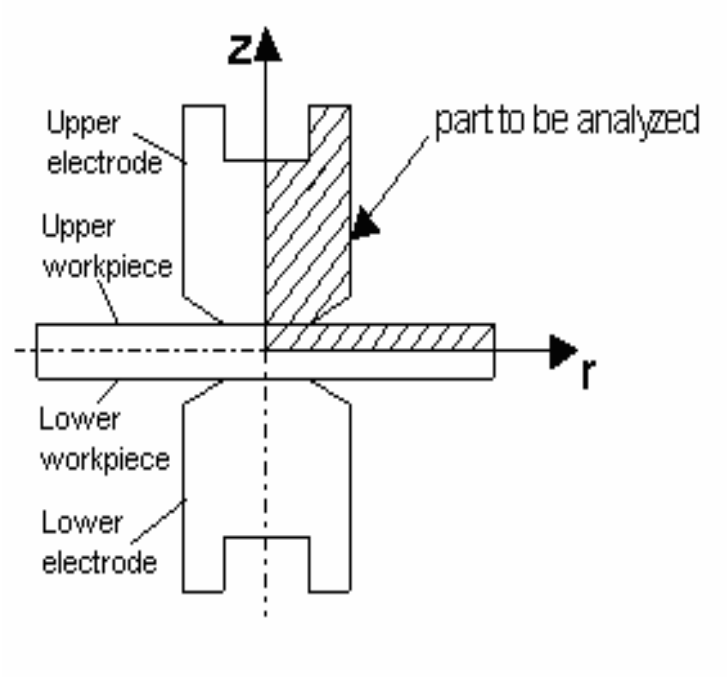

(a)

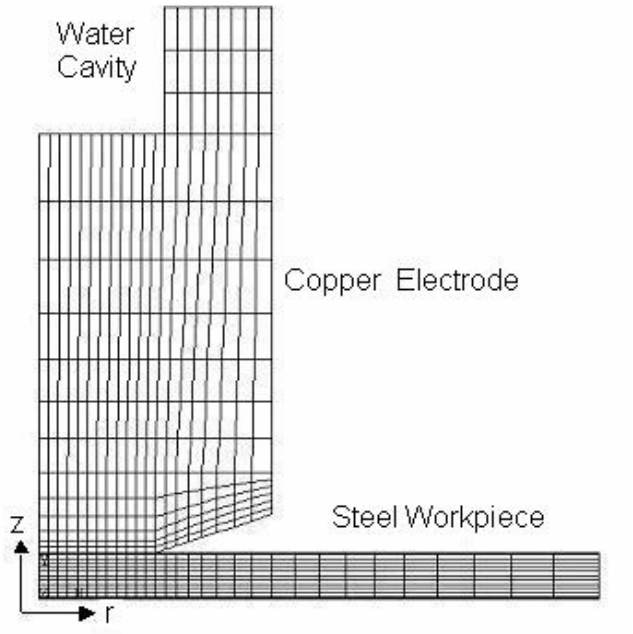

(b)

Figure 2.1 (a) Axisymetric model of spot welding setup (b) Finite element model for spot welding

All of the equations in this study are based on the column (cylindrical-polar coordinate) coordinate system, as shown in Figure 2.1. The governing equation for calculation of the electrical potential φ in the whole model is:

$$\frac{\partial}{\partial r}(\sigma \frac{\partial \varphi}{\partial r}) + \frac{\sigma}{r}\frac{\partial \varphi}{\partial r} + \frac{\partial}{\partial z}(\sigma \frac{\partial \varphi}{\partial z}) = 0 \qquad (2.1)$$

where r is the radial distance in this column coordinate system , z is the distance in the axis direction of the coordinate system, and σ is the electrical conductivity. By solving equation (2.1), the electrical potential φ is obtained. According to the electric current heat generation (q) rule:

$$q = I^2Rt \qquad (2.2)$$

where I is the current, R is the material electrical resistance, and t is the time for which current is passed. Since I = φ/R, equation (2.2) can be rewritten as:

$$q = \varphi^2 t/R \qquad (2.3)$$

The governing equation for transient temperature field distribution, which involves electrical resistance heat can be written as:

$$\rho c \frac{\partial T}{\partial t} = \frac{\partial}{\partial r}(k \frac{\partial T}{\partial r}) + \frac{k}{r}\frac{\partial T}{\partial r} + \frac{\partial}{\partial z}(k \frac{\partial T}{\partial z}) + q \qquad (2.4)$$

where ρ is the material's density, c is the heat capacity, T is the temperature, t is the time, k is the thermal conductivity, respectively. The material properties c, k and σ are temperature dependent (which is further explained in a later section). Substituting equation (2.3) in (2.4), then the equation which describe the temperature distribution with heat source of current induced Joule heat is obtained.

For stress and strain analysis, since the thermal-elastic-plastic behavior is a highly nonlinear phenomenon, the stress-strain relation is described in incremental form:

$$\{\Delta\sigma\} = [D]\{\Delta\varepsilon\} + \{C\}\Delta T \qquad (2.5)$$

where vectors $\Delta\sigma$ and $\Delta\varepsilon$ are stress and strain increment, respectively, and ΔT is temperature increment. Matrix D and vector C are materials related constant. Since residual stress is caused by heterogeneous plastic deformation of the material, temperature dependent material mechanical properties were used. Plastic deformation of material was modeled using bilinear kinematic hardening (BKIN) option in ANSYS program, which assumes the total stress range is equal to twice the yield stress and the work hardening is linear.

2.2.2 Geometrical Model and Boundary Conditions

Geometrical model. The geometrical model and the mesh division are shown in Figure 2.1. A total of 933 nodes and 835 elements (in case of thermal-mechanical analysis, there were 60 more contact elements) were used in this study. A denser mesh was used for the weld zone and the electrode portion in proximity to the workpiece.

Electrical boundary conditions. In the welding cycle, a root-mean-square (RMS) value of total current was applied uniformly on top of the copper electrode. At the faying surface of the workpieces (that is the contact regions between the two sheets being welded), the voltage was set to zero.

Thermal boundary conditions. The temperature at the water cooling cavity was set to room temperature 25^{o}C , and convection heat transfer to ambient air was specified on all the lateral surfaces of the electrode and workpiece that are not in contact.

Mechanical boundary conditions. Uniform load was applied at the top of the copper electrode during welding and holding cycle. The electrode was removed at the end of the holding cycle. At the faying surface between the electrode and the workpiece, a contact

element was used. At the faying surface between workpiece and workpiece, the vertical displacement of the part of faying surface under electrode was set to zero, and a subroutine program was used to determine if the other part of faying surface is under contact or not. If some nodes are under contact and are under pressure stress, a zero vertical displacement was applied here.

Materials properties. Temperature dependent physical and mechanical materials properties, including thermal conductivity, coefficient of thermal expansion, electrical resistance, specific heat, density and latent, elastic modulus, yield stress and Poisson's ratio, were used for both electro-thermal and thermal-mechanical analysis [10]. In this model, the contact resistance between electrode/workpiece interfaces and workpiece/workpiece faying surfaces were considered and simulated by assigning temperature and pressure dependent resistance properties to one layer of elements along the contact interfaces, which has a thickness of 0.01 mm. The value of contact resistance (equivalent contact resistance) was obtained from reference [10]. However, considering the difference of squeeze forces and the materials (sheet size) used in present study, a trial study was used to modify the contact resistance values provided in reference [10]. This contact resistance layer was not considered in the thermal-mechanical analysis.

AISI 1010 steel with 1 mm thickness was used in present study. The sheet steel has room temperature nominal yield strength of 185 MPa [17]. The physical and mechanical properties for AISI 1010 steel workpiece at elevated temperatures were referred in [18-20]. Table 2.1 shows the approximate mechanical properties for AISI 1010 steel sheet and the welded metal used in present study.

Table 2.1 Mechanical properties for AISI 1010 steel and welded metal

Temperature (^{o}C)	20	100	200	400	600	800
Elastic Modulus (GPa)	200	195	190	170	60	10
Yield Stress (MPa)	185	180	165	112	55	10

Note: Poisson's ratio for AISI 1010 steel is 0.3.

Welding conditions. In this study, the root-mean-square value of A/C welding current used was 11,000 ampere. The welding cycle had time duration of 12 cycles (0.2 s), the holding cycle had a time duration of 0.2 s (current turned off during this cycle, see Figure 2.2), and the cooling cycle had a time duration of 50 s. A squeeze force of 2225 N was used. The tapered flat shape electrode had a 3 mm radius contact area with the workpiece.

2.2.3 Analysis Flow Chart

Since spot welding is a strongly coupled model that cannot be solved directly by commercial software, an incremental method is adopted in studying the spot welding problem. First, a solid element is used to analyze the initial contact radius (between the electrode/workpiece and the workpiece/workpiece) in the model. Then a thermal-electrical coupled element is used to analyze the temperature field in the same model. The contact information from the thermal-mechanical analysis is input to the thermal-electrical analysis to determine the electrical potential distribution. After that, the thermal-mechanical solution is carried out. The temperature field from the former thermal-electrical analysis is input as a body load. After finishing the thermal-mechanical analysis, new contact information is gained. Over a given time increment, the

interactions between the electrical-thermal and thermal-mechanical analysis are obtained. This iterative procedure is applied during the whole welding cycle. A time increment of 0.001 s was used to ensure sufficient accuracy and good calculation convergence. During the holding stage, the current is set to zero, and convection is the only thermal load in the electro-thermal model. In the cooling stage, the electrode is separated (nocontact), and convection is still the only thermal load in electro-thermal model. The condition in the thermal-mechanical model is a little complicated because there is a stress release and re-equilibrium process in workpieces after separation of the electrodes. Then, the stresses continue changing with the cooling of workpieces in the electro-thermal model. When the temperature decreases to near ambient temperature (25°C), the calculated stress distribution in the thermal-mechanical model is the residual stress in the spot welded joint.

The flow chart of the analysis procedure is illustrated in Figure 2.2. Commercial finite element code ANSYS and the APDL (ANSYS Parametric Design Language) were used to deal with the incremental method involving the coupling between the electro-thermal and thermal-mechanical subroutines.

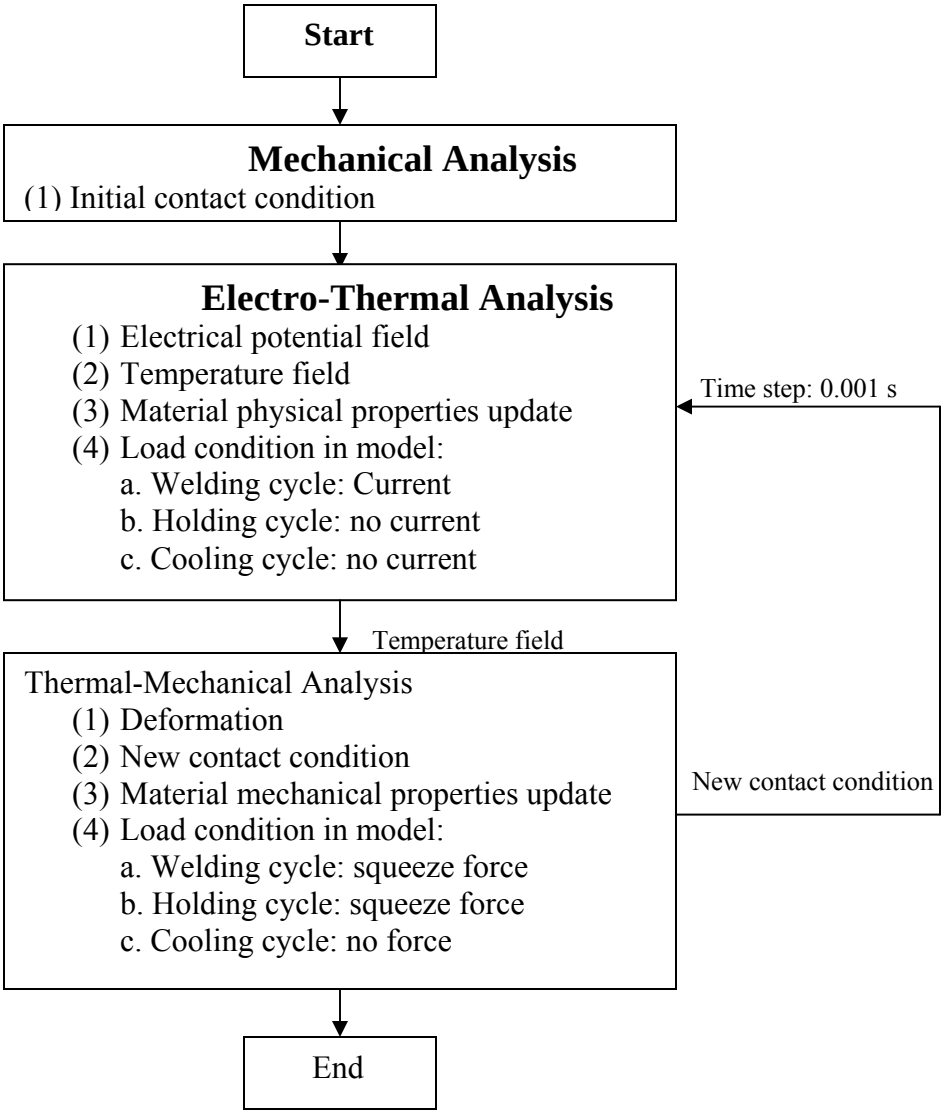

Figure 2.2 FEM program flow chart

2.3. Results and Discussion

2.3.1 Spot Nugget Shape

Figure 2.3 shows the temperature distribution in the spot welded joint. Considering 1500°C as the melting point of steel, the spot nugget (melted steel) contour appears as curve G-G in Figure 2.3. From Figure 2.3, it can be seen that the area under G-G has a

half-width of 2.20 mm and a half-height of 0.67 mm (the contact resistance layer thickness is not counted). But that is not the final nugget size because there will be some deformation in the welding zone when the weldement cools due to the electrode pressure and material shrinkage because of temperature change. According to the simulation result, the nugget has an expansion along the width of 0.02 mm, and shrinkage in height of 0.01 mm after cooling down. Therefore, the final simulated nugget size is 2.22 mm in half-width and 0.66 mm in half-height.

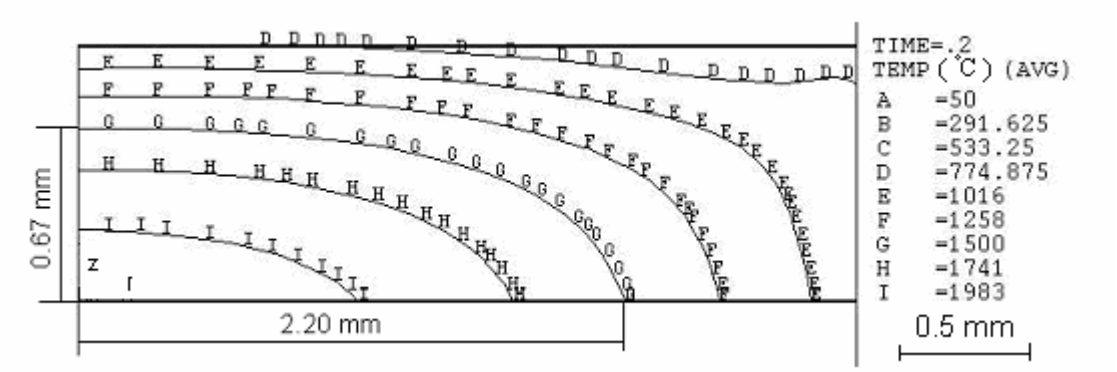

Figure 2.3 The simulated spot nugget shape

The spot welding specimen was cut along the center cross section, polished and etched to verify the spot nugget shape. Figure 2.4 shows the experimentally obtained spot nugget shape. An optical microscope was used to obtain a picture of the microstructure, as shown in Figure 2.4. The contour of the nugget is shown by a white line, which represents a change over from larger grain size (typical weld microstructure) to a finer grain size (typical HAZ microstructure). The measured spot size is 2.2 mm in half-width and 0.6 mm in half-height. It can be seen that the simulated results and measured nugget shape have good agreement.

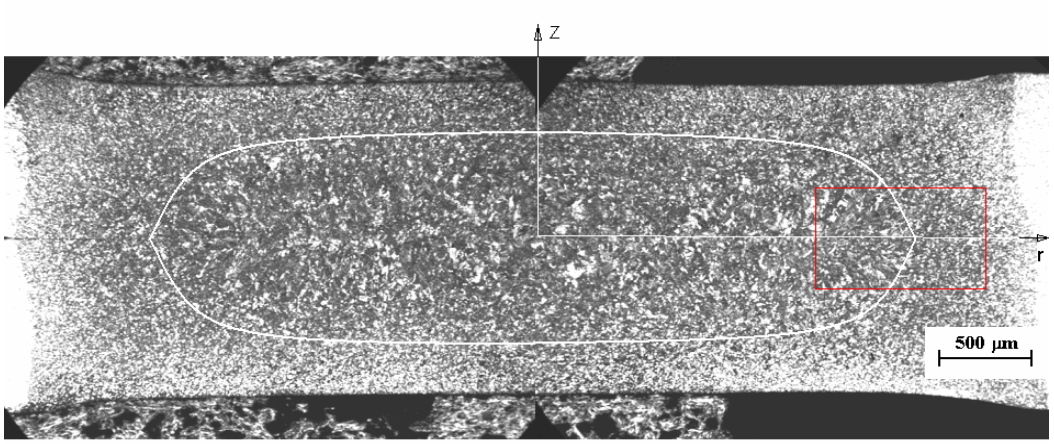

Figure 2.4 (a) Cross sectional view of the actual spot-weld, the nugget shape is shown by the white boundary

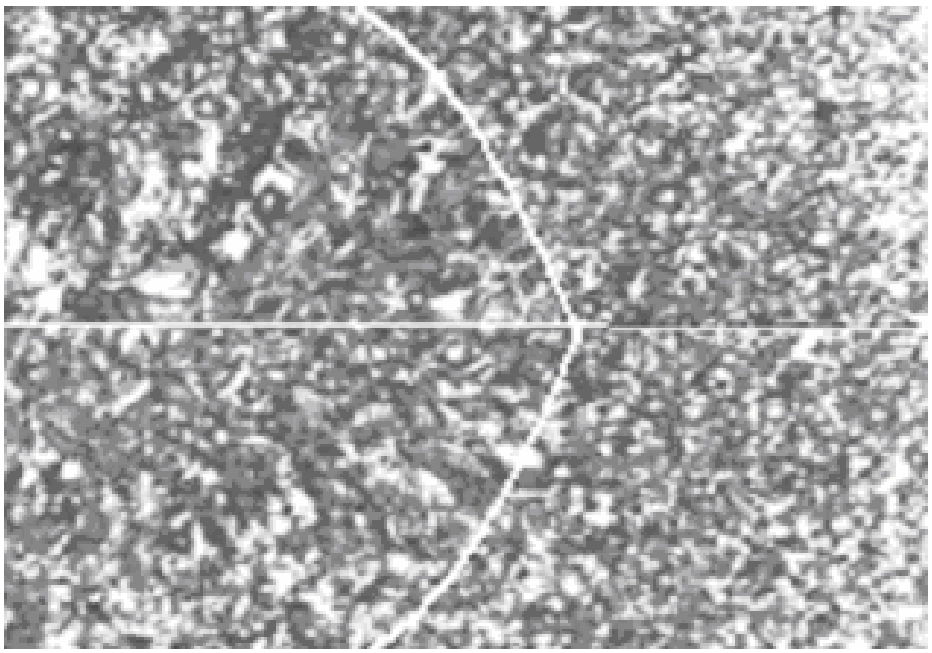

Figure 2.4 (b) Enlarged area show the difference between spot nugget and HAZ as well as base metal

2.3.2 Stress Distribution in Welding Cycle

During the welding (heating) cycle, temperature rises rapidly in the welding zone, while the expansion of hot metal is restricted by the surrounding cold metal, resulting in

compressive stress in the welding zone. Figure 2.5 (a) shows the principal stress (σ_1) distribution at end of the welding cycle. In the holding cycle, the surfaces of the welding zone have a higher cooling rate than other parts of the weld because of the water cooling effect of the electrodes. The shrinkage of the surface metal (with a higher cooling rate) is restricted by the surrounding hot weld metal, which leads to a tensile stress at the outside of welding zone while the inside hot weld metal is still under compressive stress, as shown in Figure5(b).

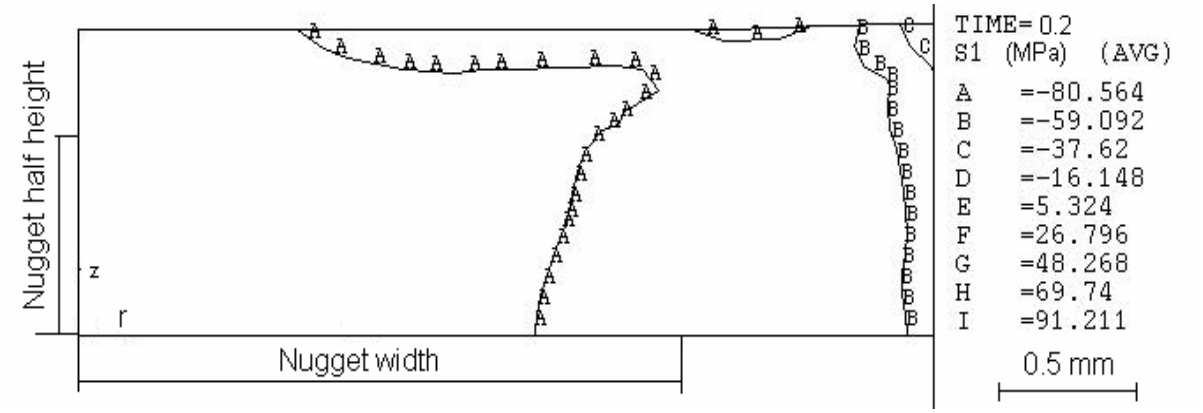

(a)

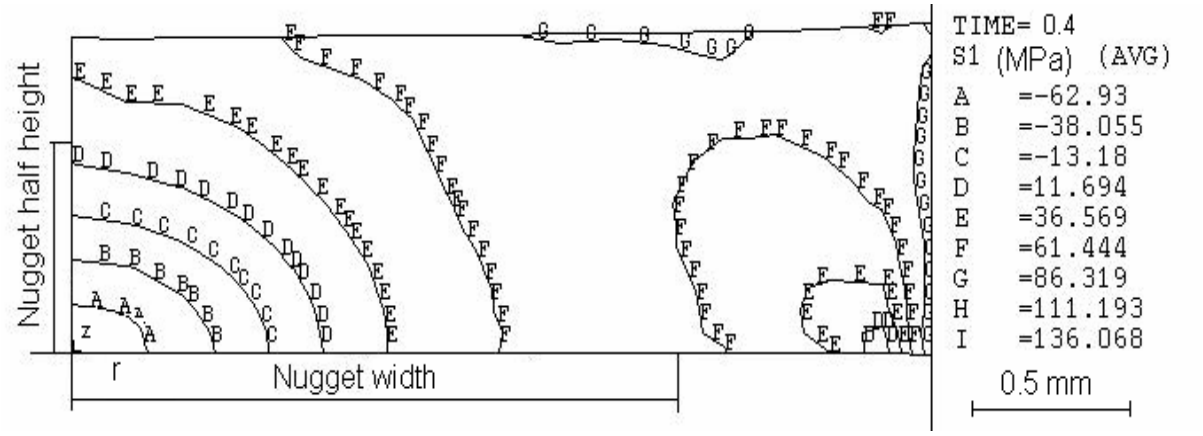

(b)

Figure 2.5 The Principal stress (σ_1) distribution during spot welding at (a) end of the welding cycle, and (b) end of the holding cycle.

2.3.3 Residual Stress Distribution

With decreasing temperature, the whole welding zone begins to shrink. Therefore, under the restriction of surrounding cold base metal, tensile residual stress dominates the welded joint area. Figure 2.6 shows the principal residual stress distribution in the spot welded joint at the end of the cooling cycle. The residual stress gradient is high outside the spot nugget, due to the high cooling rate and fine grain microstructure. This information can be valuable in the use of blind and through-hole drilling methods for residual stress determination.

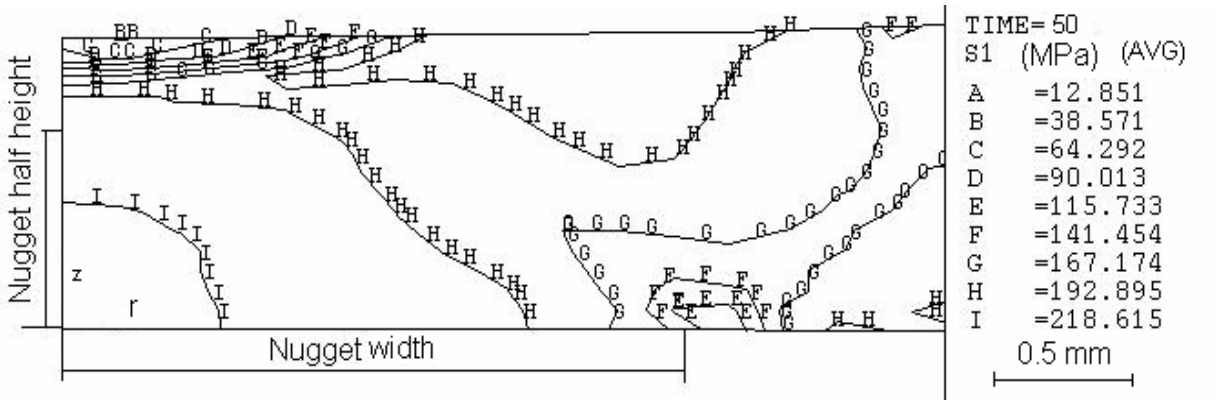

(a) Principal residual stress σ_1

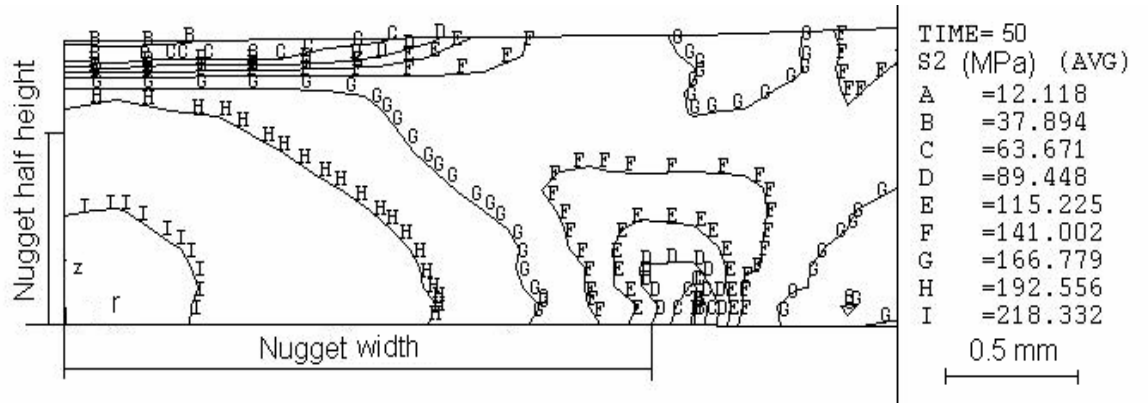

(b) Principal residual stress σ_2

Figure 2.6 Principal residual stress distribution in the spot weld

Figure 2.7 shows the principal residual stress distribution at half-depth (bottom line in present model) in the spot weld. It can be seen that the highest tensile residual stress occurs at the center of the nugget and the residual stresses decrease towards the edge of the nugget.

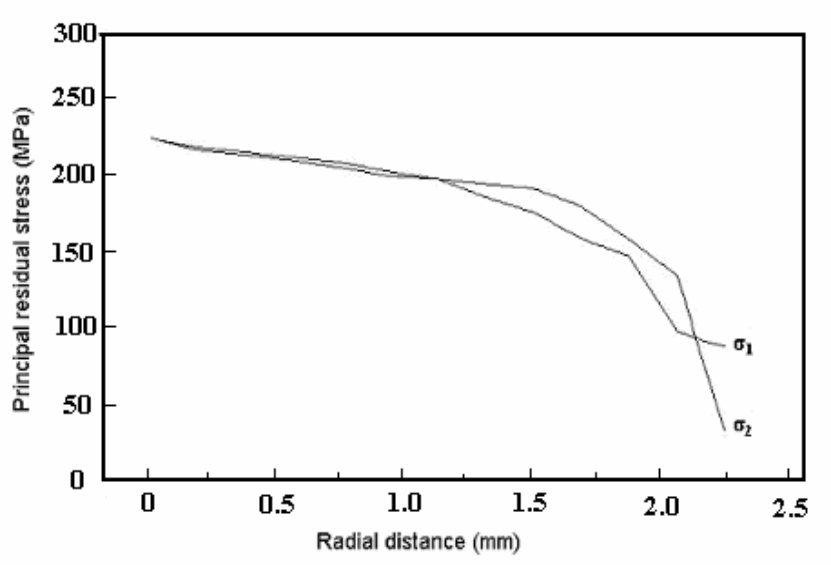

Figure 2.7 Principal residual stresses distribution at the half thickness of the spot joint

Using the technique of high sensitivity moiré interferometry in conjunction with the hole-drilling method, Khanna et al. [7] determined the residual stresses in a spot welded steel joint (the welding condition used was the same as that used in the present simulation), which is shown in Figure 2.8. Comparing Figure 2.7 and Figure 2.8, it is found that the simulated results and experimental results compare qualitatively. The maximum stress at the center and the minimum stress at the edge of the spot nugget agree with experimental results. However, in-between the FEM results show a higher value of the residual stress. This difference is possibly due to the assumption in the experimental measurements that the residual stress is uniform through the thickness of the weld. The experimental measurements [7] were made using a finite size blind hole of 0.8 mm

diameter and 0.8-1.0 mm depth. The model used for residual stress calculations assumed that the liberated displacements around the blind hole are the same as those about a through hole, since the hole depth to diameter ratio is equal to or greater than one, and the moiré displacement measurements were made close to the edge of the [12, 13].

The above simulated residual stresses results can be used in analyzing the influence of residual stress on the fatigue properties of spot welded joints, which will be discussed in future work.

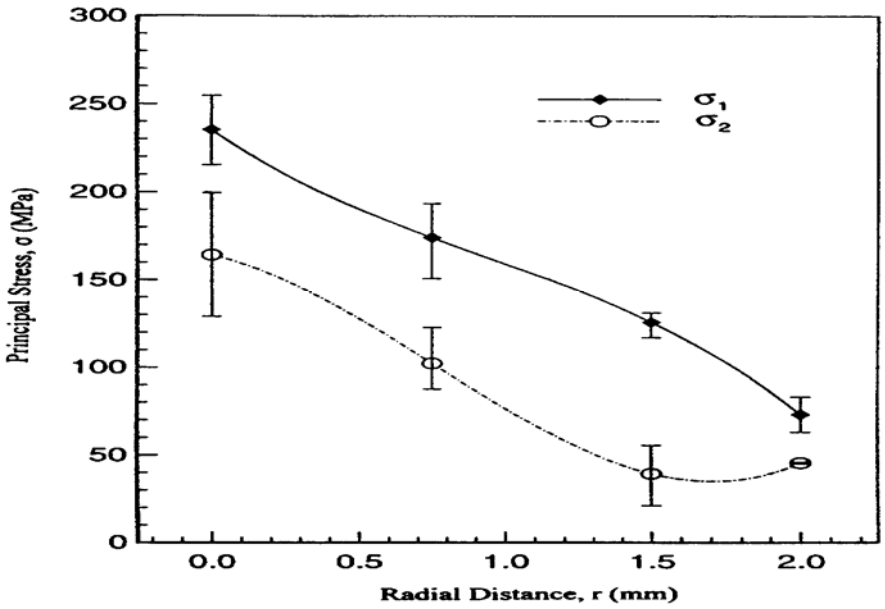

Figure 2.8 Residual stresses in spot weld determined by high sensitivity moiré interferometry [7]

2.4. Conclusions

An incremental and thermal-electro-mechanical coupled finite element model has been presented in this study for predicting residual stresses distribution and the spot nugget size in a spot welded steel joint. For comparison, the spot nugget shape and the residual stress distribution in spot joint were experimentally measured. The simulated results show good qualitative agreement with the experimental results. It has been found that in the spot nugget, a highest tensile residual stress occurs at the center of the nugget and the residual stress decreases significantly at the edge of the nugget.

2.5. Acknowledgement

The support of the National Science Foundation under grant NSF-CAREER 0196390 is gratefully acknowledged.

2.6 References:

[1] Darwish, S. M., and Al-Dekhial, S. D., 1999, "Micro-Hardness of Spot Welded Commercial Aluminium as Correlated With Welding Variables and Strength Attributes," *Journal of Materials Processing Technology*, **91,** No. 1, pp. 43-51.

[2] Anastassiou, M., Babbit, M., and Lebrun, J L., 1990, "Residual Stresses and Microstructure Distribution in Spot-Welded Steel Sheets, Relation With Fatigue Behavior," *Materials Science & Engineering A: Structural Materials: Properties, Microstructure & Processing*, **125**, No. 2, pp. 141-156.

[3] Tricoteaux, A., Fardoun, F., Degallaix, S., and Sauvage, F., 1995, "Fatigue Crack Initiation Life Prediction in High Strength Structural Steel Welded Joints," *Fatigue & Fracture of Engineering Materials & Structures*, **18**, No. 2, pp.189-200.

[4] Radaj, D., 1990, "Local Fatigue Strength Characteristic Values for Spot Welded Joints," *Engineering Facture Mechanics*, **37**, No. 1, pp. 245-250.

[5] Radaj, D., 1989, "Stress Singularity, Notch Stress and Structural Stress at Spot-Welded Joints," *Engineering Facture Mechanics*, **34**, No. 2, pp. 495-506.

[6] Satoh, T., Abe, H., Nishikawa, K and Morita, M., 1991, "On Three-Dimensional Elastic-Plastic Stress Analysis of Spot-Welded Joint under Tensile Shear Load," *Transaction of the Japan Welding Society*, **22**, No. 1, pp. 46-51.

[7] Khanna, S. K., He, Canlong, and Agrawal, H. N., 2001, "Residual Stress Measurement in Spot Welds And The Effect of Fatigue Loading on Redistribution of Stresses Using High Sensitivity Moiré Interferometry," *ASME Journal of Engineering Materials and Technology*, **123**, No. 1, pp. 132-138.

[8] Anastass, W., and Babbit, H., 1990, "Residual Stresses and Microstructure Distribution in Spot-Welded Steel Sheets: Relation with Fatigue Behavior", *Materials Sciences and Engineering*, A**125**, pp.141-156.

[9] Nied, H. A., 1984, "The Finite Element Modeling of The Resistance Spot Welding Process," *Welding Journal*, **63**, pp.s123-s132.

[10] Tsai, C. L., Jammal, O. A., and Papritan, J. C., 1992, "Modeling of Resistance Spot Weld Nugget Growth," *Welding Journal*, **71**, pp. s47-s54.

[11] Browne, D. J., Chandler H. W., Evans J. T., and Wen J., 1995, "Computer Simulation of Resistance Spot Welding in Aluminum: Part I," *Welding Journal*, **74**, No.10, pp.s339-s344.

[12] Feng, Z., Babu, S.S., Santella, M. L., Riemer, B. W., and Gould, J. E., 1998, "An Incrementally Coupled Electrical-Thermal-Mechanical Model For Resistance Spot Welding," *5th International Conference on Trends in Welding Research, Pine, Mountain, GA*, pp.1-5.

[13] Gupta, O. P., and De, Amitava, 1998, "An Improved Numerical Modeling For Resistance Spot Welding Process and Its Experimental Verification," *Journal of Manufacturing Science and Engineering*, **120**, No. 2, pp.246-251.

[14] Xu, L., and Khan, J. A., 1999, "Nugget Growth Model For Aluminum Alloys During Resistance Spot Welding," *Welding Journal*, **78**, No. 11, pp. s367-s372.

[15] Sun, X., and Dong, P., 2000, "Analysis of Aluminum Resistance Spot Welding Processes Using Coupled Finite Element Procedures," *Welding Journal*, **79**, No.8, pp. s215-s221.

[16] Chang, B. H., Shi, Y. W. and Dong, S. J., 1999, " A Study On The Role of Adhesive in Weld-Bonded Joints," *Welding Journal*, **78**, No.8, pp. s275-s279.

[17] Materials properties website: www.efunda.com

[18] *Metals Handbook*, 9th ed., Vols. 1 and 2. 1978. ASM International, Materials Park, Ohio.

[19] "High-Temperature Property Data: Ferrous Alloys". 1988. Metals Park, Ohio: *ASM International*.

[20] "Physical Constants of Some Commercial Steels at Elevated Temperatures". 1953. Edited by the British Iron and Steel Research Association. London U. K.: *Butterworths Scientific Publications*.

[21] Schajer, G. S., 1981, "Application Of Finite Element Calculations To Residual Stress Measurements", *ASME J. Engineering Materials and Technology*, **103**, No. 2, pp. 157-163.

[22] Schajer, G. S., 1988, "Measurement of non-uniform residual stresses using the hole drilling method", *ASME J. Engineering Materials and Technology*, **110**, No. 4, Part 1: pp. 338-343, Part II: pp. 344-349.

CHAPTER 3

RESIDUAL STRESSES IN SPOT WELDED NEW GENERATION ALUMINUM ALLOYS: THERMOPHYSICAL AND THEREMOMECHANICAL PROPERTIES OF 6111 AND 5754 ALUMINUM ALLOYS

Abstract

Thermophysical and thermomechanical properties of 5754 and 6111 aluminum alloys were experimentally determined between room temperature and 500°C for use as input in the numerical simulation of residual stress generated during fusion welding processes of these materials. The thermophysical properties determined included specific heat, thermal diffusivity and thermal expansion using the differential scanning calorimeter, laser flash technique and the dilatometer, respectively. Thermal conductivity was also calculated from thermal diffusivity, specific heat and density. The thermomechiancal properties determined included yield strength, elastic modulus and Poisson's ratio. The yield strength was determined using tensile test specimens in a heated chamber. The Poisson's ratio and elastic modulus were determined using resonant ultrasound spectroscopy.

3.1. Introduction

Numerical simulation is being widely used to understand manufacturing processes. For simulating thermal manufacturing processes such as welding and casting, thermophysical and thermomechanical properties of the materials are required. In this investigation, the thermophysical properties and thermomechanical properties of 5754 and 6111 aluminum alloys have been determined. These properties have been employed to numerically simulate of residual stresses generated during spot welding of sheet metals made of those aluminum alloys. These aluminum alloys are important as they are under active consideration for a future generation automotive structures. Thermophysical properties measured include specific heat, thermal conductivity, thermal expansion and density, and can be used to simulate heat transfer and solidification of the material during a welding process. Thermomechanical properties measured included yield strength, elastic modulus and Poisson's ratio, which can be used to estimate stresses and predict distortion of materials during and after welding.

It is difficult, however, to find all of the require properties in metals handbooks or other database sources. This is particularly true for new materials. Unfortunately, new materials are usually the objective for numerical studies because numerical simulation has been a powerful method to optimize or study manufacturing processes of new materials [1-4]. Some investigations have been done by previous researchers on the thermophysical and thermomechanical properties of new materials [5,6], which show how to determine those properties for numerical simulation purposes.

For comparison purposes, some aluminum alloys, which can be found in handbooks, have been referred in this paper. For example, 5052 and 5456 aluminum alloys can be

compared to 5754 aluminum alloy, while 6061 and RR131D aluminum alloys can be compared to 6111 aluminum alloy. The mean chemical compositions of these alloys are listed in Table 1 [7,8].

Table 3.1 The chemical compositions of 5754, 6111 and some reference aluminum alloys

Alloy	Mg	Si	Cu	Fe	Mn	Cr	Zn	Ti
5754	2.6-3.6	0.4	0.1	0.4	0.5	0.3	0.2	0.15
6111	0.5-1.0	0.7-1.1	0.5-0.9	0.4	0.15-0.45	0.1	0.15	0.1
5052	2.2-2.8	0.25	0.1	0.4	0.1	0.15-0.35	0.1	-
6061	0.8-1.2	0.4-0.8	0.15-0.4	0.7	0.15	0.04-0.35	0.25	0.15
5456	4.7-5.5	.25	.1	.4	0.5-1.0	0.02-0.2	.25	.2
RR131D	1.4	0.5	0.3	0.3	0.1	0.2	0.45	0.12

The measured property data have been used to simulate residual stresses in a spot welded joint using the thermo-electrical-mechanical finite element analysis, which will be presented in a separate paper. It should be noted that the measurement methods mentioned in the present study are not unique for determining some thermal properties of materials; some other options are also available.

3.2. Determination of thermo-physical properties as a function of temperature

The thermo-physical properties of 5754 and 6111 aluminum alloys that have been measured are thermal expansion, specific heat and thermal conductivity. Brief details of the experimental techniques used and the results are given below.

3.2.1 Differential dilatometry for measurement of thermal expansion of aluminum alloys

Differential dilatometry is a method in which the thermal expansion of a sample is measured relative to that of a reference material. In conventional dilatometry, the reference material is usually the measuring system itself, and this can be considered a special case of the differential method. A primary advantage of the method is that a single test can suffice to determine the difference in expansion between two materials [9,10].

Figure 3.1 shows the schematic diagram of a differential dilatometer. The expansion of the sample and reference are transmitted by means of two push rods. The differential expansion is measured by means of a differential transformer. A furnace is used to heat the sample and reference. The specimen tested had the dimension of 5 mm in width, 5 mm height, and 25 mm length. Helium gas flowing at a rate of 5 ml/minute was used to purge the dilatometer during testing.

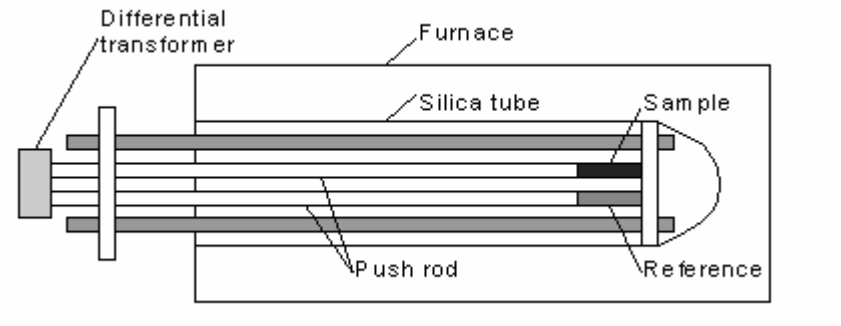

Figure 3.1 Schematic diagram of the differential dilatometer

A sample was measured in both heating and cooling cycles. At each cycle, a very short temperature ranged was used to calculate the coefficient of thermal expansion at specified temperature by computer program. The average values of coefficient of thermal expansion at heating and cooling cycles were used to draw the mean coefficient of

thermal expansion data points curves. Figure 3.2 shows the mean coefficients of thermal expansion of 5754 and 6111 aluminum alloys. For comparison, aluminum alloys 5052 and 6061 have also been cited in Figure 3.2 [11].

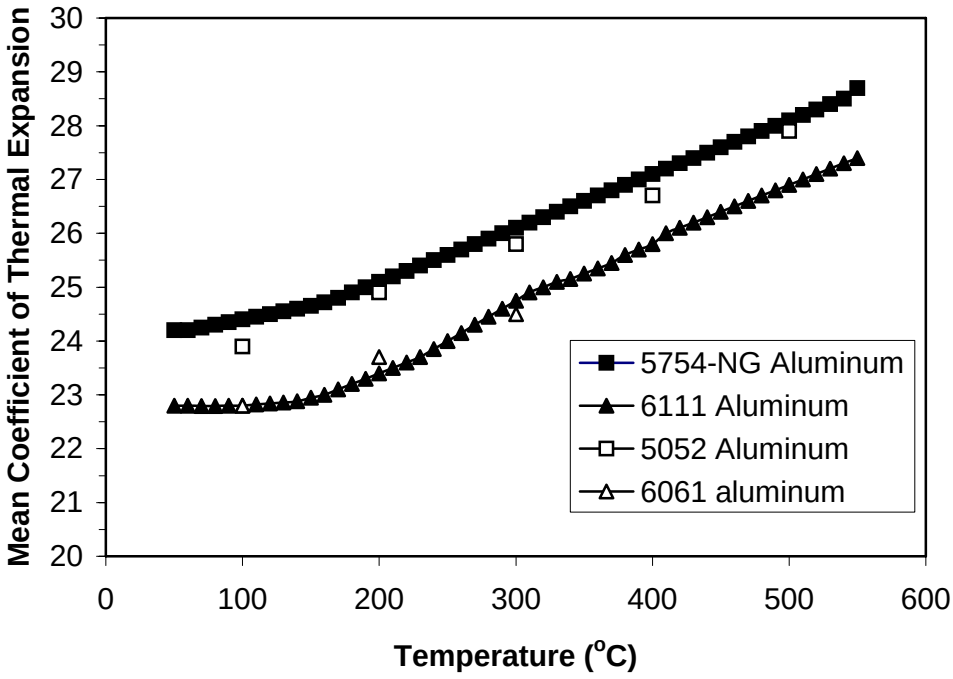

Figure 3.2 Mean coefficient of thermal expansion of 5754 and 6111 aluminum alloys, as well as 5052 and 6061 aluminum alloys.

3.2.2 Differential scanning calorimetry (DSC) for measurement of specific heat

Differential scanning calorimetry (DSC) is a technique in which the difference in energy inputs into a specimen and a reference material is measured as a function of temperature while the substance and reference material are subjected to a controlled temperature program. The difference in heat flow into the test material and a reference material due to energy changes in the material is continually monitored and recorded.

DSC measurement provides a rapid, simple method for determining the specific heat capacity of a material [8]. The ASTM standard E 1269-01 was referred [12].

The specimens used in DSC were disks of 6 mm diameter and 1.5 mm thickness. ASTM E1269-95 standard was used to determine the specific heats. Samples were heated and cooled at rates of 20°C/min in Argon flowing at 50 ml/min. A Sapphired disk of similar dimensions was used as the standard material. Figure 3.3 shows the values of specific heat of 5754 and 6111 aluminum alloys as a function of temperature. For 6111 aluminum the dip in the specific heat around 275°C and the peak around 375°C is possibly due to precipitation and solutionization events occurring in the alloy and are not related to the heat capacity of the alloy. Specific heat of pure aluminum has been shown in Figure 3.3 for comparison [13].

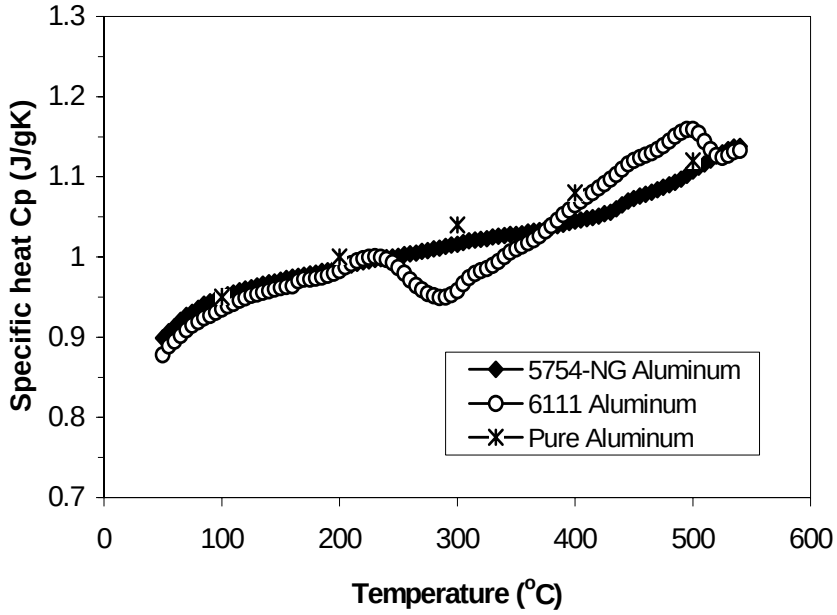

Figure 3.3 Specific heat of 5754 and 6111 aluminum alloys, as well as pure aluminum

3.2.3 Laser flash for measurement of thermal diffusivity and thermal conductivity

Thermal diffusivity, α, is a measure of transient heat flow and is defined by the equation below:

$$\alpha = k/(\rho C_p) \tag{3.1}$$

where k is thermal conductivity, ρ is density, and C_p is specific heat. However, thermal diffusivity α has been measured independently using the 'Laser Flash' method, and not using the above equation as it is very difficult to measure thermal conductivity.

In the laser flash method, the front face of a small disk-shaped specimen is subjected to a very short burst of radiant energy coming from a laser or a xenon flash lamp, with the irradiation time being of the order of one millisecond or less. The resulting temperature rise of the rear surface of the specimen is recorded and measured and thermal diffusivity values are computed from temperature rise versus time data by using the expression:

$$\alpha = 1.37L^2 / (\pi^2 t_{1/2}) \tag{3.2}$$

where L is the thickness of the specimen, $t_{1/2}$ is a specific time at which the rear surface temperature reaches half its maximum value. The above equation is the Parker equation that assumes no heat loss, however we used Clark and Taylor correction to the Parker values in the data analysis.

Figure 3.4 schematically shows the instrument for measuring diffusivity of a material using the laser flash method. The specimens used in laser flash method are disks of 6 mm diameter and 1.5 mm thickness. The test temperatures ranged from room temperature to 500 ˚C. Figure 3.5 shows the thermal diffusivity of 5754 and 6111 aluminum alloys as a function of temperature.

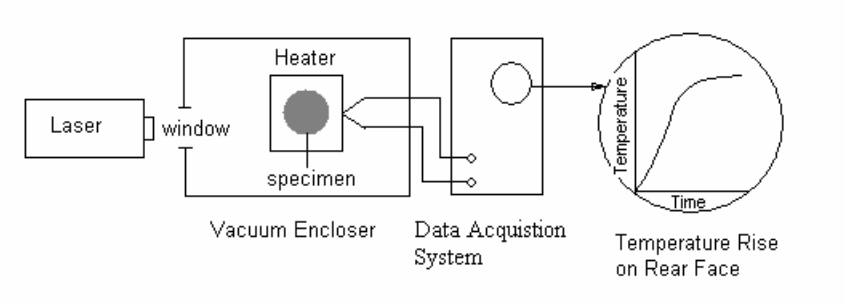

Figure 3.4 Schematic of laser flash apparatus for measuring thermal diffusivity of a material

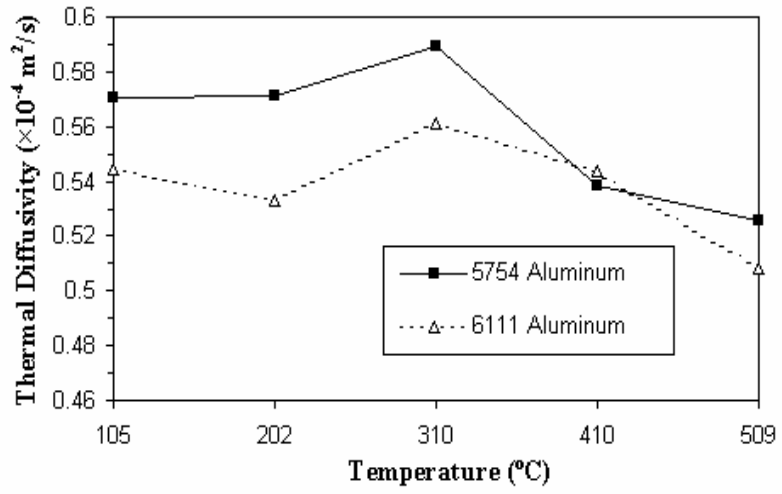

Figure 3.5 Thermal diffusivity of 5754 and 6111 aluminum alloys

Since it is very difficult to measure thermal conductivity, it was calculated using the expression:

$$k = \rho \alpha C_p \tag{3.3}$$

The density has been assumed constant at 2700 kg/m^3 for both aluminum alloys. Substituting density, measured specific heat and thermal diffusivity into equation (3.3), thermal conductivity can be obtained. Figure 3.6 shows calculated thermal conductivity as a function of temperature.

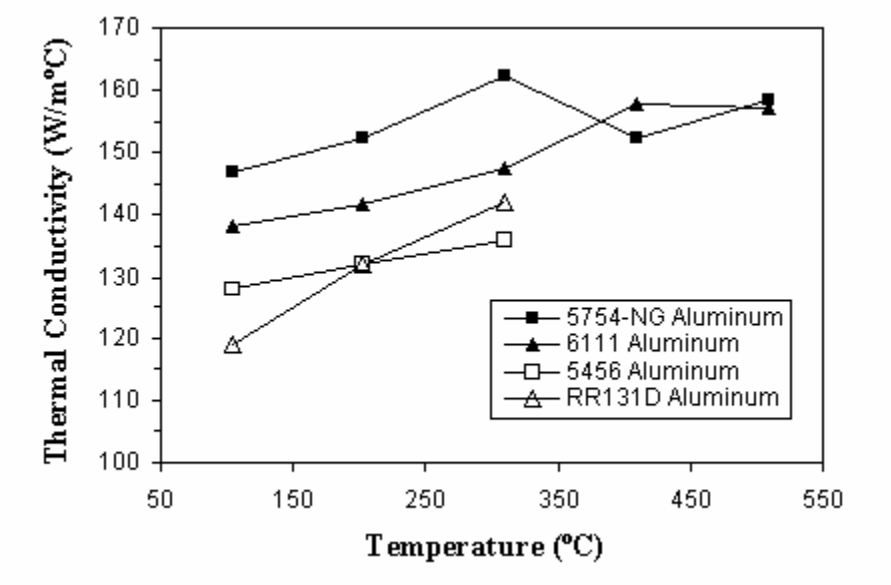

Figure 3.6 Thermal conductivity of 5754 and 6111 aluminum alloys, as well as 5456 and RR131D aluminum alloys

3.3. Determination of thermo-mechanical properties as a function of temperature

The following thermo-mechanical properties of 5754 and 6111 aluminum alloys were measured: Yield strength, Elastic Modulus, Tangent Modulus and Poison's ratio. All of these properties were determined as a function of temperature.

3.3.1 High temperature tensile test for measurement of the yield strength and Elastic Modulus

High temperature tensile tests were performed on a 200 KN Instron Model 4507 testing machine. ASTM standard E-21 was followed for the elevated temperature tension tests on the two aluminum alloys.

The dimensions of the specimen are shown in Figure 3.7. The specimen thickness was 3.24 mm for 5754 aluminum and 2.0 mm for 6111 aluminum (6111 was not

available in thicker stock). End tabs, which are schematically shown in Figure 3.8, were welded to test specimens to strengthen the region where mechanical load is transferred to the specimen by pin-loading.

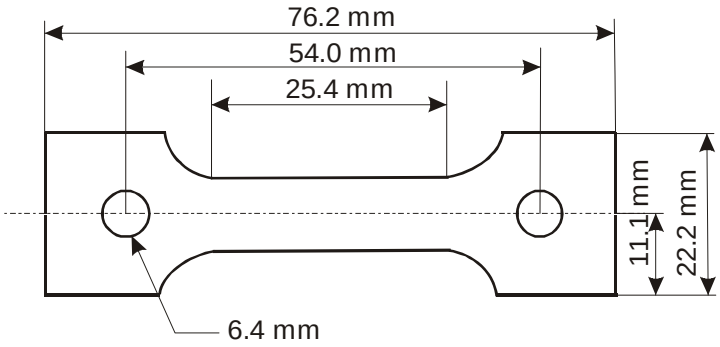

Figure 3.7. Schematic diagram of tensile specimen

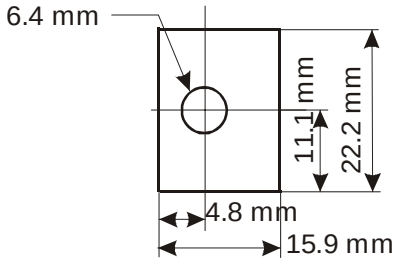

Figure 3.8. Schematic diagram of tab welded to the end of tensile specimen

Figure 3.9 shows typical tensile stress-strain curves of 5754 and 6111 alloys as a function of temperature. Table 2 lists the mechanical properties obtained from the tensile tests on 5754 and 6111 alloys. It should be noted that the slope of an apparently linear region was used to estimate the value of the yield strength corresponding to 0.2% strain. The elastic moduli listed in Table 2 are average values obtained by approximating the stress-strain region over 0.2% strain with a linear region. The tangential modulus was obtained corresponding to 2% strain for a simplified linear hardening stress-strain curve, which will be used in numerical simulation of spot welding process.

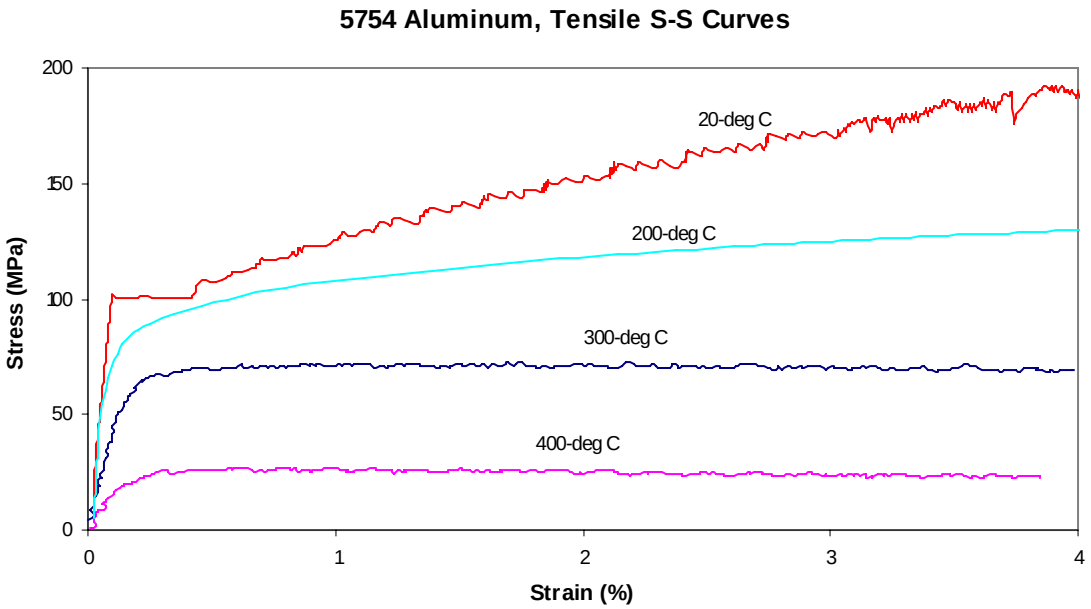

(a)

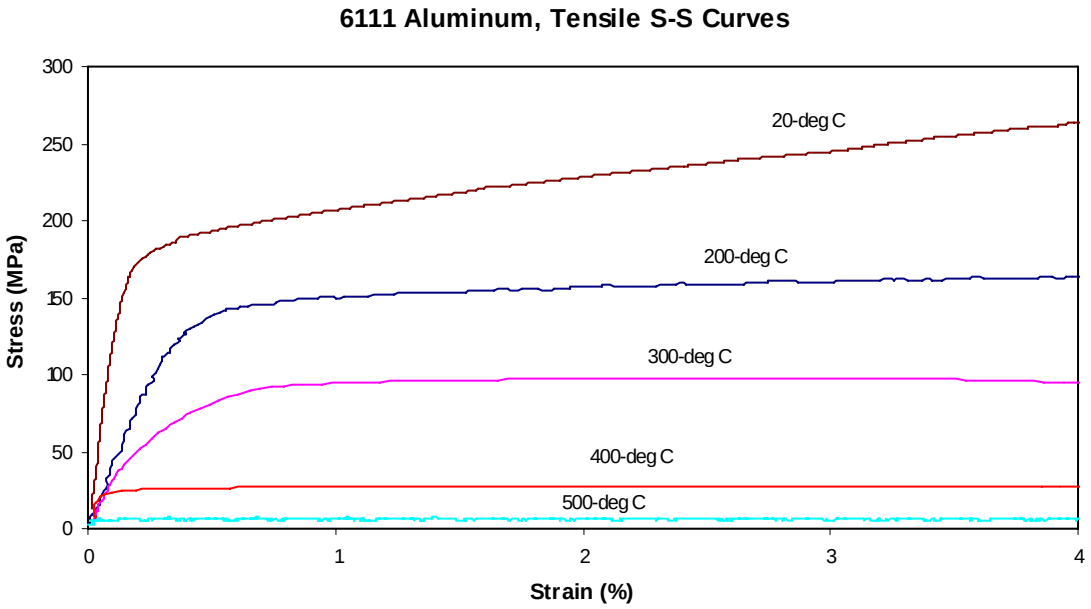

(b)

Figure 3.9 Typical tensile stress-strain curves of a) 5754 and b) 6111 aluminum alloys as a function of temperature

Table 3.2 Mechanical properties for 6111 and 5754 aluminum alloys

Temperature (^{o}C)		20	200	300	400	500
	Material					
Yield Strength (MPa)	5754	99.8	91.1	63.0	24.3	7.0
	6111	178.1	142.5	81.1	25.3	5.7
Elastic Modulus (GPa)	5754	73.9	38.2	34.1	13.3	2.3
	6111	80.7	38.4	36.1	30.5	15.3
Tangential Modulus (GPa)	5754	2.4	1.45	0.23	0.05	0.02
(2 % strain)	6111	1.95	1.05	0.42	0.09	0.05

3.3.2 Resonant ultrasound spectroscopy (RUS) techniques for measurement of the elastic modulus and poison's ratio

3.3.2.1 The principle of RUS

RUS technique is based on measuring the spectrum of mechanical resonances for a sample of known shape. An approximate spectrum is previously calculated from the known sample dimensions, its mass, and a set of assumed elastic constants. The measured spectrums of mechanical resonances are compared with the theoretically calculated spectrum. The true set of elastic constants is then calculated by a recursive regression method that varies the assumed elastic constants until matching the calculated resonant spectrum with experimental one. A multidimensional minimization of the error between the measured and calculated spectra enables deducing all the elastic constants of the solid from a single frequency scan. More details of this technique can be found elsewhere [14-

18]. Over the last 10 years, RUS has become a versatile laboratory technique for measuring elastic constants, ultrasonic attenuation, thermodynamic properties, structure phase transitions, etc. in solids. The available results demonstrate that RUS can be used on small samples with high precision [17].

3.3.2.2 Instrumentation

Figure 3.10 shows a block diagram of the RUS system. For tests at elevated temperatures, the sample and waveguides that support the sample and that transmit the signal to the transducers, which are located outside the furnace, are placed in a heating chamber. The waveguides used in this investigation were made of aluminum oxide. Disk shaped test specimens were 20 mm diameter disks and 2 mm thickness for 6111 aluminum and 3.2 mm thickness for 5754 aluminum.

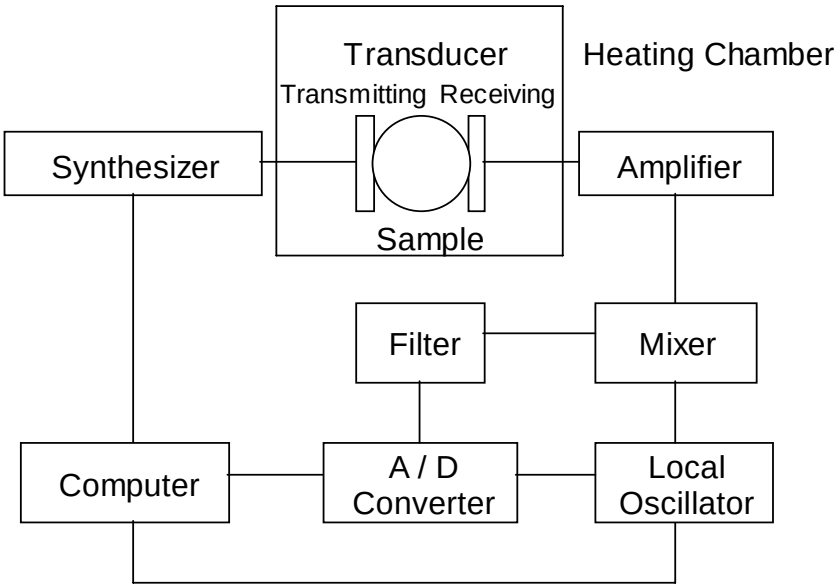

Figure 3.10. Block diagram of a typical RUS swept excitation measurement system

3.3.2.3 Results

Figure 3.11 shows a typical resonance spectra of an 5754 disk sample in RUS at room temperature.

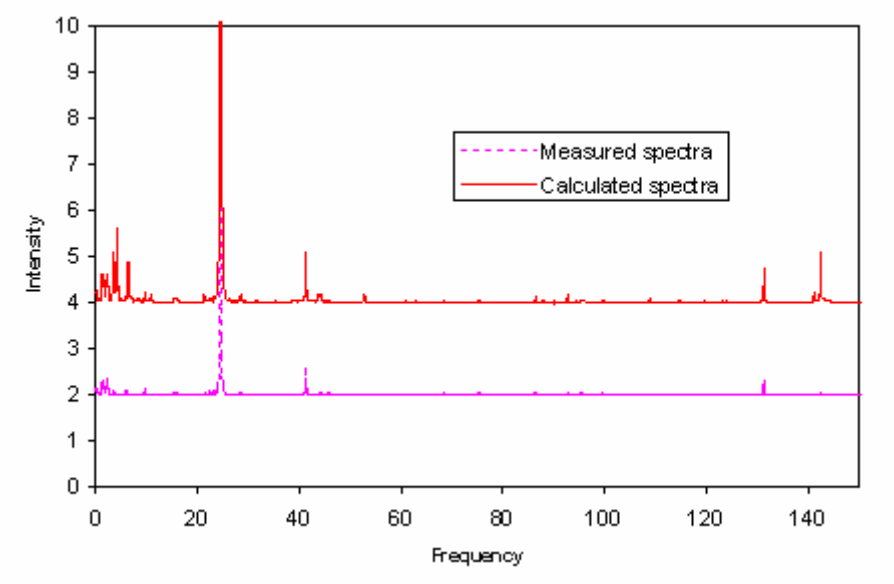

Figure 3.11. Typical resonance of the aluminum cylinder sample in RUS

After the fitting process, the measured results can be obtained. Figure 3.12 and Figure 3.13 show the measured Poisson's ratio and Young's moduli of 5754 and 6111 aluminum. It may be noticed that the Poisson's ratio of 5754 aluminum alloy remains relatively constant while that of 6111 aluminum alloy keeps decreasing with the temperature. From a mechanics view point, Poisson's ratio is related to elastic modulus, E, and shear modulus, G, that means the response to stretching and shear deformation modes does not change with the temperature in the same manner for the sample in which we observed increase in Poisson's ratio with temperature. From a metallurgical viewpoint, precipitations, dissolutions, and other factors in materials should be

considered to explain the different Poisson's ratio results. To understand this more clearly, it is necessary to do further detailed analysis.

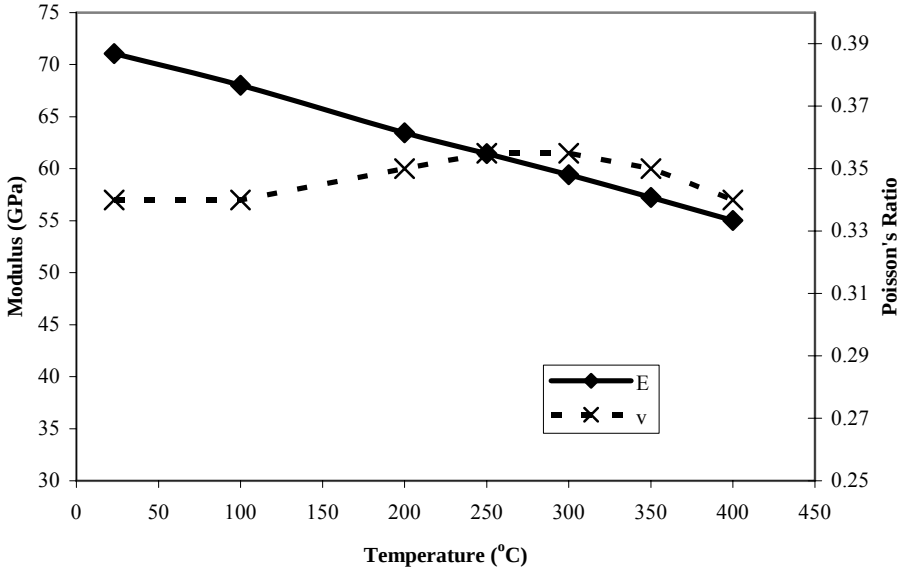

Figure 3.12 Measured Poisson's ratio and Young's modules of aluminum 5754

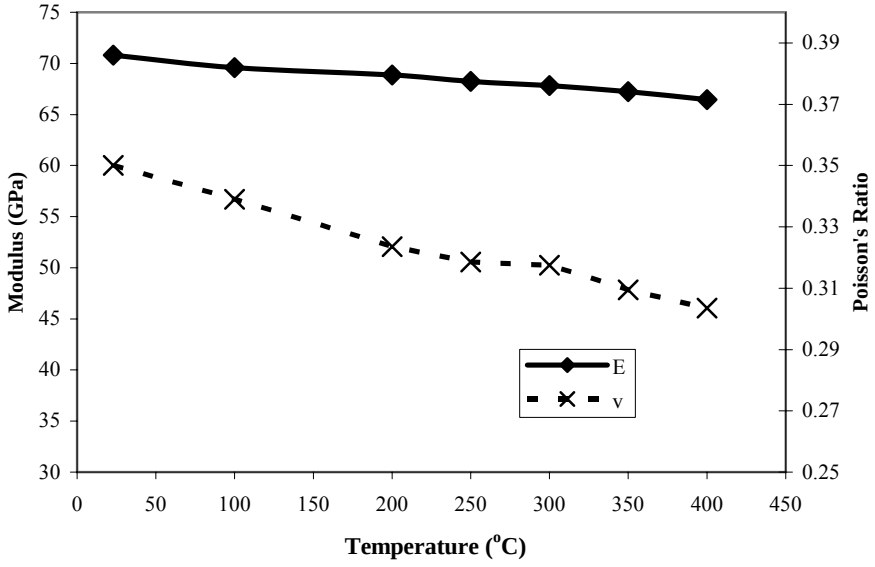

Figure 3.13 Measured Poisson's ratio and Young's modules of aluminum 6111

It should be noted that the elastic modulus obtained by RUS matches very well with what is obtained from tensile test only at room temperature. Above 200 ˚C, however, there are very significant differences between results from RUS and tensile test. These differences result from the viscoplastic behavior of aluminum at high homologous temperatures and the difference in strain rates between the RUS and tensile test experiments. It is postulated that the elastic modulus values obtained from the RUS method are more accurate and more suited for use in finite element based residual stress estimation in a welding process as welding involves rapid cooling and high strain rates.

3.4. Summary

The physical and mechanical properties of two aluminum alloys, 5754 and 6111, were experimentally determined between 20°C and 500°C. It was found that these aluminum alloys have similar thermo-physical properties, such as specific heat, thermal conductivity and thermal expansion. The thermo-mechanical properties, however, are quite different. 6111 aluminum alloy has a significantly higher yield strength and elastic modulus than that of 5754 alloy.

3.5 Acknowledgements:

The support of the National Science Foundation under grant NSF Career 0196390 is gratefully acknowledged. Research sponsored by the Assistant Secretary for Energy Efficiency and Renewable Energy, Office of FreedomCAR and Vehicle Technology Program, as part of the High Temperature Materials Laboratory User Program, Oak Ridge National Laboratory, managed by UT-Battelle, LLC for the U.S. Department of Energy under contract number DE-AC05-00OR22725 is also acknowledged.

3.6 References:

[1] M. Hval, R. H. Johnson, and C. Thaulow, Strength and Deformation Properties of Welded Aluminium Structures with Reference to Local Design and Material Properties, American Welding Society, pp. 167-182, 1995.

[2] L. H. Kallien, and R. Rosch, Development of a New Four Cylinder Crankcase for the High Pressure Die Casting Process Using Simulation Tools, ASM International, Advances in Aluminum Casting Technology, pp. 199-203, Oct. 1998.

[3] R. Kopp, Some Current Development Trends in Metal-Forming Technology, Journal of Materials Processing Technology, vol. 60, no. 1-4, pp. 1-9, 25 June 1996.

[4] C. L. Tsai, W. L. Dai, D. W. Dickinson and J. C. Papritan, Analysis and Development of a Real-Time Control Methodology in Resistance Spot Welding, Welding Journal, vol. 70, Dec., 1991, p. 339s-51s.

[5] R. B. Dinwiddie, H. Wang, W. Porter, J. Jo and L. S. Knipple, Thermophysical Properties of an HY-100 Weldment, 24th International Thermal Conductivity Conference, Pittsburgh, USA, 1997.

[6] M. Anwander, A. Hadrboletz, B. Weiss and B. Zagar, Thermal and mechanical properties of micromaterials using laseroptical strain sensors, Proceedings of Spie - the International Society for Optical Engineering, v3897, 1999. p. 404-413.

[7] ASM Handbook, (Formerly Tenth Edition, Metals Handbook), Volume 2, Properties and Selection: Nonferrous Alloys and Special-Purpose Materials, pp. 19-20, ASM International, 1990.

[8] ASM Handbook, ASM International, 1970.

[9] W. A. Plummer, Differential Dilatometry- A Powerful Tool, AIP Conference Proceedings, Series Editor: Hugh C. Wolfe, Number 17, Editors: R. E. Taylor and G. L. Denman, American Institute of Physics, New York, 1974.

[10] W. D. Porter and P. J. Maziasz, Thermal Expansion Data On Several Iron- And Nickel-Aluminide Alloys, Scrita Metallurica et Materialia, Vol.29, 1993, 1043-1048.

[11] Y.S. Touloukian, R. K. Kirby, R. E. Taylor, and P. D. Desai, "Thermal Expansion – Metallic Elements and Alloys," pp. 1028-1033 in Thermophysical Properties of Matter, Vol. 12, IFI/Plenum Co., New York, (1977).

[12] ASTM standard: E 1269-01, Standard Test Method for Determining Specific Heat Capacity by Differential Scanning Calorimetry.

[13] Y.S. Touloukian and E. H. Buyco, "Specific Heat - Metallic Elements and Alloys," pp. 1-5 in Thermophysical Properties of Matter, Vol. 4, IFI/Plenum Co., New York, (1970).

[14] Albert Migliori and John L. Sarrao (eds.), Resonant Ultrasound Spectroscopy, A Wiley-Interscience Publication, New York, 1997.

[15] Albert Migliori and Timothy W. Darling, Resonant Ultrasound Spectroscopy for Materials Studied and Non-destructive Testing, Ultrasonics, vol (34), 1996, 473-476.

[16] A. Migliori, J. L. Sarrao, William M. Visscher and et al, Resonant Ultrasound Spectroscopic Techniques for Measurement of the Elastic Moduli of Solids, Physics B, Vol. (183), 1993, 1-24.

[17] Y. He, R. B. Schwarz, T. Darling and et al, Elastic Constant and Thermal Expansion of Single Crystal γ-TiAl From 300 to 750 K, Materials Science and Engineering A vol. (239-240), 1997, 157-163.

[18] Georage W. Rhodes, Resonant Ultrasound Spectroscopy for Discontinuity Detection in Both Metallic and Nonmetallic Parts, Materials Evaluation, Vol. (58), Mar, 2000, 421-427.

CHAPTER 4

RESIDUAL STRESSES IN SPOT WELDED NEW GENERATION ALUMINUM ALLOYS: FINITE ELEMENT SIMULATION OF RESIDUAL STRESSES IN A SPOT WELD IN 5754 ALUMINUM ALLOY

Abstract

An incremental thermo-electro-mechanical coupled finite element model has been developed for predicting the residual stress field in a 5754 aluminum alloy spot welded joint. The complete spot welding process, including squeezing, welding, holding and cooling cycles, as well as the temperature and stress histories during those cycles in the welded joint have been investigated. All the required thermo-physical and thermo-mechanical properties used were experimentally measured. The results show that tensile residual stress predominates the spot nugget area. The highest tensile residual stress, with a value close to the materials yield strength, occurs around the center of the nugget. The residual stress value decreases slightly towards the edge of the spot nugget.

4.1. Introduction

Aluminum alloys are being actively considered as substitute materials for steel in the automotive industry. This substitution is being propelled by the need for greater fuel economy in automobiles. Theoretical calculations based on conventional automotive designs have estimated that a 40 % reduction in body weight can possibly increase fuel efficiency over 7 % [1]. In addition, the evolution of advanced metallurgy technology has led to the development of new aluminum alloys with higher strength-to-weight ratio, better weldability, enhanced formability, and improved corrosion resistance relative to conventional aluminum alloys [2].

Although some new welding techniques have been used to manufacture automotive structures, such as laser beam welding [3-4] and friction stir welding [5-7], electrical resistance spot welding (or spot welding) is still a major method of joining sheet metal in the automotive industry. Spot welding joins metal parts together with a localized, permanently bonded connection. Compared with other welding processes, resistance spot welding is fast, easily automated and easily maintained. Figure 4.1 shows a schematic diagram of the spot welding setup. The application of the appropriate squeezing pressure, results in the formation of a contact interface between the two work pieces or sheets. Then a high electric current is passed that results in localized melting of the metal sheets between the electrodes. When electric current is turned off, molten metal cools down and solidifies under the pressure of the electrodes, resulting in the formation of a spot weld nugget. The electrodes are then retracted. When the welded region cools down, residual stresses are generated due to the local heterogeneous thermal cycle, heterogeneous thermo-plastic deformation, and some phase transformation induced by plastic

deformation (i.e. phase transformation induced deformation). Residual stresses significantly affect stress corrosion cracking and hydrogen-induced cracking and also fatigue strength in these weldments [8].

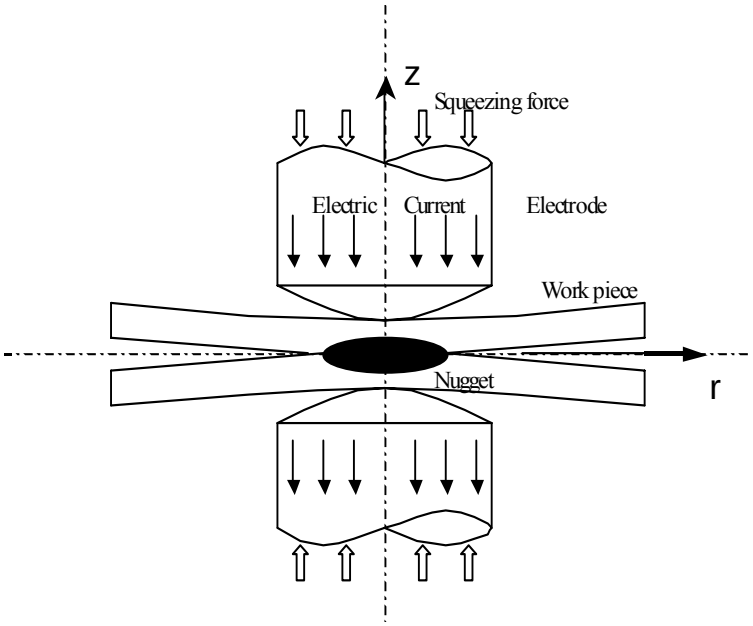

Figure 4.1 Schematic diagram of spot welding setup

Due to the complexity involved in the measurement of residual stresses, there has been an increasing use of numerical simulation procedures for estimating or predicting residual stress in weldments [9]. However, previous numerical simulations on spot welding have mainly focused on the temperature distribution, nugget growth, electrode design, welding parameters optimization, etc. [10-14]. The complete welding process simulation for residual stress prediction has not been investigated. To study residual stresses in a spot welded joint, however, the whole welding process, which includes squeezing cycle, welding (heating) cycle, holding cycle, and cooling cycle, should be considered in the simulation.

Since spot welding is a strongly coupled process that cannot be solved directly by commercial software, a sequentially coupled finite element model was used in previous investigations [14-15]. Sequentially coupled model simulates the temperature field and stress field in the spot weld in a sequential order. Under this condition, the contact radii between the electrode/workpiece and faying interface are assumed to remain constant during the whole welding process. This is not actually true because contact radii are the result of competition between thermal expansion and electrode squeezing force, thus they vary during the welding process. Later, an incrementally coupled thermal-electro-mechanical model was developed [11-14]. In the coupled thermal-electro-mechanical model at predetermined small time increments, the contact radii from thermo-mechanical analysis are input to the electrical-thermal analysis as electrical and thermal boundary conditions. Then the temperature distribution from electrical-thermal analysis is input to the thermo-mechanical analysis as a body load. This iterative procedure is applied during the whole welding process. Since the simulated contact condition at electrode/workpiece and faying interface is more close to the true contact status, this incrementally coupled model leads to more accurate results, compared with the previous sequential coupled model.

In this study, an incrementally coupled finite element model has been established to study the complete spot welding process, and temperature dependent physical and mechanical material properties determined in a previous investigation [16] have been used. The material that has been investigated is 5754 aluminum alloy. The chemical composition of 5754 aluminum is shown in Table 4.1 [17]. The history of internal stress

generation and the final residual stress distribution in the spot welded aluminum joint has been obtained. The growth of the spot weld nugget has also been studied.

Table 4.1 Chemical composition of 5754 aluminum alloy (wt. %)

Si	Fe	Cu	Mn	Mg	Cr	Zn	Ti
0.40	0.40	0.10	0.50	2.6~3.6	0.30	0.20	0.15

4.2. Finite Element Model and Analysis

4.2.1 Modeling the spot welding process

The spot welding process can be divided into four cycles as explained below:

(1) Pre-squeezing cycle: workpieces are deformed under a pre-squeezing force, which develops a good workpiece/workpiece, workpiece/electrode contact. Pre-squeezing cycle is followed immediately by the heating cycle.

(2) Heating cycle: workpieces are heated by passing current, while the squeezing force is kept constant.

(3) Holding cycle: current is cut off but the squeezing force is maintained. The workpieces start cooling.

(4) Cooling cycle: squeezing force is removed. The spot welded joint and workpiece cool down to room temperature. Residual stresses are developed in the welded joint.

It can be seen that the spot welding process involves a complex coupling among thermal, electrical and mechanical induced deformation processes. Since such a strongly coupled model cannot be solved directly by commercially software available, an

incremental method has been adopted using APDL (ANSYS Parametric Design Language) in ANSYS commercial software. At first, a solid element is used to analyze the initial contact radius (between the electrode/workpiece and the workpiece/workpiece) in the model. Then a thermo-electrical coupled element is used to analyze the temperature field in the same model. The contact information from thermo-mechanical analysis is input to the thermo-electrical analysis to determine the electrical potential distribution. After that, the thermo-mechanical solution is carried out. The temperature field from the former thermo-electrical analysis is input as a body load. After finishing the thermo-mechanical analysis, new contact information is gained. Over a given time increment, the interactions between the electrical-thermal and thermo-mechanical analysis are obtained. This iterative procedure is applied during the whole welding cycle. A time increment of 0.001 s was used to ensure sufficient accuracy and good calculation convergence. During the holding cycle, the current is set to zero, and convection is the only thermal load in the thermo-electrical model. In the cooling cycle, the electrode is separated (non-contact), and convection is still the only thermal load in thermo-electrical model. The condition in the thermo-mechanical model is a little complicated because there is a stress release and a re-equilibrium process occurs in the workpieces after separation of the electrodes. The internal stresses continually change during cooling of the workpieces in the thermo-electrical model. When the temperature decreases to near ambient temperature (25°C), the calculated internal stress distribution in the thermo-mechanical model is the residual stress in the spot welded joint. This simulation process is schematically shown in Figure 4.2.

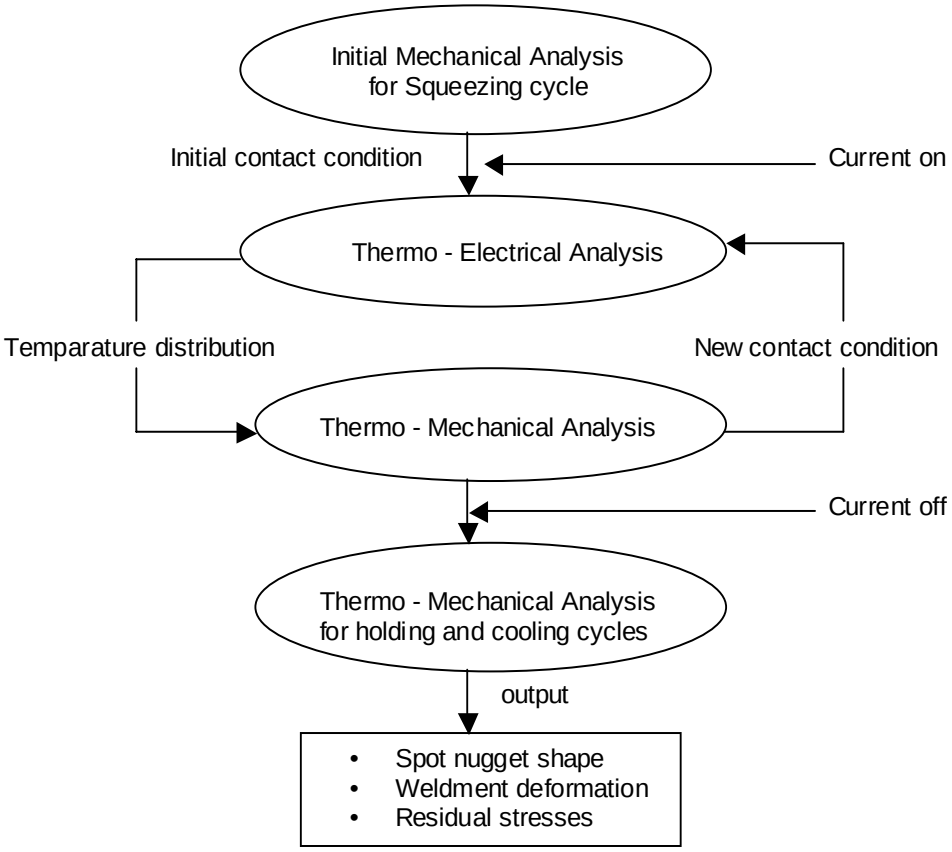

Figure 4.2 Flow chart for finite element based simulation of the spot welding process

4.2.2 Geometric model

Dome type electrodes are typically used in aluminum and aluminum alloy spot welding. Because of symmetry, only one quarter of the model is analyzed in the axisymmetric problem of spot welding, which is shown in Figure 4.3. The mesh divisions in the finite element analysis (FEA) for thermo-electrical analysis and thermo-mechanical analysis are shown in Figure 4.4. The mesh in thermo-electrical analysis contains 995 elements, while there are 2815 elements (which includes 1940 contact elements) in the thermo-mechanical analysis. A more dense mesh was used in the spot

nugget forming area, which has a higher temperature gradient (and therefore higher stress gradient) than anywhere else.

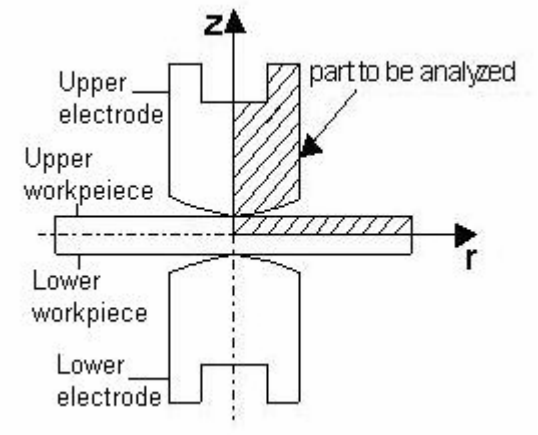

Figure 4.3 Part to be analyzed in a symmetric model

It may be noticed that the mesh for thermo-electrical analysis shown in Figure 4.4 is a little different from that for thermo-mechanical analysis. This is because no contact element is available for thermo-electrical analysis as in the case of thermo-mechanical analysis. Thus a death and birth technique was used to simulate the contact and separation condition in thermo-electrical analysis, as shown in Figure 4.4 (a) and Figure 4.5. The death and birth of elements in thermo-electrical analysis is controlled by the contact information from thermo-mechanical analysis. The contact condition between the faying surfaces in thermo-electrical analysis can be simulated by setting the thermo-electrical model boundary values, which is also controlled by the contact information from thermo-mechanical analysis.

In Figure 4.4 (b), it may be seen that there are two kinds of contact elements used. One is node to surface contact element, which is for simulating the contact condition between the dome shaped electrode and the workpiece. The second is a surface to surface

contact element, which simulates the contact condition between the two faying surfaces (i.e. workpiece to workpiece).

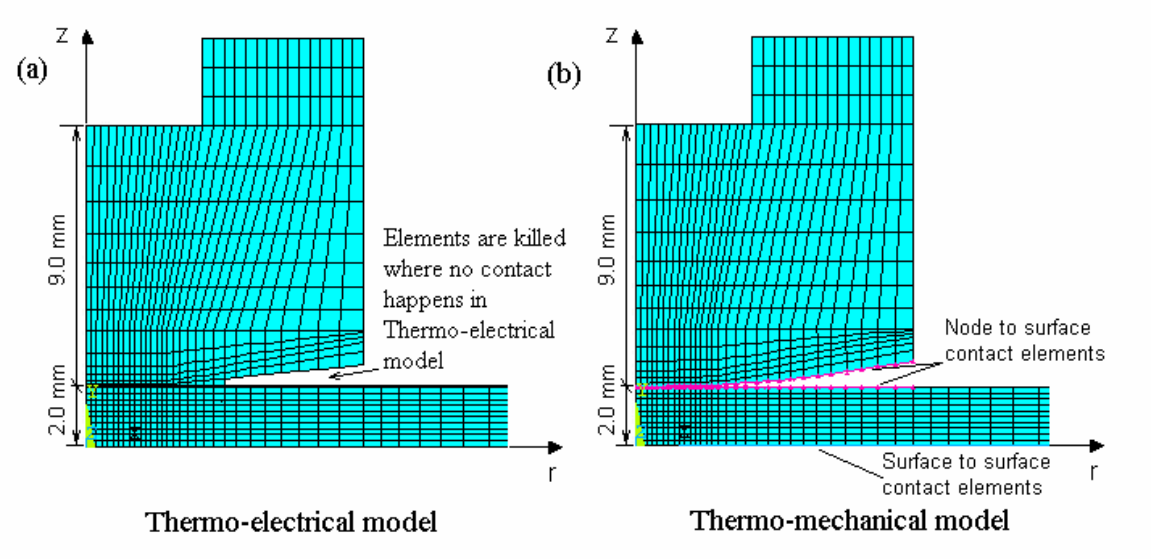

Figure 4.4 FEM mesh for (a) thermo-electrical analysis and, (b) thermo-mechanical analysis

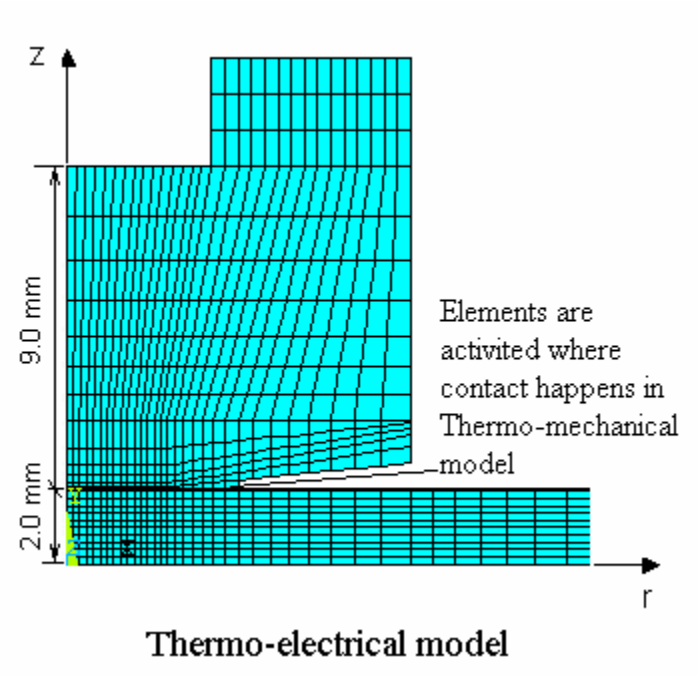

Figure 4.5 The contact condition after elements become death in thermo-electrical analysis

4.2.3 Basic theory

All the equations in this study are based on the cylindrical coordinate system, as shown in Figure 4.4. The governing equation for calculation of the electrical potential φ in the whole model is:

$$\frac{\partial}{\partial r}(\sigma \frac{\partial \varphi}{\partial r}) + \frac{\sigma}{r}\frac{\partial \varphi}{\partial r} + \frac{\partial}{\partial z}(\sigma \frac{\partial \varphi}{\partial z}) = 0 \qquad (4.1)$$

where r is the radial distance in this column coordinate system, z is the distance in the axis direction of the coordinate system, and σ is the electrical conductivity. By solving equation (4.1), the electrical potential φ is obtained. According to the electric current heat generation (q) rule:

$$q = I^2Rt \qquad (4.2)$$

where I is the current, R is the material electrical resistance, and t is the time for which current is passed. Since I = φ/R, equation (4.2) can be rewritten as:

$$q = \varphi^2 t/R \qquad (4.3)$$

The governing equation for transient temperature field distribution, which involves electrical resistance heat can be written as:

$$\rho c \frac{\partial T}{\partial t} = \frac{\partial}{\partial r}(k \frac{\partial T}{\partial r}) + \frac{k}{r}\frac{\partial T}{\partial r} + \frac{\partial}{\partial z}(k \frac{\partial T}{\partial z}) + q \qquad (4.4)$$

where ρ is the material's density, c is the heat capacity, T is the temperature, t is the time, and k is the thermal conductivity, respectively. The material properties c, k and σ are temperature dependent. Substituting equation (4.3) in (4.4), the equation which describe the temperature distribution generated by passing electric current is obtained.

For stress and strain analysis, since the thermal-elastic-plastic behavior is a highly nonlinear phenomenon, the stress-strain relation is described in incremental form:

$$\{\Delta\sigma\} = [D]\{\Delta\varepsilon\} + \{C\}\Delta T \quad (4.5)$$

where vector $\Delta\sigma$ and $\Delta\varepsilon$ is stress and strain increment, respectively, ΔT is temperature increment. Matrix D and vector C are materials related constant [18]. Since residual stress is caused by heterogeneous plastic deformation of the material, temperature dependent mechanical properties of the material were used [16]. Plastic deformation of material was modeled using bilinear kinematic hardening (BKIN) option in ANSYS program, which assumes the total stress range is equal to twice the yield stress and the work hardening is linear.

4.2.4 Boundary conditions and materials properties

Electrical boundary conditions. In the welding cycle, a root-mean-square (RMS) value of total alternating current was applied uniformly at the top of the copper electrode. At the faying surface of the workpieces, the voltage of the nodes was set to zero if the nodes were under contact according to the contact information from thermo-mechanical analysis.

Welding conditions. For the 5754 aluminum alloy, the value of A/C welding current used was RMS of 8,000 amperes, with duration of 3 cycles (0.05 s) for preheating; 29,000 amperes, with duration of 3 cycles (0.05 s) for welding; 32,000 amperes, with duration of 5 cycles (0.083 s) for post heating. The holding cycle had a time duration of 0.168 s, and the cooling cycle had a time duration of 150 s. A squeeze force of 7500 N was used. The dome shaped electrode had a radius of 50.8 mm. The thickness of both aluminum sheets used was 2.0 mm.

Thermal boundary conditions. The temperature at the water cooling cavity was restrained to 25 ºC, and convection heat transfer to ambient air was specified on all the lateral surfaces of the electrode and workpiece that are not in contact. The coefficient of heat transfer was set to 12 W/(m^2 ºC) [18].

Mechanical boundary conditions. Uniform pressure was applied at the top of the copper electrode during welding and holding cycles. The electrode was retracted at the end of the holding cycle. In the cooling cycle, some contact elements at the faying surface, where the highest temperature reached is the melting point of the material, were set to always contact because of the solidification of liquid metal.

Materials properties. Temperature dependent physical and mechanical material properties, including thermal conductivity, coefficient of thermal expansion, specific heat, density, elastic modulus, yield stress and Poisson's ratio, were measured in a previous investigation [16] and were used for both thermo-electrical and thermo-mechanical analysis. It should be noted that mechanical properties of the aluminum alloy were kept unchanged beyond the temperature of 500 ºC up to melting of the alloy. Electrical resistance of the workpiece and electrode materials were obtained from reference [18], which are listed in Table 4.2. In this model, the contact resistance between electrode/workpiece interface and workpiece/workpiece faying surfaces were considered and simulated by assigning temperature and pressure dependent resistance properties to one layer of elements along the contact interfaces, which had a thickness of 0.05 mm. The value of contact resistance (equivalent contact resistance) was estimated from references [19-20], as listed in Table 4.2. It may be noticed that the contact resistance layer was not considered in the thermo-mechanical analysis.

Table 4.2 Electrical resistance of aluminum alloy and estimated contact resistance between electrode/workpiece and workpiece/workpiece

Temperature (ºC)	20	200	300	400	500
Aluminum alloy resistance ($\times 10^8$ Ω·m)	5.8	7.7	8.8	9.8	20.5
Copper electrode resistance ($\times 10^8$ Ω·m)	2.64	3.99	5.19	6.01	7.48
Contact resistance between electrode/workpiece ($\times 10^8$ Ω·m)	580	370	280	98	20.5
Contact resistance between workpiece/workpiece ($\times 10^8$ Ω·m)	290	190	140	49	20.5

4.3. Results and Discussion

4.3.1 Spot nugget size and contact radius history in electrode/workpiece and workpiece/workpiece

Figure 4.6 shows the temperature distribution in the spot welded joint after the welding (heating) cycle. Considering 600^{o}C as the melting point of aluminum, the spot nugget (melted aluminum) contour is shown in Figure 4.6. It may be seen from Figure 4.6 that the spot nugget size for 5754 aluminum alloy has a radius of 3.23 mm and a half-height of 1.05mm (the contact resistance layer thickness is not counted). These results agree with the experimentally measured nugget radius of about 3.5 mm [21]. There would be small changes in the spot nugget size due to expansion or shrinkage of the material when cooling down to room temperature. Expansion along the centerline of the nugget was found to be 0.02 mm, and the shrinkage along the height of the nugget was 0.01 mm when the weld cools down to room temperature.

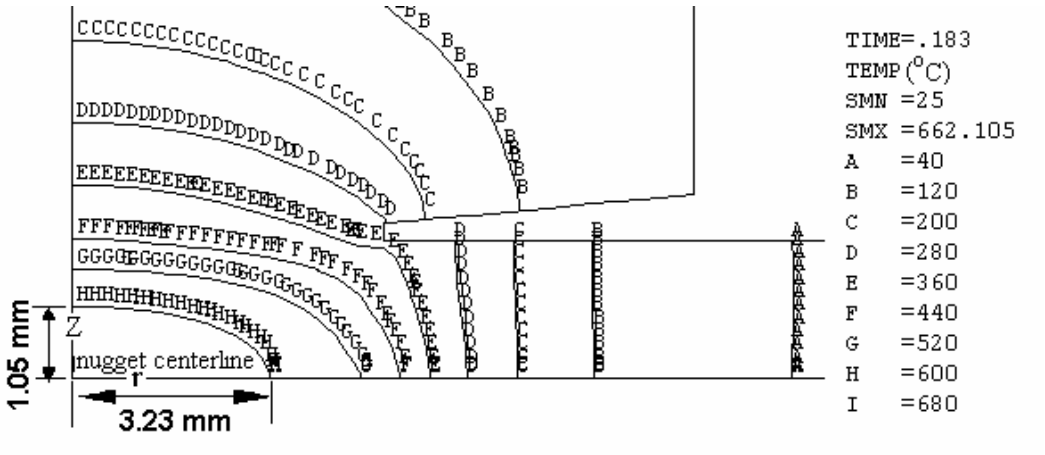

Figure 4.6 Simulated spot nugget shape and size for 5754 aluminum alloy sheets of 2mm thickness

Figure 4.7 shows the contact radius changes in electrode/workpiece and workpiece/workpiece during pre-squeezing cycle, heating cycle and holding cycle. It should be noted that the contact radius in Figure 4.7 excludes materials expansion due to heating. It can be seen that from squeezing cycle to heating cycle (0.0 to 0.183 s), the contact radius keeps increasing in both electrode/workpiece and workpiece/workpiece contact areas. The contact area becomes larger during the heating cycle due to softening of materials at higher temperatures, while the squeezing force is kept the same. In the holding cycle (0.183 to 0.351 s), the contact areas begin to decrease due to the solidification of the weld and increase in the material's strength with decreasing temperature.

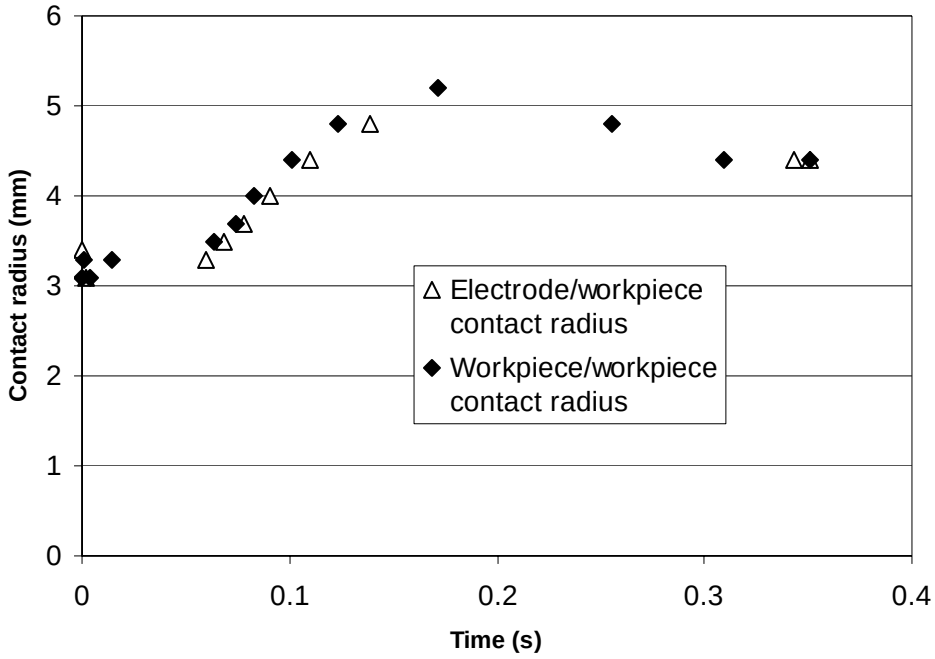

Figure 4.7 The contact radius history in electrode/workpiece and workpiece/workpiece

4.3.2 Internal stress development in the spot nugget during the welding process

The formation of residual stress in the spot welded joint is due to local plastic deformation caused by non-uniform temperature distribution during the welding process. Figures 4.8 and 4.9 show the temperature and maximum principal stress σ_1 distribution history, respectively, along the centerline (which is shown in Figure 4.6) of the spot nugget during the whole welding process.

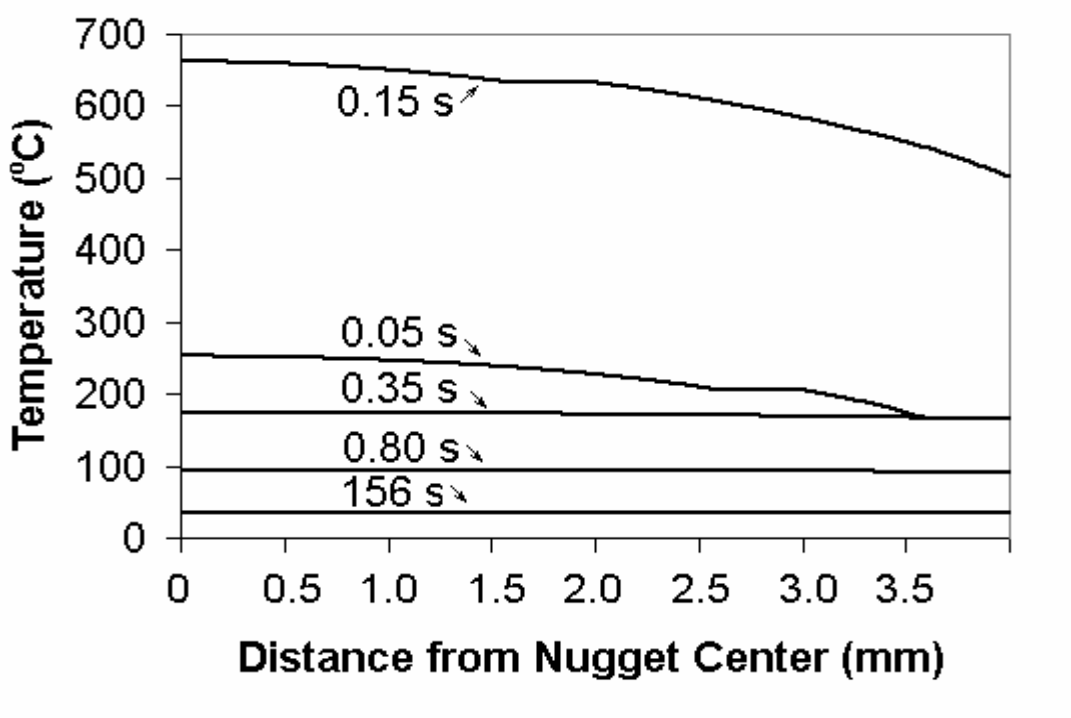

Figure 4.8 Temperature history along the centerline of spot nugget during welding

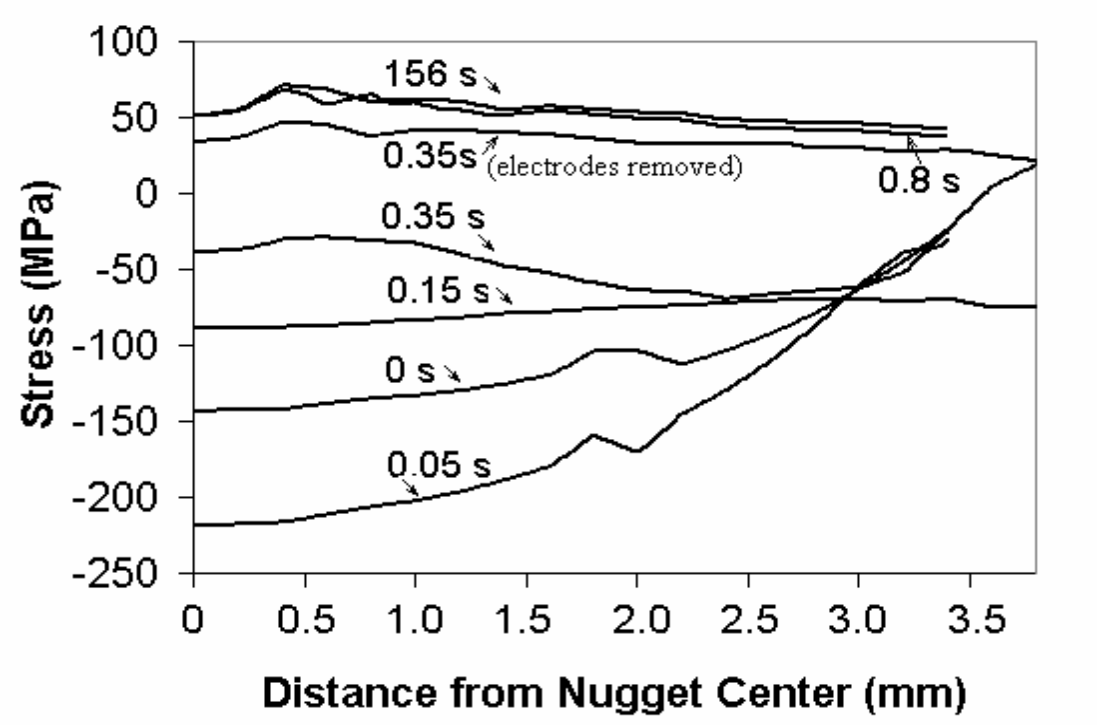

Figure 4.9 Principle stress σ_1 history along the centerline of spot nugget during welding

It may be seen from Figure 4.9 that high compressive stress develops in the spot nugget center when the temperature starts rising in the nugget, for example, when the welding time is 0.05s. When the temperature reaches the melting point of aluminum alloy at the welding time of 0.15 s, the compressive stress in the nugget becomes more uniform and decrease to a lower value of approximately 90 MPa. During the holding cycle, in which current was shut off but the load is maintained, temperature drops rapidly and the compressed metal in the spot nugget begins to shrink, which results in the development of tensile stresses. At the end of the holding cycle, the squeeze load was removed and the electrodes were separated from the workpiece, when tensile stresses formed in the nugget, as shown in Figure 4.9 at the welding time of 0.35 s. During the cooling cycle, the temperature decrease from about 180 ^{o}C to 25 ^{o}C, and the internal stresses do not change significantly during this cooling period from 0.35 s (electrode removed) to 156 s.

4.3.3 Residual stress distribution in aluminum spot welded joint

Figures 4.10 and 4.11 show the principal residual stress distribution in a 5754 aluminum spot weld. For comparing, Figure 4.12 shows the internal stress distribution in the spot weld at the end of the holding cycle. It may be seen from Figure 10 and 11 that tensile residual stress predominates the spot nugget area. The highest tensile residual stress, with a value close to the material's yield strength, occurs in the center area of the nugget. The tensile residual stress decreases slightly towards the edge of the spot nugget. The maximum residual stress of about 75 MPa occurs at the center and close to the surface of the weld, and then decreases to about 50 MPa at the half thickness of the spot

nugget, which is at the origin of the coordinate system shown in Figure 4.3. It may be noted that the residual stress states shown in the spot weld region only are all tensile in nature. Residual stresses are internal stresses and are self equilibrated stresses. However, if we chose a larger domain that includes the spot weld and the surrounding regions then we would obtain a global residual stress state that is self-equilibrated.

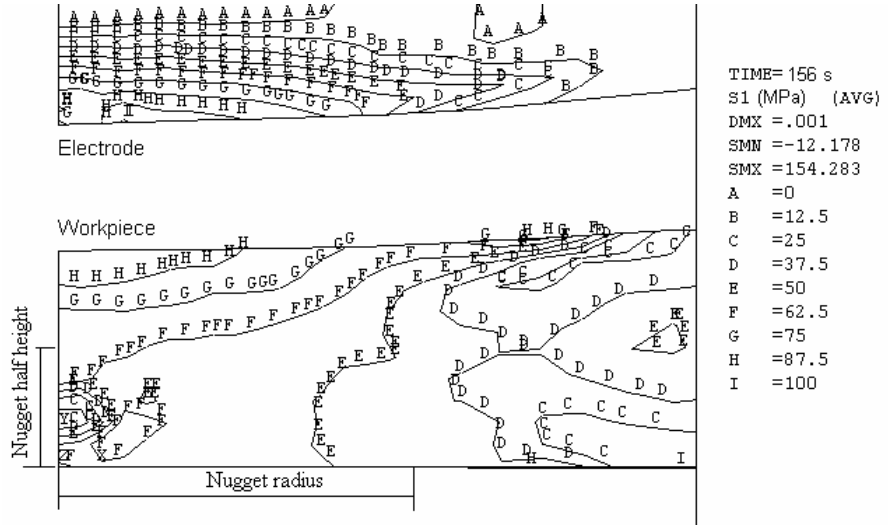

Figure 4.10 Principal residual stress σ_1 in aluminum spot welded joint

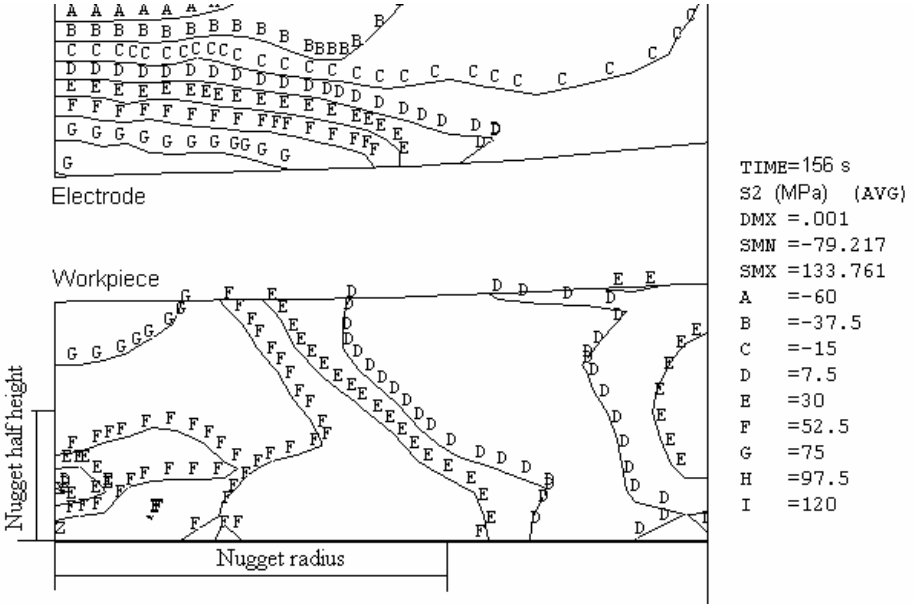

Figure 4.11 Principal residual stress σ_2 in aluminum spot welded joint

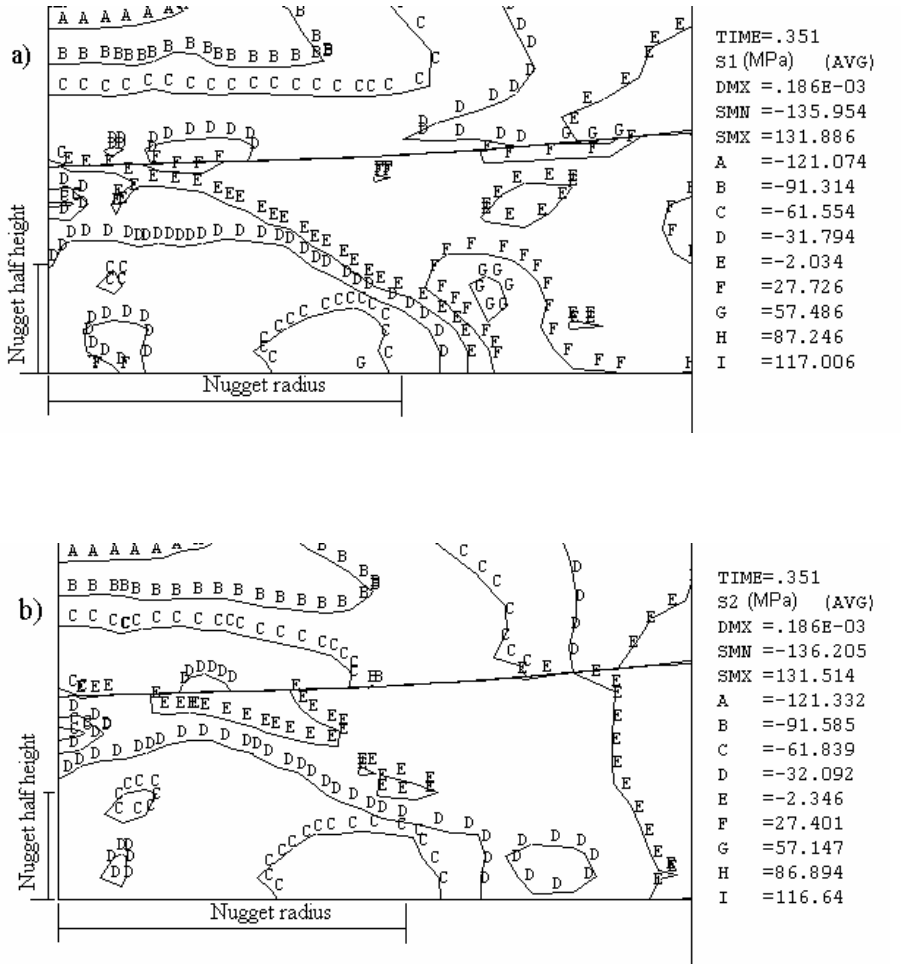

Figure 4.12 Internal stress a) principal stress σ_1 and b) principal stress σ_2 distribution in aluminum spot welded joint at end of the holding cycle

4.4. Conclusions

In this investigation, a two-dimensional axisymmetric finite element model was developed to determine the temperature distribution, internal stress development history and the welding residual stress distribution in 5754 aluminum alloy spot welded joints. A coupled thermo-electrical-mechanical finite element model with temperature dependent physical and mechanical material properties was employed. All material properties used were measured by experiments. The temperature and internal stress development history

in the spot welded joint provides a fundamental understanding of the deformation produced and the internal stresses generated in the welded region. Quantitative determination of these quantities should provide important data for safer and more durable design of thin sheet aluminum structures for automotive structures.

4.5 Acknowledgement:

The support of the National Science Foundation under grant NSF-CAREER 0196390 is gratefully acknowledged. Discussions with Wallace D. Porter, Hsin Wang, Miladin Radovic and Edgar Lara-Curzio, The High Temperature Materials Laboratory, Oak Ridge National Laboratory, Oak Ridge, Tennessee, USA, are appreciated.

4.6 References:

[1] Venkat, S.; Albright C. E.; Ramasamy S. and Hurley J. P., 1997, "CO_2 Laser Beam Welding of Aluminum 5754-O and 6111-T4 Alloys," *Welding Journal*, **76**, July, pp. 275s-282s.

[2] Irving, B., 1992, "Blank Welding Forces Automakers to sit up and take notice," *Welding Journal*, **71**, No.9, pp.39-45.

[3] Birch, S., 1999, "Laser-welding aluminum alloys," *Automotive Engineering International*, **107**, No.11, Nov, p.71.

[4] Hirose, A.; Todaka, Hirotaka; Yamaoka, Hiroto, 1999, "Quantitative evaluation of softened regions in weld heat-affected zones of 6061-T6 aluminum alloy- characterizing of the laser beam welding process," *Metallurgical and Materials Transactions Part A, Physical Metallurgy and Materials Science*, **30A**, No.8, Aug, pp.2115-2120.

[5] Jin H.; Saimoto, S. and Ball, M., 2001, "Characterisation of microstructure and texture in friction stir welded joints of 5754 and 5182 aluminium alloy sheets," *Materials Science and Technology*, **17**, No.12, Dec., pp. 1605-14.

[6] Cederqvist, L. and Reynolds, A. P., 2001, "Factors affecting the properties of friction stir welded aluminum lap joints," *Welding Journal*, **80**, No.12, Dec., pp. 281S-287S.

[7] Kalee, S., 1997, "TWI works on friction stir welding for lightweight automotive structures," *Metallurgia*, **64**, Apr, p. 119.

[8] Masubuchi, K., Analysis of Welded Structures, Pergamon, Oxford, 1980.

[9] Murphy, Y. V. L. N.; Rao G. V.; and Iyer P. K.; 1996, "Numerical Simulation of Welding and Quenching Processes Using Transient Thermal and Thermo-Elasto-Plastic Formulations," *Computers and Structures*, **60**, No.1, pp.131-154.

[10] Xu, L., and Khan, J. A., 1999, "Nugget Growth Model For Aluminum Alloys During Resistance Spot Welding," *Welding Journal*, **78**, No. 11, pp. s367-s372.

[11] Browne, D. J., Chandler H. W., Evans J. T., and Wen J., 1995, "Computer Simulation of Resistance Spot Welding in Aluminum: Part I," *Welding Journal*, **74**, No.10, pp.s339-s344.

[12] Feng, Z., Babu, S.S., Santella, M. L., Riemer, B. W., and Gould, J. E., 1998, "An Incrementally Coupled Electrical-Thermo-mechanical Model For Resistance Spot Welding," *5th International Conference on Trends in Welding Research, Pine, Mountain, GA*, pp.1-5.

[13] Gupta, O. P., and De, Amitava, 1998, "An Improved Numerical Modeling For Resistance Spot Welding Process and Its Experimental Verification," *Journal of Manufacturing Science and Engineering*, **120**, No. 2, pp.246-251.

[14] Tsai, C. L., Jammal, O. A., and Papritan, J. C., 1992, "Modeling of Resistance Spot Weld Nugget Growth," *Welding Journal*, 71, pp. s47-s54.

[15] Nied, H. A., 1984, "The Finite Element Modeling of The Resistance Spot Welding Process," *Welding Journal*, 63, pp.s123-s132.

[16] Sanjeev K. Khanna, Xin Long, Wallace D. Porter, Hsin Wang, **Ken C. Liu**, Miladin Radovic and Edgar Lara-Curzio, Residual stresses in spot welded new generation aluminum alloys Part A – thermophysical and thermomechanical properties of 6111 and 5754 aluminum alloys, *Science and Technology of Welding and Joining*, vol.10 No.1, 2005, pp.82-87.

[17] ASM Handbook, Vol. 2, December, 2000, Properties & Selection: Nonferrous Alloys & Special Purpose Materials, American Society of Metals.

[18] Murakawa, H., Kimura, H. and Ueda, Y., 1995, "Weldability Analysis of Spot Welding on Aluminum Using FEM," *Transactions of Japan Welding Research Institute*, **24**, pp.101-111.

[19] Tsai, C. L.; Dai, W. L.; Dickinson, D. W. and Papritan, J. C., 1991, "Analysis and Development of a Real-Time Control Methodology in Resistance Spot Welding", *Welding Journal*, **70**, pp.s339-s351.

[20] Babu, S. S.; Santella, M. L.; Feng, Z.; Riemer, B. W. and Cohron J. W., 2001, "Empirical Model of Effects of Pressure and Temperature on Electrical Contact Resistance of Metals", Science and Technology of Welding and Joining, **6**, pp. 126-132.

[21] Krause, A., Ford Motor Co., personal communication.

CHAPTER 5
EFFECT OF FATIGUE LOADING AND RESIDUAL STRESS DISTRIBUTION ON SUB-MICROSCOPIC DEFORMATION MECHANISMS IN A SPOT WELDED JOINT

Abstract

The evolution of microstructure in as-welded and post-heating residual-stress-relieved spot-welded steel sheets during fatigue testing has been studied. It has been found that under high fatigue load, the dislocation density at the edge of the spot welded zone (also known as the "weld nugget") is much higher than that in nugget center area, which indicates that significant plastic deformation occurred in the edge of the weld nugget during fatigue testing. Under low fatigue load, the dislocation density is significantly lower in both edge and center areas in the weld nugget. The effect of post-heating on the microstructure (mainly dislocation morphology) is more dislocations could be generated during fatigue test for both high and low loading. Post-heating results in strength decrease of spot welded joint while it releases the residual stress in it, which makes the fatigue life of welded sheet decrease under low fatigue loading condition.

5.1. Introduction

During spot welding process, when the current is turned off, the volume of molten metal cools down and solidifies beginning from its outer edges. The volume of metal from the work pieces that has undergone heating, melting, fusion, and resolidification is called the weld nugget. The large temperature gradients created by the intense local heating during the welding process followed by rapid cooling, and also phase changes in the solidifying metal, induce heterogeneous deformations in the metal resulting in the development of internal stresses. These internal or remaining stresses are known as residual stresses.

In order to increase the reliability of products, studies on the mechanical properties (including fatigue properties) of the spot welded joint has been attracting a lot of interest [1-6]. It is known that the mechanical properties of a welded joint are not only determined by the microstructure of weld zone metal, but also by the residual stresses introduced by the heterogeneous thermal cycle during welding. Residual stresses play an important role in influencing the fatigue life and other mechanical properties of the spot welded structure. For instance, when the interaction between residual stresses and external loads occurs, the local area that has the highest tensile residual stress is a potential source for crack initiation and growth in the weld or heat affected zone (HAZ).

The fatigue process in a metal is usually associated with microstructural changes, such as dislocations generation and motion, during the initiation period of a fatigue crack. For example, numerous sub-grains form in parent grains in metal during cyclic stressing [7]. The boundaries of those sub-grains are made up of heavily jogged, scalloped and tangled dislocations. The density of dislocations within the boundaries changes as the

fatigue test progresses. Thus, fatigue behavior, residual stress and microstructure of a spot weld are all interrelated. Hence, the objective of this study was to qualitatively determine dislocation density and dislocation redistribution in the spot-weld as a function of fatigue cycles for as-welded and residual stress relieved spot welds. When a spot welded sample is subjected to tensile shear fatigue loading there is a redistribution of residual stresses and this occurs in conjunction with dislocation generation and motion as a function of the number of fatigue cycles at various depths in the thickness direction of the spot weld. It is hypothesized that changes in the dislocation distribution are related to the residual stress distribution in the spot weld, which in turn affect final failure.

5.2. Brief review of experimental and numerical investigation of residual stress distribution in a spot weld

Residual stresses are defined as self-equilibrating stresses existing in materials under uniform temperature conditions without external loading. Such stresses being self-equilibrating, the resultant force and the resultant moment produced by them is zero. Residual stresses can be also generated due to elastic-plastic loading, machining, welding, forming, heat-treating, coatings, etc.

Generally, we can distinguish three main kinds of residual stress according to the distance over which they can be observed [8]. The first kind of residual stress, termed *macroscopic*, is long-range in nature, extending over at least several grains of the material. The second kind, often called *structural micro stress*, covers a distance of one grain or a part of the grain. It can occur between different phases and have different

physical characteristics, or between embedded particles, such as inclusions and the matrix. The third kind of residual stress ranges over several atomic distances within the grain, and is equilibrated over a small part of the grain. In this study we are only concerned with the first kind of residual stress or the macroscopic residual stress field.

A significant effort has been devoted to the measurement of residual stresses in different kinds of welds such as butt weld, fillet weld, etc., in medium to thick plates of various steels [9]. The first series of techniques consist of nondestructive methods, such as X-ray diffraction, neutron diffraction method, ultrasonic method, and the magnetic method. These are based on the relationship between the physical or crystallographic parameters and the residual stress state. The other series of techniques consist of the mechanical methods. These methods mainly involve the measurement of macroscopic engineering strains which are released when material is removed mechanically or by etching from parts loaded by residual stress and subsequent calculation of the residual stress as a function of the strain measured using elasticity theory. The main techniques are the hole drilling method, ring core method, bending deflection method, and sectioning method. These methods have been widely used for measuring residual stresses through the thickness of thick welds. All these methods are sensitive to the macroscopic residual stress.

However, due to the small size of spot weld, it is very difficulty to measure the residual stress experimentally. High sensitivity moiré interferometry with hole drilling [9] and X-ray methods [10-13] have been tried to measure residual stress in spot welded joint. With moiré methods in conjunction with hole drilling, the average through-

thickness residual stresses are obtained, while the X-ray method gives the residual stresses in the surface layers of the weld, though etching techniques have been used for through-thickness stress measurement using X-rays.

In addition to experimental methods, numerical study of residual stress by finite element analysis (FEA) has been developed with the advances in computer hardware and finite element analysis (FEA) software. In 1984, a thermal-electro-mechanical coupled model was introduced by Nied [14]. Since then, coupled spot welding models have been developed by many researchers to focus on different aspects of the spot welding process, such as temperature distribution, nugget growth, electrode design, welding parameters optimization, etc. [14-20]. Figure 5.1 shows the comparison between experimental and simulated residual stress distribution in mild steel spot welded joints [9, 20]. It can be seen that the highest tensile residual stress occurs at the center of the nugget and the residual stresses decrease towards the edge of the nugget. Similar results can also be found in Refs 10-13. Khanna et.al. [9] also found that after high amplitude loading (in low cycle fatigue), residual stress decreases in the center of the spot nugget and increases in the edge of the spot nugget such that the final residual stress in the edge area is nearly equal to that in center region, as listed in Table 5.1 and Table 5.2. No further explanation about this phenomenon could be found in their study.

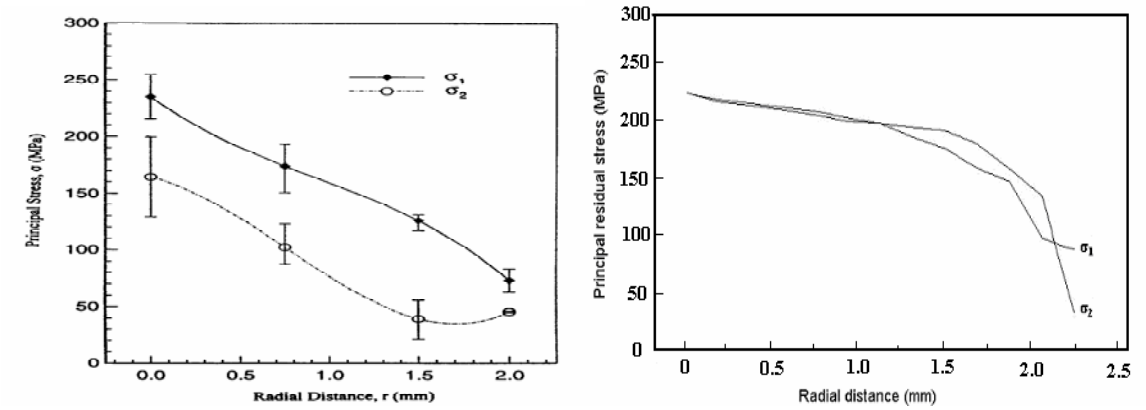

(a) (b)

Figure 5.1 Residual stress distribution in a spot weld in mild steel sheet, obtained using: (a) Moiré interferometry [9] and (b) finite element method [20].

Table 5.1 Residual stress in spot weld nugget

	At center	At edge
Single face	252.0 199.6 254.7 Average: 235.4	63.2 83.2 - Average: 73.2
Double face	247.3 236.0 - Average: 241.7	75.2 87.5 69.1 Average: 77.3

Table 5.2 The effect of fatigue loading on residual stress in a spot weld nugget

Spot welded sample	Interrupted during high load fatigue test (10,000 cycles) (MPa)	
	At center	At edge
Single face	168.5 156.7 134.8 175.6 Average: 158.9	-
Double face	200.0 158.4 154.1 Average: 170.8	177.6 104.7 - Average: 141.2

5.3. Fatigue behavior of low carbon spot welded sheet and microstructure observation of fatigued spot welded sheet

5.3.1 Fatigue test

5.3.1.1 Materials and specimen

The nominal chemical composition and nominal mechanical properties of cold rolled AISI 1020 mild steel sheet is shown in Table 3 and Table 4, respectively. The typical microstructure of AISI 1020 is mainly ferrite with some pearlite. Some of the specimens were post-heat reated to relieve residual stresses in the spot welded joint. During post-heat treatment, specimens were slowly heated to 650 °C and held 2 hours, then the cooled down slowly in the furnace. Figure 2 shows the microstructure of a spot-welded joint (including base metal, heat affected zone and weld metal) under an optical microscope. No significant grain coarsening was found after post-heat treatment.

Table 5.3 Nominal chemical composition of mild steel AISI 1020 (wt %)

C	Mn	P	S
0.18-0.23	0.30-0.60	0.04 (max)	0.05 (max)

Table 5.4 Nominal mechanical properties of mild steel AISI 1020

Tensile strength (Mpa)	Yield strength (Mpa)	Elongation (%)
395	295	37

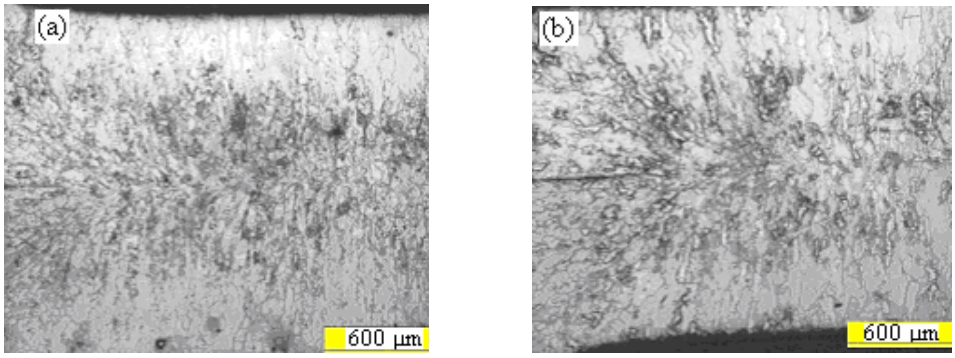

Figure 5.2 Microstructure of (a) as-welded specimen and (b) post-heated specimen.

Specimens used for fatigue tests were of the tensile shear type, as shown in Figure 5.3. The thickness of the specimen was 1.0 mm, the length 180 mm and the width 30 mm. 45 mm long tabs of the same thickness as the specimen were glued at each of the specimen to reduce bending deformation at the joint. The diameter of spot nugget was measured as about 6.5 mm for all of the samples.

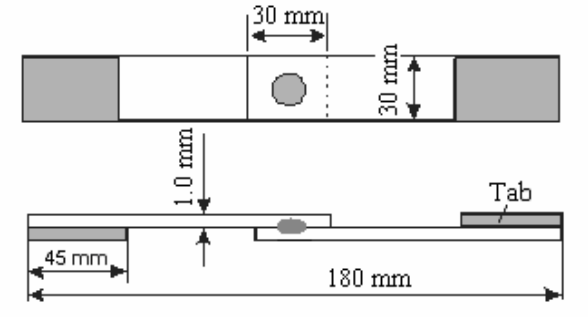

Figure 5.3 Tensile shear type fatigue specimen

5.3.1.2 Fatigue test procedure

An Instron universal testing machine was used to conduct load-controlled tension-tension fatigue tests. The specimens were subjected to varying sinusoidal loading with a

load ratio of R=0.1, at a frequency of 10 Hz. During the fatigue test, the maximum load, minimum load, maximum and minimum cross head displacement, and the frequency were monitored by using the Instron Wave Maker Data Acquisition software and 8800 Plus digital controller.

5.3.1.3 Fatigue test results

Quasi-static tension tests were conducted to obtain the peak load in a spot welded AISI 1020 steel tensile shear specimen in an as-welded condition and after post-heat residual stress relief condition as listed in Table 5.5. The corresponding load vs. displacement curves are shown in Figure 5.4. It can be seen that after post-heat treatment, the tensile strength of spot welded sheet is decreased by about 8% and yield strength of the joint is decreased by about 20%.

Table 5.5 Quasi-static tension strength of spot welded AISI 1020 steel sheets

As-welded (kN)	Post-heated (kN)
5.20	4.82

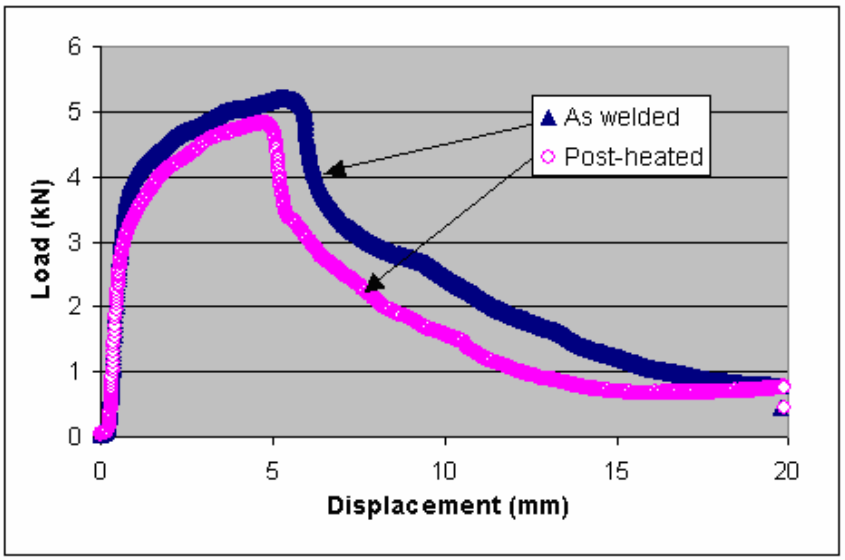

Figure 5.4 Quasi-static loading tests of spot welded AISI 1020 steel sheet

Table 5 shows the fatigue tests used in the present study. Since the objective of this study is to investigate the relationship among microstructure, residual stress and fatigue behavior of spot welded steel sheet, special fatigue test processes were designed as shown in Table 4. In the fatigue tests, low loads (such as for specimens AW4, PH3 and PH5) and high loads (such as for specimens AW2, AW8 and PH8) were used to determine the fatigue life of as-welded and post-heated specimens at both high fatigue cycles and low fatigue cycles. Then, a series of fatigue specimens were stopped during the fatigue tests at the beginning (e.g. specimens AW7, AW10, PH9 and PH7), middle (e.g. specimens AW5), and ending (e.g. specimens AW5, AW9, PH10 and PH6) periods of the fatigue lives under loads which were determined according to the above fatigue failure tests. Those unfailed fatigue specimens (that are when the tests were stopped) were used for transmission electron microscopy (TEM) observation.

Table 5.5 Fatigue test of as received and after annealed spot welded AISI 1020 sheet

Specimen #	Amplitude (kN)	Max. Load (kN)	Min. Load (kN)	Cycles to failure	Cycles to stop the test
As-welded (AW)					
AW2	0.96	2.13	0.21	70,618	
AW4	0.68	1.5	0.15	586,235	
AW8	1.49	3.30	0.33	13,214	
AW5	0.54	1.2	0.12		1,000,000
AW6	0.54	1.2	0.12		500,000
AW9	1.49	3.30	0.33		9,000
AW10	1.49	3.30	0.33		1,000
Post-heated (PH)					
PH8	1.49	3.30	0.33	20,469	
PH3	0.54	1.20	0.12	874,300	
PH5	0.54	1.20	0.12	789,067	
PH6	0.54	1.20	0.12		500,000
PH10	1.49	3.30	0.33		9,000

5.3.2 TEM observation

5.3.2.1 Specimen preparation

Thin foil TEM samples were prepared with the material cut from the unfailed fatigue specimens using a low speed diamond saw. The normal direction of the thin foils was parallel to the specimen axis. Two locations (one in spot nugget center, the other one at the edge of the spot nugget) in the spot welded sheets were excised to make TEM samples, as shown in Figure 5.5. It should be noted that the samples from the edge of the spot nuggets were under the highest tensile stress during fatigue loading, due to the stress concentration during tensile loading [12].

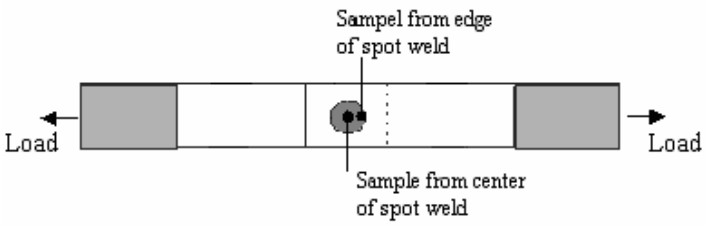

Figure 5.5 TEM samples location from spot welded steel sheet

The thin foils were mechanically ground on both sides to a thickness of about 100 μm. Discs of 3 mm diameter were punched from these foils. Focused ion beam milling (FIB) was used on the samples to further reduce the thickness of the samples to approximately 2 μm. A Gallium-liquid metal source was used to generate the ion beam. Once sample preparation was complete, a Hitachi HF-2000 field -emission TEM operated at 200 KV was used for analysis.

5.3.2.2 Microstructure and dislocation morphology in as-welded specimens

TEM observations were made on samples excised from the center and the edge of the sopt-weld nugget. Under sinusoidal tension-tension fatigue load, microstructures in the fatigued specimens have various dislocation morphologies at different fatigue periods. It should be noted that figures shown in this paper are typical microstructures in the investigated specimens. They are indented to show the general case in each condition. It was also found that the grain size in post-heated specimens are generally larger than in as-welded specimens, which indicates the recrystallization of grains during post-heat treatment.

Figure 5.6 shows a moderate dislocation density at the center of spot nugget. Dislocations generated in the center of spot nugget are possibly due to plastic deformation

under the high tensile residual stress generated in the welded joint during the solidification process.

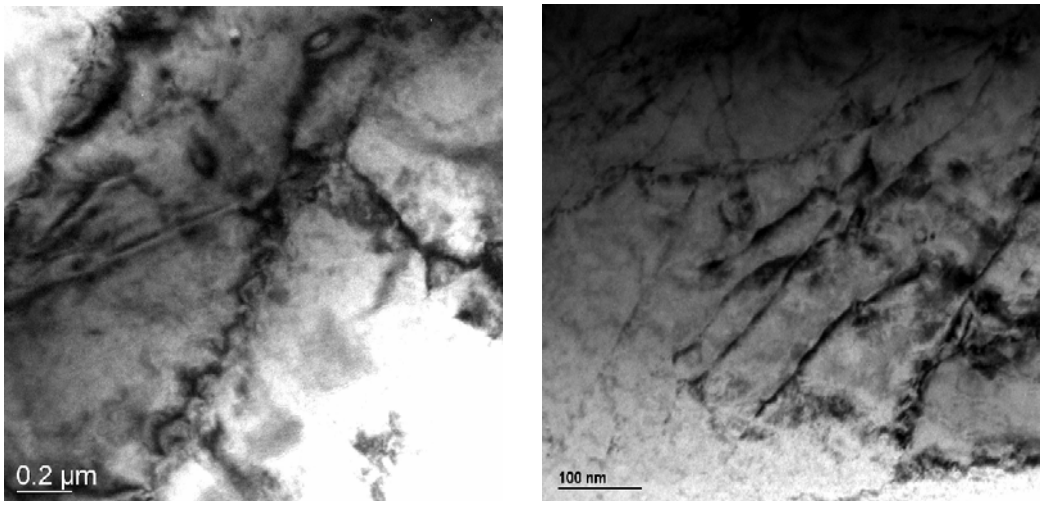

(a) (b)

Figure 5.6 Microstructure at the center of spot nugget in as-welded mild steel specimen

In the spot nugget edge area, low dislocation density has been found in as-welded sample, as shown in Figure 5.7.

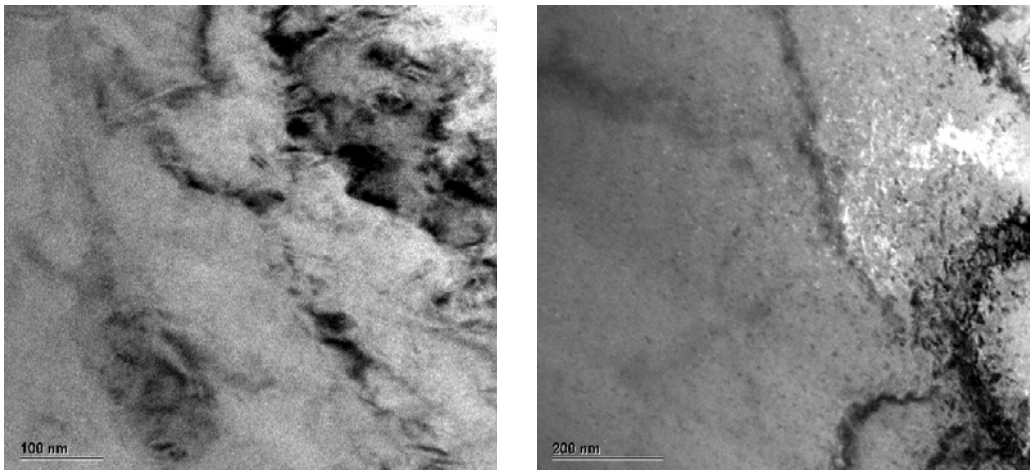

(a) (b)

Figure 5.7 Microstructure at the edge of spot nugget in as-welded mild steel specimen.

After post-heated, samples show very low dislocation density at the edge of spot nugget similar to that of as-welded samples, which is shown in Figure 5.8.

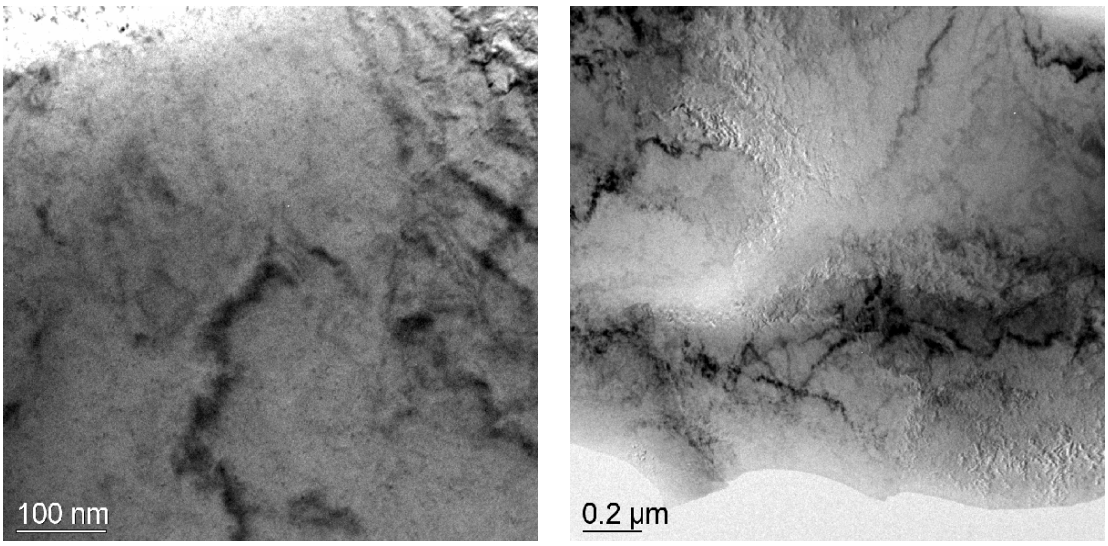

(a) (b)

Figure 5.8 Microstructure at the edge of spot nugget in post-heated mild steel specimen.

5.3.2.3 Effects of high fatigue load on dislocations distribution in as-welded samples

Under high fatigue load (max. load 3.3 kN, load amplitude 1.49 kN), as-welded specimens have a fatigue life of about 13,214 cycles (sample number AW8). Figure 5.9 shows microstructure and dislocations distribution in the center of spot nugget in as-welded specimen AW10, which was stopped at 1,000 cycles during the fatigue test. It can be seen that no significantly dislocation tangle can be found. However, in the spot nugget edge area, a high density of dislocations and dislocations tangles are presented, which is shown in Figure 5.10. This indicates that significant plastic deformation occurred at the edge area of the spot nugget, which agrees with that edge area is the stress concentration area during fatigue tests, as mentioned above.

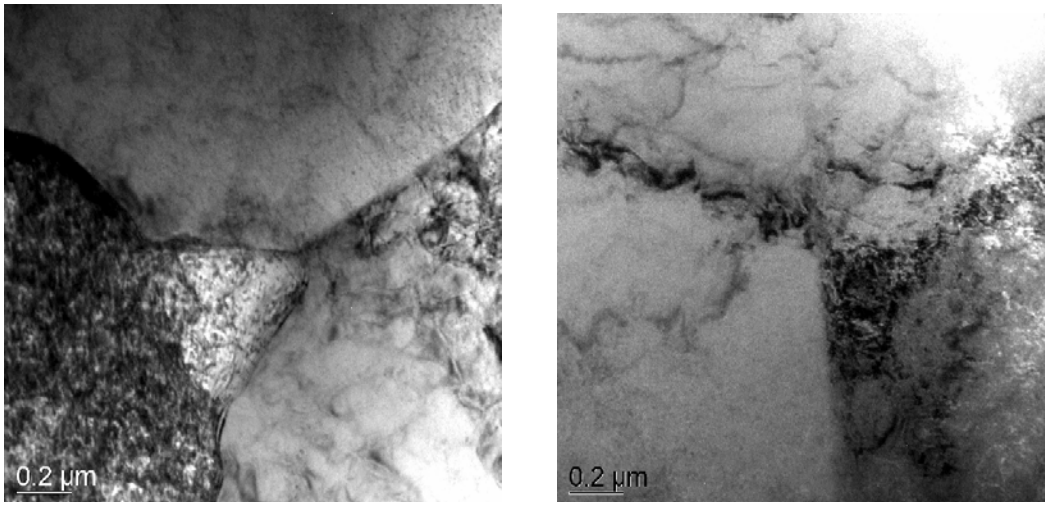

(a) (b)

Figure 5.9 Microstructure and dislocation at the center of as-welded specimen (sample number AW10, stopped at 1,000 cycles during fatigue test)

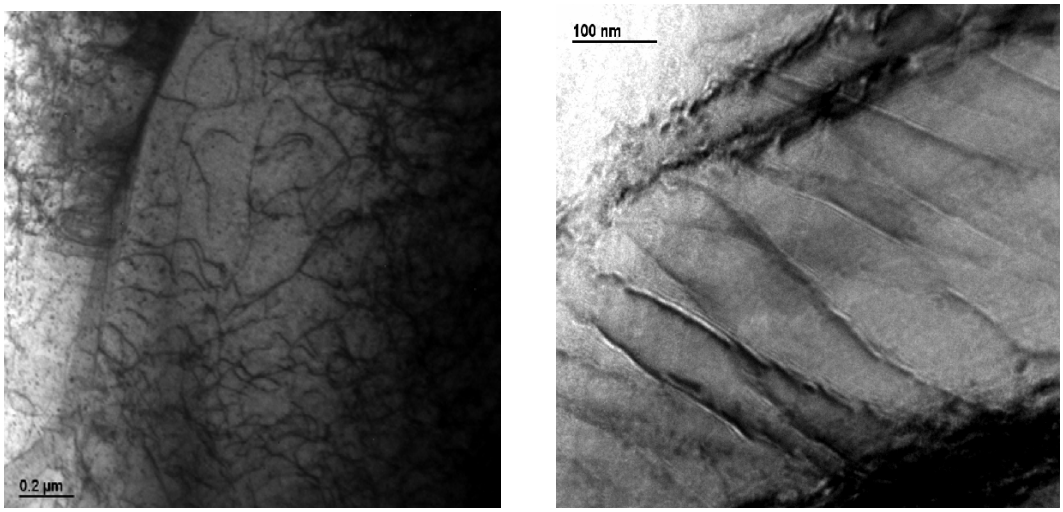

Figure 5.10 Microstructure and dislocation at the edge of as-welded specimen (sample number AW10, stopped at 1,000 cycles during fatigue test).

5.3.2.4 Effects of low fatigue load on dislocations distribution in as-welded samples

Under low fatigue load (max. load 1.2 kN, load amplitude 0.54 kN), as-welded specimens have fatigue life greater than 1,000,000 cycles, and post-heated specimens have fatigue life of about 800,000 cycles. Under low fatigue load, plastic deformation is very limited in a spot welded sheet; thus the dislocation structure is not expected to change significantly as occurs in specimens under high fatigue load. Figure 5.11 shows microstructure and dislocations morphology at the edge of spot nugget in as-welded specimen AW6, which was stopped at 500,000 cycles during fatigue testing. It can be seen that no significantly dislocation tangle are presented.

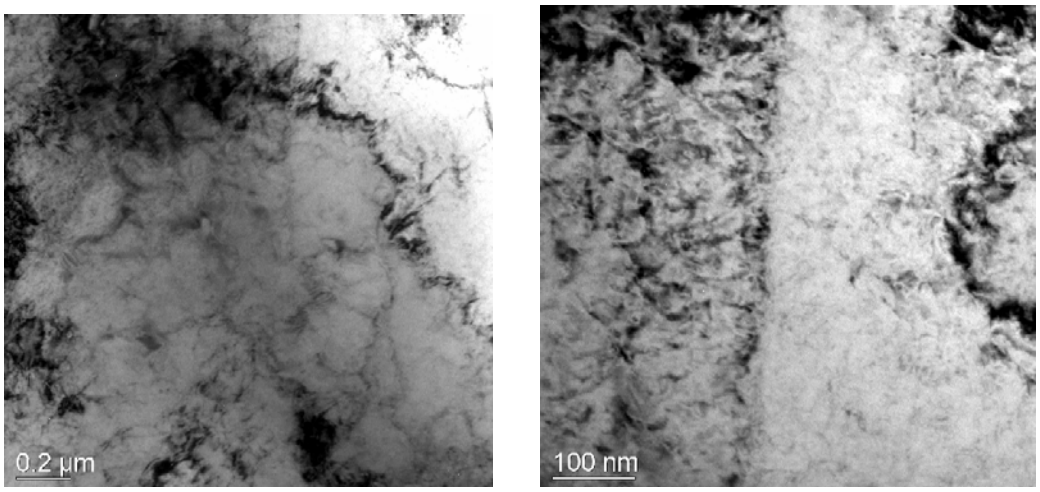

(a) (b)

Figure 5.11 Microstructure and dislocation distribution at the edge of spot nugget in as-welded specimen (sample number AW6, stopped at 500,000 cycles).

For low fatigue load, after 1,000,000 cycles fatigue test, the dislocations morphologies of in as-welded sample do not change significantly, as shown in Figure 5.12.

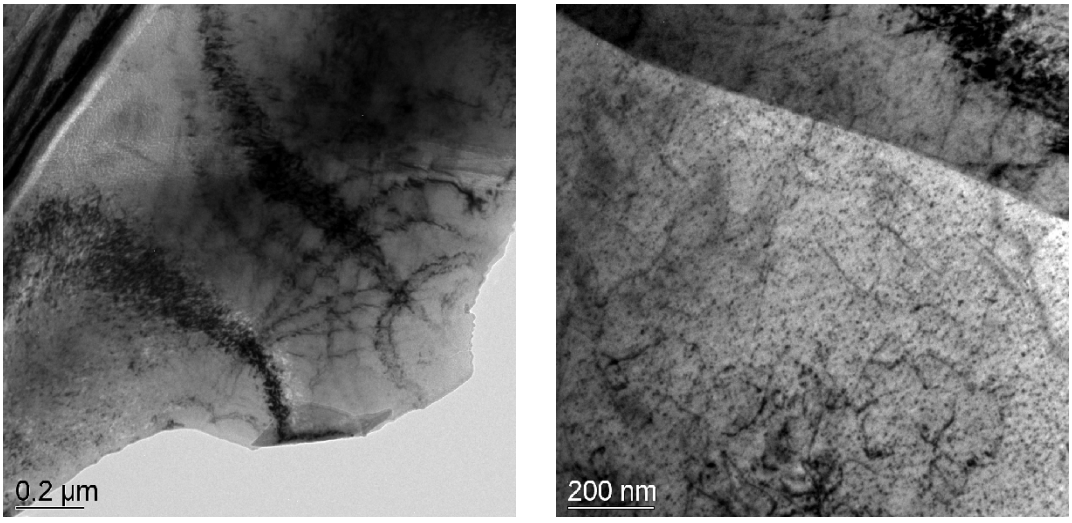

(a) (b)

Figure 5.12 Microstructure and dislocation distribution at the edge of spot nugget in as-welded specimen (sample number AW6, stopped at 1,000,000 cycles).

5.3.2.4 Effects of post-heated treatment on dislocation morphology of spot welded samples

(a) High-load fatigue samples

Under high fatigue load (max. load 3.3 kN, load amplitude 1.49 kN), post-heated specimens have a fatigue life of about 20,469 cycles (sample number PH8). Figure 5.13 shows the dislocations at the edge of the post-heated sample which was stopped at 9000 cycles under a fatigue load amplitude of 1.49 kN. It can be seen that no dislocations are present at the edge of post-heated sample. This is quite different from what was observed in the as welded sample (Figure 5.13), which showed a dense dislocation structure. Possible explanations for this behavior are that at the low number of fatigue cycles dislocation generation occurred in a narrow band, which was not captured and observed in the TEM sample used. Also it may be possible that the parent sheet metal recrystallized more than the spot-weld and was

relatively softer (with a lower yield strength) compared to the spot-weld causing initial yielding in the sheet metal outside the HAZ of the spot nugget, and hence no dislocations were observed in the edge of the spot weld at the low number of fatigue cycles.

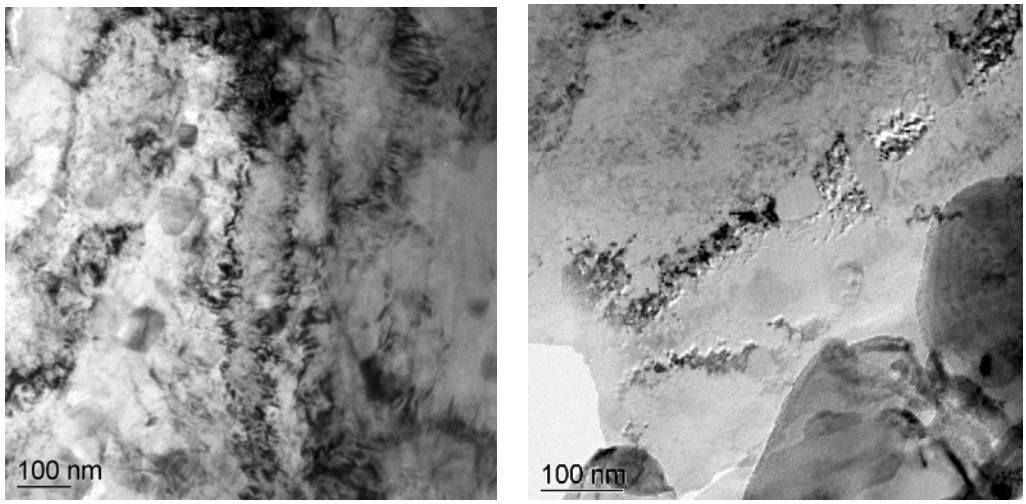

(a) (b)

Figure 5.13 Microstructure and dislocations at the edge of the spot nugget in post heated specimen (sample number PH10, stopped at 9000 cycles).

(b) Low-load fatigue samples

A large number of dislocations were observed in low load amplitude post-heated specimens subjected to a much higher number of fatigue load cycles, as shown in Figure 5.14. This situation is also different from that which occurs in as-welded samples, e.g. as shown in Figure 5.11. This may be caused by the relative lower yield strength of post-heated materials, which results in easier plastic deformation under low load and thus the yielding and dislocation structures are more widespread around the spot nugget.

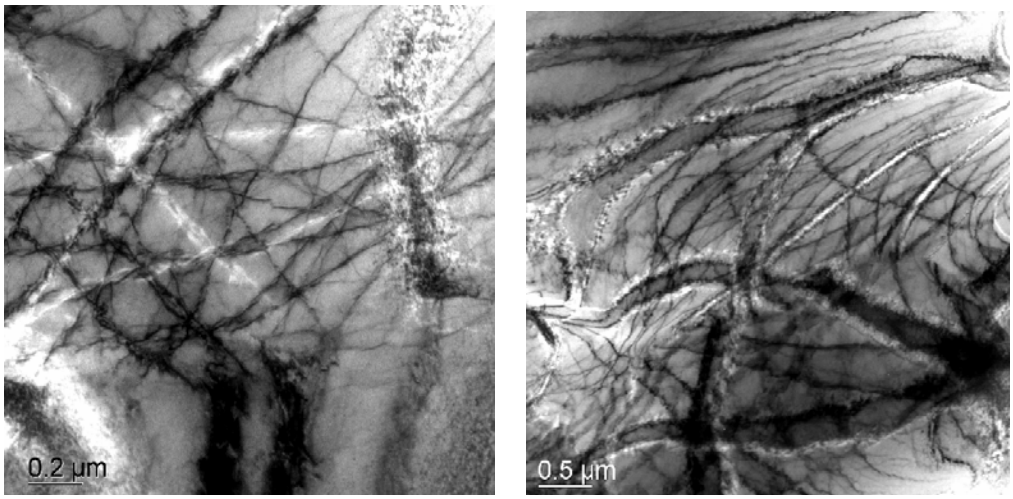

(a) (b)

Figure 5.14 Microstructure and dislocations at the edge of the spot nugget in as post-heated specimens (sample number PH6, stopped at 500,000 cycles).

5.4. Discussion

The TEM microstructures observed in as-welded and post-heated fatigued specimens can be described as follows: under high fatigue load, the high density of dislocations at the edge of the spot nugget indicates significant plastic deformation happened in this area, while much lower dislocation density in the nugget center area indicates less plastic deformation occurred. Under low fatigue load, the dislocation density is significantly lower in both edge and center areas in the spot nugget. The effect of post-heating on the microstructure (primarily dislocation morphology) is that more dislocations are generated during fatigue testing in both high and low loading. It is believed that post-heating decreases the welded joint strength, and therefore allows plastic deformation to occur more easily during fatigue testing, which leads to high dislocation density.

The residual stress decrease in the spot nugget center and increase in the edge, which was also reported in Ref [9], can also be explained based on the current study. With high fatigue load, significant plastic deformation can occur in the spot nugget, especially in the

spot edge area. Residual stress is therefore released to some degree, which leads to a decrease in the residual stress at the center of spot nugget. Since it is a self-equilibrating stress, residual stress redistributes after fatigue plastic deformation, which may lead to the increase of residual stress in the edge area of spot nugget. To get the detailed residual stress redistribution, a finite element structural analysis is needed.

Under low fatigue load, however, it is believed that residual stress would not be significantly released during loading. Therefore, tensile residual stress in the spot nugget will decrease the specimen's fatigue strength. After a residual-stress-relieving post-heat treatment, it was presumed that fatigue life would be increased. However, experiments showed that the fatigue life of post-heated specimens significantly decreased. This may be caused by reduced material's strength after post-heating. The beneficial effect of residual-stress-relieving is overcome by the detrimental effect of lower yield strength.

5.5. Conclusions

The present study was conducted to investigate the relationships of microstructure and residual stress effects on the fatigue behavior of spot welded steel sheets. It was found that under high fatigue load, dislocation density in the spot nugget edge is much higher than that in the nugget center area, which indicates significant plastic deformation occurred in the edge of spot nugget during fatigue testing. Under low fatigue load, the dislocation density is significantly lower in both edge and center areas of the spot nugget. The effect of post-heating (residual stress relieving) on the microstructure (primarily dislocation morphology) is that more dislocations are generated during fatigue testing for both high and low loading. Post-heating results in lower yield strength of the spot welded joint, which makes the fatigue life of a welded sheet decrease under low fatigue loading conditions.

5.6 References:

[1] Darwish, S. M., and Al-Dekhial, S. D., 1999, "Micro-Hardness of Spot Welded Commercial Aluminium as Correlated With Welding Variables and Strength Attributes," *Journal of Materials Processing Technology*, **91,** No. 1, pp. 43-51.

[2] Anastassiou, M., Babbit, M., and Lebrun, J L., 1990, "Residual Stresses and Microstructure Distribution in Spot-Welded Steel Sheets, Relation With Fatigue Behavior," *Materials Science & Engineering A: Structural Materials: Properties, Microstructure & Processing*, **125**, No. 2, pp. 141-156.

[3] Tricoteaux, A., Fardoun, F., Degallaix, S., and Sauvage, F., 1995, "Fatigue Crack Initiation Life Prediction in High Strength Structural Steel Welded Joints," *Fatigue & Fracture of Engineering Materials & Structures*, **18**, No. 2, pp.189-200.

[4] Radaj, D., 1990, "Local Fatigue Strength Characteristic Values for Spot Welded Joints," *Engineering Facture Mechanics*, **37**, No. 1, pp. 245-250.

[5] Radaj, D., 1989, "Stress Singularity, Notch Stress and Structural Stress at Spot-Welded Joints," *Engineering Facture Mechanics*, **34**, No. 2, pp. 495-506.

[6] Satoh, T., Abe, H., Nishikawa, K and Morita, M., 1991, "On Three-Dimensional Elastic-Plastic Stress Analysis of Spot-Welded Joint under Tensile Shear Load," *Transaction of the Japan Welding Society*, **22**, No. 1, pp. 46-51.

[7] Frost N. E.; Marsh K. J. and Pook, L. P. (eds), Metal Fatigue, Oxford University Press, 1974, pp6-35.

[8] Lu, J., ed., 1995, *Handbook of Measurement of Residual Stresses*, The Fairmont Press, Georgia.

[9] Khanna, Sanjeev K; He, Canlong and Agrawal, Hari N., Residual Stress Measurement in Spot Welds and the Effect of Fatigue Loading on Redistribution of Stresses Using High Sensitivity Moiré Interferometry, *ASME Journal of Engineering Materials and Technology*, vol. 123, 2001, pp.132-138.

[10] Bae, D. H., Sohn, I. S. and Kong, J. K., Assessing the Effects of Residual Stresses on the Fatigue Strength of Spot Welds, *Welding journal*, vol. 82, 2003, pp. 18s-23s.

[11] Anastassiou, M.; Babbit, M. and Lebrun, J. L., Residual Stress and Microstructure Distribution in Spot-Welded Steel Sheets: Relation with Fatigue Behavior, *Materials Science and Engineering*, A125, 1990, pp141-156.

[12] Henrysson H.-F.; Abdulwahab, F. and Josefson, B. L.; Residual Stresses in Resistance Spot Welds: Finite Element Simulations, X-Ray Measurements and Influence on Fatigue Behavior, *Welding World*, vol.43, 1999, pp55-63.

[13] Lee, Yung-Li; Pan, Jwo; Hathaway, Richard B. and Barkey, Mark E. (eds), Fatigue Testing and Analysis (Theory and Practice), Elsevier Butterworh-Heinemann, USA, 2005.

[14] Nied, H. A., 1984, "The Finite Element Modeling of The Resistance Spot Welding Process," *Welding Journal*, **63**, pp.s123-s132.

[15] Tsai, C. L., Jammal, O. A., and Papritan, J. C., 1992, "Modeling of Resistance Spot Weld Nugget Growth," *Welding Journal*, **71**, pp. s47-s54.

[16] Browne, D. J., Chandler H. W., Evans J. T., and Wen J., 1995, "Computer Simulation of Resistance Spot Welding in Aluminum: Part I," *Welding Journal*, **74**, No.10, pp.s339-s344.

[17] Feng, Z., Babu, S.S., Santella, M. L., Riemer, B. W., and Gould, J. E., 1998, "An Incrementally Coupled Electrical-Thermal-Mechanical Model For Resistance Spot Welding," *5th International Conference on Trends in Welding Research, Pine, Mountain, GA*, pp.1-5.

[18] Gupta, O. P., and De, Amitava, 1998, "An Improved Numerical Modeling For Resistance Spot Welding Process and Its Experimental Verification," *Journal of Manufacturing Science and Engineering*, **120**, No. 2, pp.246-251.

[19] Xu, L., and Khan, J. A., 1999, "Nugget Growth Model For Aluminum Alloys During Resistance Spot Welding," *Welding Journal*, **78**, No. 11, pp. s367-s372.

[20] Long, Xin; Khanna, Sanjeev K., Numerical Simulation of Residual Stresses in a Spot Welded Joint, *ASME Journal of Engineering Materials and Technology*, vol. 125, 2003, pp.222-226.

CHAPTER 6
FATIGUE AND FRACTURE BEHAVIOR OF SPOT WELDED ADVANCED HIGH STRENGTH STEEL SHEET

Abstract

Fatigue properties testing and failure characterization of high strength spot welded steels, such as DP600 GI, TRIP600 and HSLA340Y GI, have been conducted. Tensile shear and coach peel samples have been used in this investigation. HSLA samples were used as the baseline material for comparison. Random loading fatigue tests were also conducted using DP600 GI and HSLA340Y GI spot welded samples. Microhardness was measured to study the hardness change across the weld nugget. Under low load and high cycles situation all the materials show very similar fatigue strength. Crack initiation and propagation during the fatigue loading history has been experimentally determined and discussed. Microhardness tests show that DP600 GI sample have the highest hardness, about 420 HV in weld nugget and 250 HV in base metal, followed by TRIP600, about 400 HV in weld nugget and 220 HV in base metal, and HSLA340Y GI, about 320 HV in weld nugget and 160 HV in base metal. It was also found that both DP600 GI and HSLA340Y GI show some softening during high load and low cycles fatigue tests. Random loading fatigue tests show that DP600 GI has lower fatigue strength compared to HSLA340Y GI for both tensile-shear and coach-peel samples.

6.1. Introduction

With the increasing of fuel efficiency requirement, new materials are needed for decreasing automobile weight. Aluminum alloys and advanced high strength steel (AHSS) are under investigating for substituting currently used low-carbon steels and high strength low alloy (HSLA) steels. Although aluminum alloy has only one-third of steel density, it can not be used largely on economic cars in a short period of time due to its high costs (materials cost and fabrication cost) [1]. From economic point of view, with possibly similar cost of HSLA steels, AHSSs are more likely to be chosen for making lighter-weight vehicles. AHSSs, such as dual-phase steel DP600 GI and transformation induced plasticity steel TRIP600, have yield strength over 550 MPa, compared to conventional high strength steels within the range of 210-550 MPa. Therefore, thinner AHSS sheets, which decrease weight of automobile, can be used in automobile without losing any strength. Another advantage of AHSS is that it has quite higher yield to tensile ratio than that of HSLA steels at the same class, which results in a high level of crash energy absorption and a good formability in stamping.

Although some other joining techniques are more and more being used, spot welding still remains the primary joining method in automobile manufacturing so far. A typical vehicle contains more than 3000 spot welds [2]. In the past, fatigue behavior is not a major concern when use relative thick mild steel sheet in automotive. For AHSS steels, however, it was found significant fatigue damage which is related to the reduction in sheet thickness [3-4]. Previous studies also show that fatigue strength of high strength steels spot welded joint is not higher than that of mild steels [5-6]. Therefore, it becomes

a major concern to investigate the performance of spot welded joint in AHSSs for getting better fatigue design.

To study the fatigue properties of spot welded joint of AHSS, it is necessary to understand the microstructure nature of materials and to conduct fracture (fatigue) mechanics analysis.

AHSS is obtained by controlled cooling from an intercritical annealing process followed by lower-temperature austenite transformation [2,7]. Depending on different alloy elements and cooling process, AHSS has different finial microstructure. DP steel is consisted of ferrite and martensite, and the mechanical properties are controlled by the martensite volume-fractioni and ferrite grain size. TRIP steel is consisted of ferrite, bainite and austenite. Retained austenite plays a very important role in the TRIP steel's mechanical performance. When TRIP steel is subjected to a plastic deformation in manufacturing or in service, the retained austenite can transform to maternsite accompanying with a large elongation. This is so called transformation-induced plasticity (TRIP) effect.

Since AHSS is obtained by controlled cooling, welding heat input can significantly affect the microstructure of AHSS in welded joint, which results in the change of mechanical properties (including fatigue properties) in this area.

For studying the fatigue properties of a structure, the loading type is a very important factor to be considered. In real service of mechanical components, typical cyclic loadings are almost random in nature and vary in magnitude. Therefore, understanding of the fatigue behavior of AHSS spot welds under variable amplitude random loading is essential for the fatigue design of automotive components. The first step for doing

random loading test is to measure the loading parameters at specific points on the structure under real operating conditions and get the load-time history, as it is shown in Figure 1 (it should be noted that Figure 6.1 only shows a part of the loading history. The original history has 198,886 events in total). And then, each time history is converted to a fatigue spectrum for that event consisting of load range versus number of cycles by using cycle counting procedures. Racetrack counting method was used in this study. This method is useful for condensing histories to those events that do the most of the damage. Thus the condensed histories accelerate the fatigue testing and permit focusing of attention on a few significant events. The details of this method can be found in refer [6].

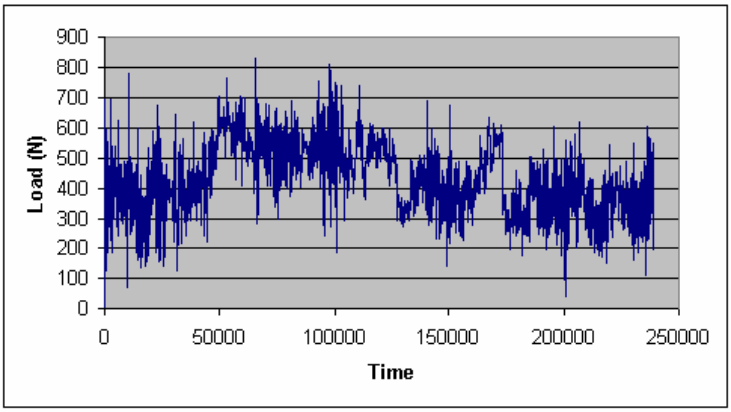

Figure 6.1 Part of the random loading history

The purpose of this study is to experimentally investigate the fatigue properties of AHSS steels (DP600 GI and TRIP600) and HSLA340Y GI in both coach peel and tensile shear specimens under tension-tension sinusoidal and random fatigue loads. The fatigue crack initiation and propagation has been studied and the failure mechanisms were also discussed.

6.2. Experimental Procedure

6.2.1 Materials and specimen

The nominal chemical composition and nominal mechanical properties of AHSS steels and HSLA steel are shown in Table 6.1 and Table 6.2, respectively [2].

Table 6.1 Chemical compositions of AHSS steels and HSLA steel (wt. %)

Steel	C	Mn	P	S	Si	Cu	Ni	Cr	Mo	Al	V	Cb
DP600 GI	0.081	1.760	0.017	0.006	0.013	0.040	0.02	0.19	0.180	0.048	0.002	0.004
TRIP600	0.101	1.470	0.002	0.001	1.536	0.016	0.02	0.05	0.010	0.027	0.005	0.005
HSLA340Y GI	0.053	0.620	0.008	0.005	0.214	0.052	0.02	0.01	0.000	0.039	0.001	0.016

Table 6.2 Mechanical properties of AHSS steels and HSLA steel

Steel	0.2% offset YS, MPa	UTS, MPa	Uniform Elong %	Total Elong %
DP600 GI	432.6	671.4	13.6	22.1
TRIP600	420.9	672.8	20.6	29.3
HSLA340Y GI	369.2	448.5	15.9	31.7

Specimens for fatigue tests are tensile shear type and coach peel type, as shown in Figure 6.2. Samples were supplied by Auto Steel Partnership. The thickness of DP600 GI and TRIP600 samples are 1.5 mm, while the thickness of HSLA340Y GI samples are 1.6 mm. Tensile shear type specimens have length of 217 mm and width of 39 mm. In the case of wide tensile shear specimen, the length is 283 mm and width 124 mm. Coach peel specimens have length of 155 mm and width of 39 mm. In tensile shear specimen, 35 mm

long taps with appreciated thickness were stick at each of the specimen in order to reduce bending deformation at the joint. The diameter of spot nugget was measured as about 7.0 mm for all of the samples.

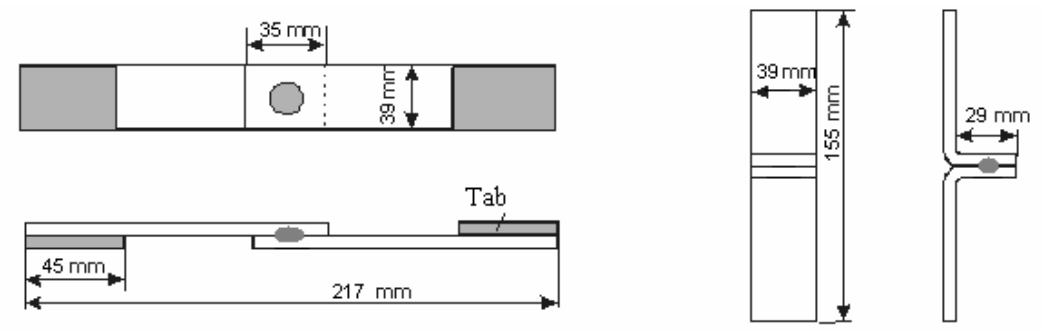

Figure 6.2 (a) Tensile shear type and (b) coach peel type fatigue specimens

6.2.2 Fatigue test procedure

An Instron universal testing machine was used to conduct load-controlled tension-tension fatigue test. The samples were subjected to various sinusoidal load with a load-ratio R=0.1 or R=0.3, at a frequency of 5 Hz for coach peel sample and 10 Hz for tensile shear sample. For the case of R=0.3, a constant load amplitude was set when compared with that of R=0.1. Thus, the maximum, minimum and mean load in R=0.3 case are different from that of R=0.1 case. The maximum dynamic load used was typically about 60 % of the maximum load obtained during a quasi – static tensile test. During the fatigue test, the maximum load, minimum load, maximum and minimum cross head displacement, and the frequency were monitored by using the Instron Wave Maker Data

Acquisition software and 8500 Plus digital controller. For the random loading test, a loading history file was provided by Sheet Steel Fatigue Taskforce of Auto Steel Partnership. Then a fatigue cycle file was condensed by using Racetrack counting method according to ASTM Standard E-1049 [6]. The condensed tensile shear time history includes 7,744 events and coach peel includes 10,958 events, compared to the 198,886 events in the original file.) Figure 6.3 shows the condensed tensile shear fatigue history file. Since the original random loading history was scale to maximum load of 1000 N, the loads were multiply by 11 or 6 for tensile shear samples and times 1.8 or 1.0 for coach peel samples during the real fatigue tests.

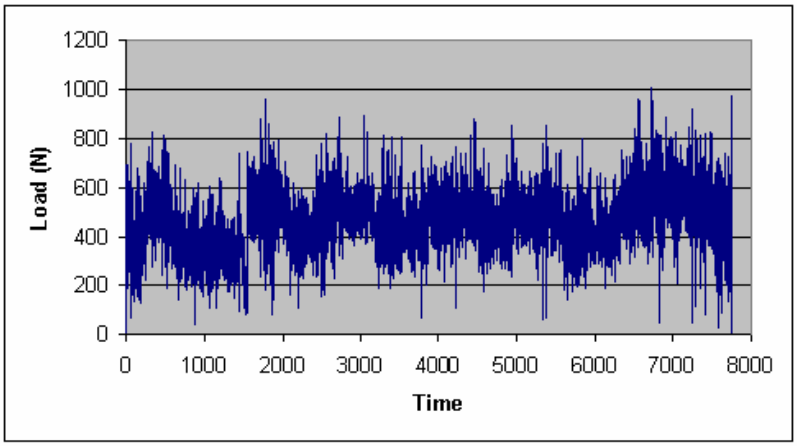

Figure 6.3 Condensed tensile shear fatigue history

For microstructure and fracture morphology observation of the fatigue failure sample, fatigue samples were cut along the center of the spot nugget in the direction of the length of sample. The cross section of the cut samples was polished and then etched. The etchant used was 3% Nital (3mL HNO_3 and 97 mL alcohol).

Microhardness tests were conducted on the surface of the sectioned and polished samples used for microstructure observation. A Micromet II microhardness tester was used to conduct the test with a load of 300g wickers indenter.

6.3. Results and discussion

6.3.1 Quasi-Static tension

Quasi-static tension test were conducted on tensile shear and coach peel samples for each of the materials. The ultimate tension strengths of spot welded samples are listed in Table 6.3. Figure 6.4 shows the load vs. displacement curves for various samples. It can be seen from Table 6.3 and Figure 6.4 that TRIP600 tensile shear samples has the highest tensile strength among three kinds of materials (32% higher than that of HSLA340Y GI sample and 13% higher than that of DP600 GI). For coach peel samples, however, the situation is just the reversion of tensile shear case. HSLA340Y GI has the highest tensile strength and TRIP600 has the lowest one. Compared to Table 6.2, it can be seen that the strength of tensile shear spot welded samples are coincident with base materials strength. It is easy to understand that spot welded joint weak the coach peel samples, especially for TRIP600 and DP600 GI materials, which causes the unusual strength performance of them. It will be discussed in the following context in detail.

Table 6.3 Static ultimate tension strength of tensile shear and coach peel samples

Material	Tensile shear (kN)	Coach peel (kN)
DP600 GI	20.95	3.64
TRIP600	23.58	3.29
HSLA340Y GI	17.82	4.84

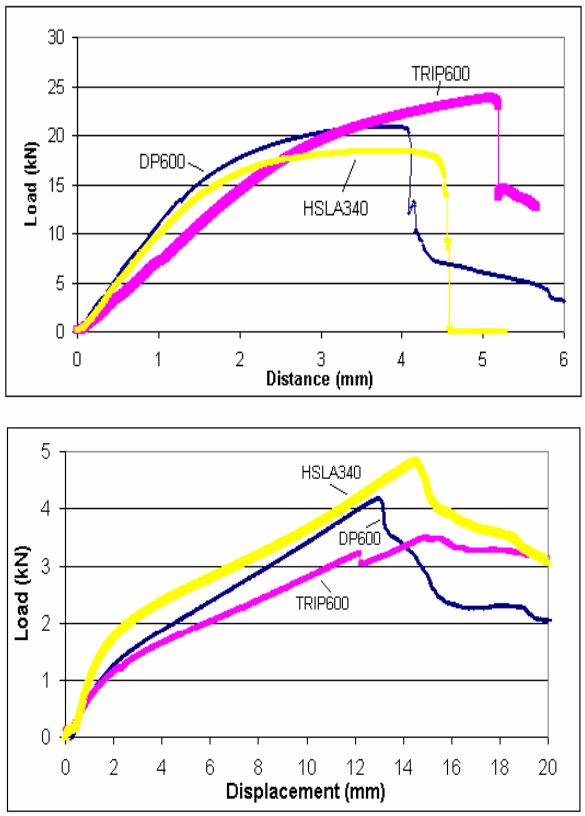

Figure 6.4 Static loading tests of (a) tensile shear samples and (b) coach peel samples

6.3.2 Fatigue properties

The fatigue life curves of three materials are shown in Figure 6.6. It can be seen from Figure 6.5 that the fatigue strength of DP600 GI samples is very similar to that of HSLA340Y GI samples, and both of them are slightly higher than that of TRIP600 samples under high load in both tensile shear and coach peel conditions. Under low load, all of samples show very similar fatigue strength in each of tensile shear and coach peel groups. For tensile shear samples, the fatigue strength of DP600 GI and TRIP600 welded joint is about 5~6 % of the static joint strength. For coach peel samples, the above value is about 4 %. As it is mentioned before, a high strength of base materials doesn't necessarily mean high fatigue strength of spot welded joint. The obtained results agree

with previous study that the spot weld fatigue performance is independent of base materials strength at low load and high cycles. Another interesting phenomena is that TRIP600 samples, which has a high static tensile strength in base material and tensile shear samples, doesn't show a good performance at high load and short cycles.

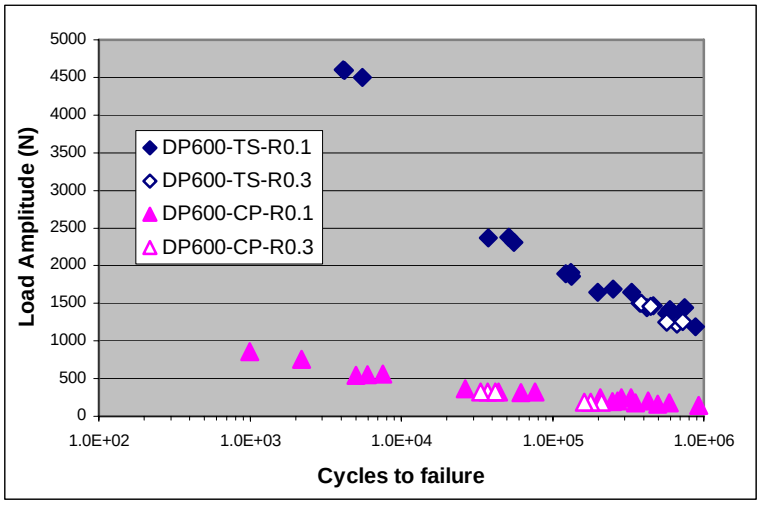

(a)

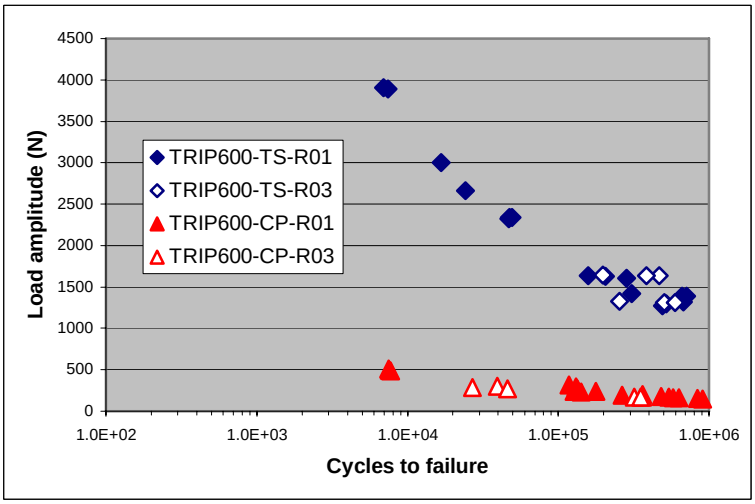

(b)

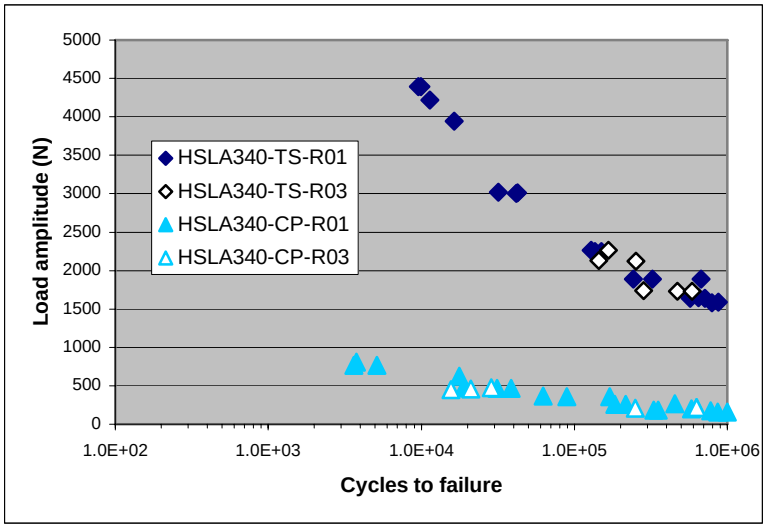

(c)

Figure 6.5 Load vs. cycles to failure curves for (a) DP600 GI, (b) TRIP600 and (c) HSLA340Y GI (hollow symbols in each curves represent R ratio 0.3, all others are 0.1.)

6.3.3 Microstructure and fatigue crack characterization

6.3.3.1 Tensile shear samples

Microstructures and fatigue crack surface morphologies were carefully studied to analysis the fatigue fracture mechanism of above three materials. Figure 6.6 and 6.7 show the microstructure and fatigue crack path in DP600 GI spot welded joints. The microstructures of DP600 GI and TRIP600 spot joint do not show something special under optical microscopy with low magnitude, compared to ordinary spot weld joint. Coarse column dendritic crystals in the spot nugget surrounded by about 0.8 thick Heat Affected Zone (HAZ) areas for all of three materials spot welded joints.

It has been observed that at high load and low cycles, fatigue crack in a tensile shear sample propagates along the workpieces interface and into the spot nugget for a short distance (from HAZ of spot nugget to edge of nugget, about 0.8 mm), and then propagates perpendicular to the workpieces interface to complete fracture, as shown in Figure 6.6 (b). For the case of low load and high cycles, the crack directly propagates

perpendicular to the workpiece interface from the HAZ area of spot nugget, as shown in Figure 6.6 (c).

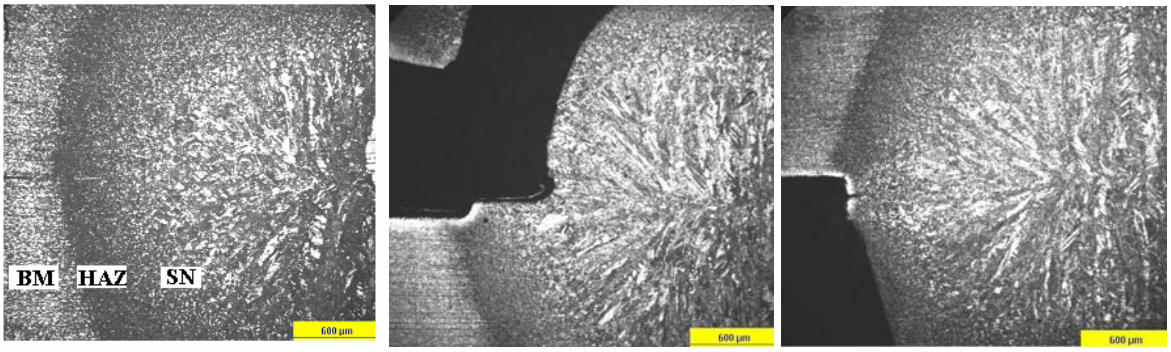

(a) (b) (c)

Figure 6.6 DP600 GI fatigue tensile shear sample microstructures and failure models: (a) without fatigue test, (b) with fatigue test of 51,360 cycles, (c) with fatigue test of 1647,440 cycles. (All pictures at 5X magnification). Note: **BM**-Base Metal, **HAZ**-Heat Affected Zone, **SN**-Spot Nugget

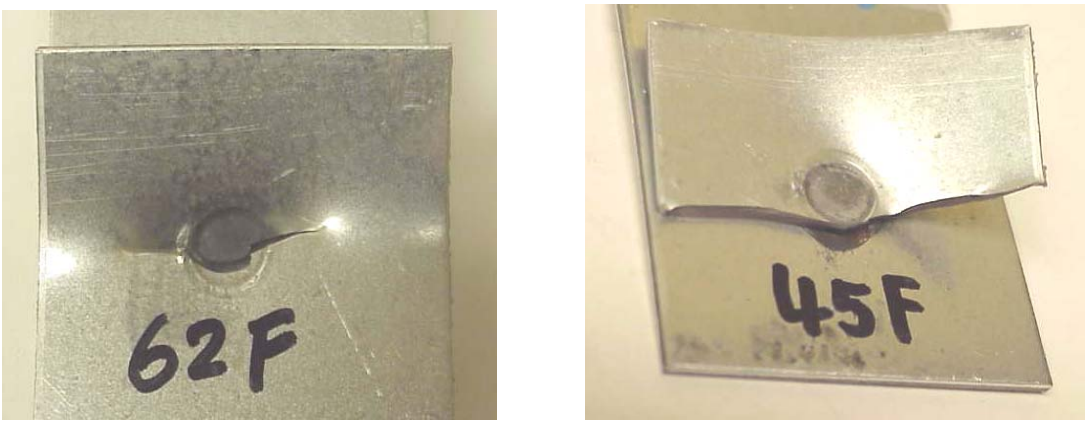

(a) (b)

Figure 6.7 DP600 GI tensile shear fatigue sample failure modes: (a) with fatigue of 55,350 cycles, and (b) 2043,850 cycles.

Unlike DP600 GI spot weld, it was found that a “tongue” formed between the two workpiceces of TRIP600 tensile shear samples around the spot nugget, which is shown in Figure 6.8 (a). This tongue is usually the initiation place of the fatigue crack no matter in high load or low load conditions as shown in Figure 6.8 (b) and (c) and Figure6.9. This could be the reason for the low fatigue strength of TRIP600 spot welded joints even though they have a high quasi-static tensile strength.

It has been reported in a previous study [2] that TRIP steels need high current intensity and high squeeze force to be spot welded. This may be the cause for “tongue” formation during welding. The tongue may form a very weak interfacial bond with the base material due to its surface oxidation [2], or directly forms a sharp crack-like notch as shown in Figure 6.7 (a). Under the application of a fatigue load, the sharp crack-like notch easily forms a crack. It is interesting to note that the crack path is not along the HAZ border as in the case of DP600 GI spot weld, but only through the base metal.

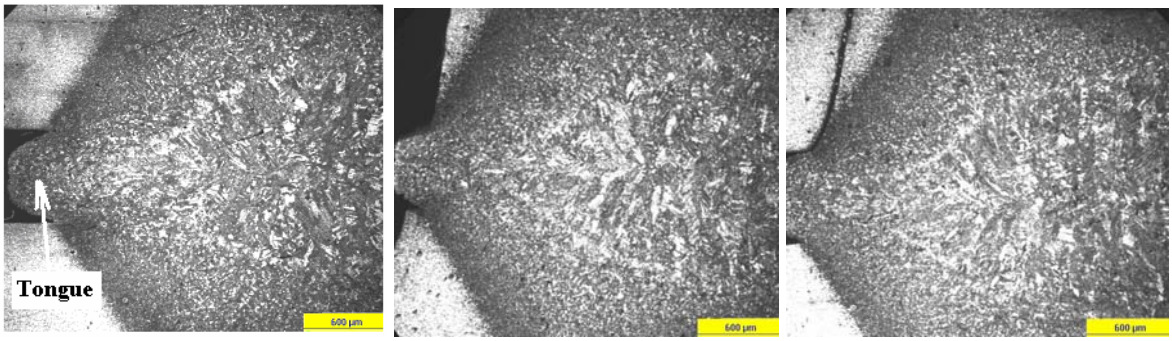

(a) (b) (c)

Figure 6.8 TRIP600 fatigue tensile shear sample microstructures and failure modes: (a) without fatigue test, (b) with fatigue test of 6,920 cycles, (c) with fatigue test of 677,748 cycles (5X)

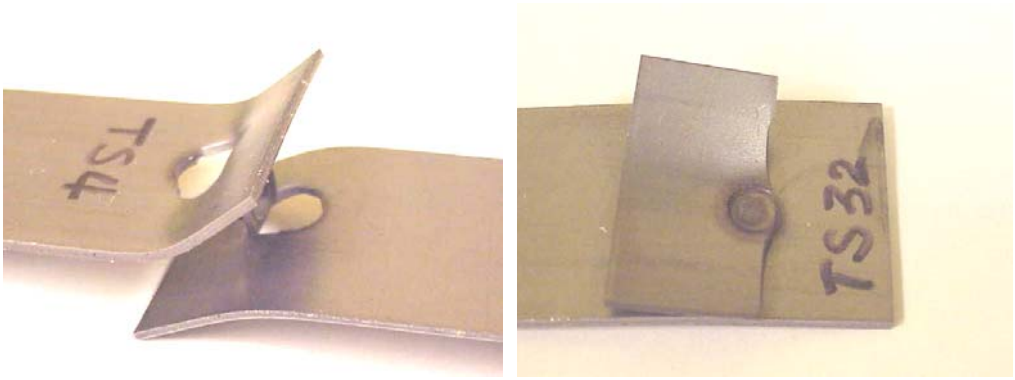

(a) (b)

Figure 6.9 TRIP600 tensile shear fatigue sample failure modes: (a) with fatigue of 7,415 cycles, and (b) 491,733 cycles.

The crack path in HSLA340Y GI tensile shear samples is different from that in DP600 GI or TRIP600 samples. From Figure 6.10 and Figure 6.11, it can be seen that crack propagates along the workpiece interface into the weld nugget for a very short distance in both high fatigue load and low fatigue load conditions. However, it is another crack that is perpendicular to the workpiece interface which causes the final fatigue failure. For high load condition, this perpendicular crack starts in the HAZ area, while for low load condition, it starts in the base metal adjacent to the HAZ area.

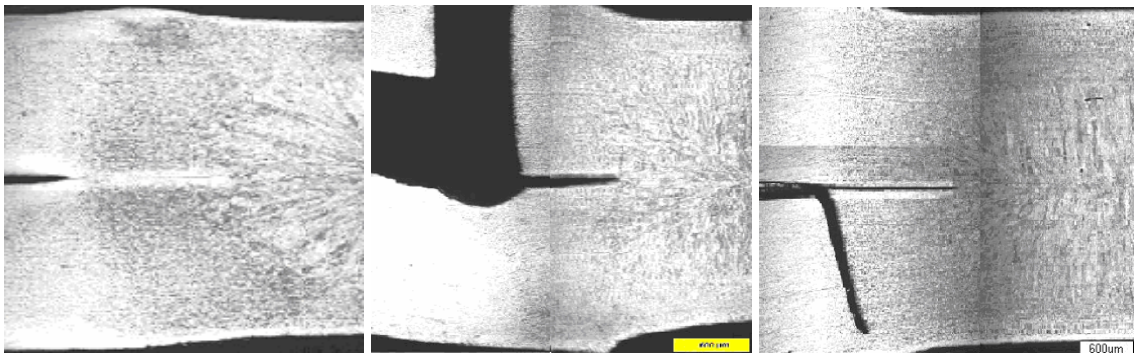

(a) (b) (c)

Figure 6.10 HSLA340 fatigue tensile shear sample microstructures and failure modes: (a) without fatigue test, (b) with fatigue test of 9,571 cycles, (c) with fatigue test of 1728,126 cycles (5X)

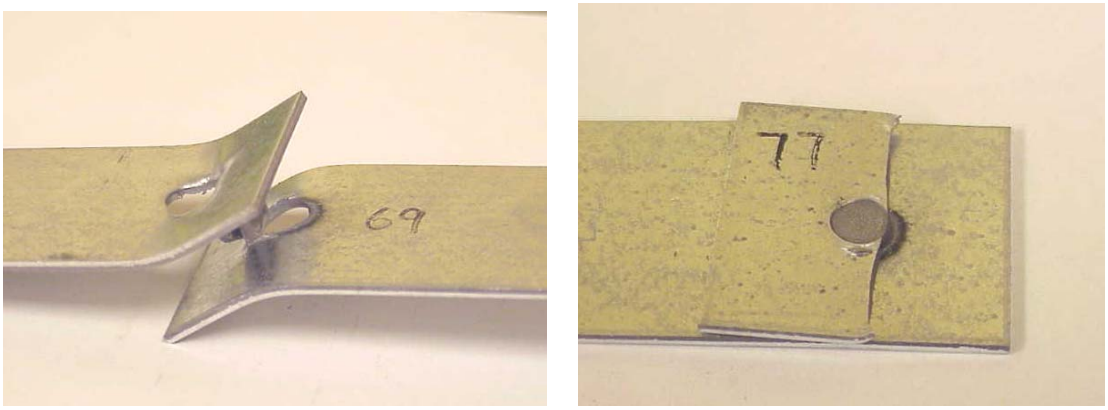

(a) (b)

Figure 6.11 HSLA340Y GI tensile shear fatigue sample failure modes: (a) with fatigue of 9,972 cycles, and (b) 793,992 cycles.

6.3.3.2 Coach peel samples

The fatigue fracture morphology of coach peel samples was similar for all three types of materials studied. At high load and low cycles, crack propagates parallel to the weld interface and into the spot nugget for a short distance, and then propagates perpendicular to the weld interface till complete fracture, as shown in Figures 6.12 and

6.13 (a). For the case of low load and high cycles, the crack propagates parallel to the weld interface and into the spot nugget for a relatively long distance, as shown in Figure 13 (b).

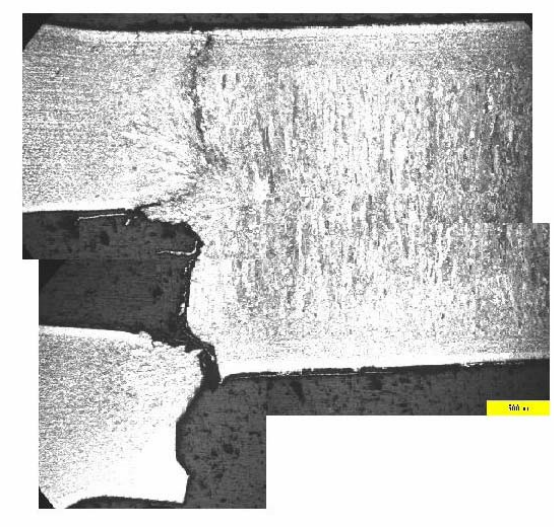

Figure 6.12 HSLA340Y GI coach peel sample fatigue failure at of 5,103 cycles (5X)

(a) (b)

Figure 6.13 DP600 GI coach peel fatigue sample failure modes: (a) with fatigue of 995 cycles, and (b) 1524,765 cycles.

6.3.4 Microhardness determination

Microhardness tests were conducted along the centerline (1/2 thickness) of spot joint and ¼ thickness of spot nugget on the cross section surfaces on each of the materials. Since the results of centerline and ¼ thickness are very similar, only results of centerline are shown in Figure 6.14. In each curves, microhardness from distance 0 to 3.5 mm show the hardness of weld nugget, from 3.5 mm to about 4.5 mm show the hardness of HAZ and beyond 4.5 mm show the hardness of base metal. It can be seen from Figure 6.14 that DP600 GI spot joint has the highest hardness, about 420 HV in weld nugget and 250 HV in base metal, followed by TRIP600, about 400 HV in weld nugget and 220 HV in base metal, and HSLA340Y GI, about 320 HV in weld nugget and 160 HV in base metal. It also can be found that both DP600 GI and HSLA340Y GI show somewhat softening during high load and short cycles fatigue test. This is coincident with previous study [7,8]. But at low load and long cycles test, all of three materials do not show any significant softening or hardening effect.

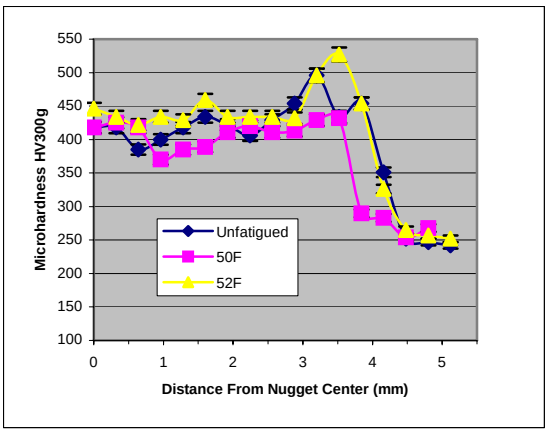

(a) DP600 GI

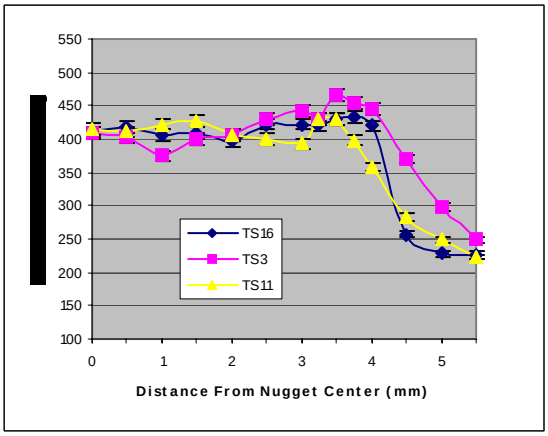

(b) TRIP600

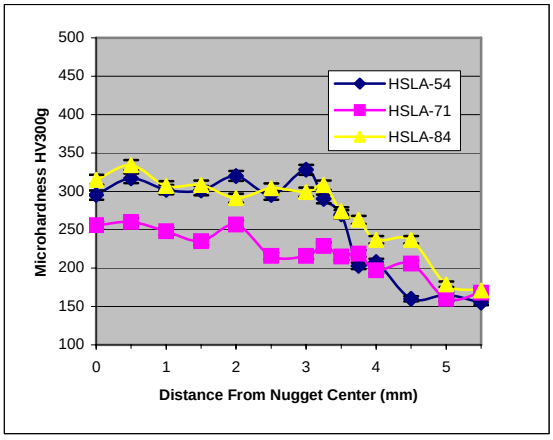

(c) HSLA 340

Figure 6.14 Microhardness of (a) DP600 GI, (b) TRIP600 and (c) HSLA340Y GI weld

6.3.5 Spectrum loading fatigue test

Spectrum loading fatigue test results are shown in Table 6.4. It can be seen that DP600 GI has much lower fatigue strength compared to HSLA340Y GI with both tensile-shear samples and coach peel sample. However, for coach peel samples with load scaling factor of 1.0, both the materials exhibited similar fatigue strength. is the fatigue response of spot welds under random loading is different from the results obtained with constant load amplitude fatigue tests, in which DP600 GI and HSLA340Y GI have very similar fatigue strengths. Thus DP600 GI and HSLA340Y GI spot welded samples have a different response to the load interaction and sequence effects during random loading, which can not be explained by the Miner linear damage rule [6].

Table 6.4 Spectrum loading fatigue tests for DP600 GI and HSLA340Y GI samples

Specimen type	Scale	Cycles to failure	
		DP600 GI	**HSLA340Y GI**
Tensile shear	X11	187,158	296,909
		195,489	328,110
	X6	1,591,074	3,443,103
		2,035,769	3,500,000 (running out)
Coach peel	X1.8	184,087	397,935
		295,268	464,585
	X1.0	1,883,017	1,930,433
		2,636,914	2,285,532

6.4 Conclusions

An experimental investigation of the fatigue properties of DP600 GI, TRIP600 and HSLA340Y GI spot welded samples led the following conclusions:

(1) Fatigue strength, under constant amplitude sinusoidal fatigue loading, of spot welded DP600 GI samples is very similar to that of HSLA340Y GI samples, and both of them are slightly higher than that of TRIP600 samples under high fatigue loads for both tensile shear and coach peel samples. Under low fatigue loads, all the three materials show very similar fatigue strength for both tensile shear and coach peel specimens.

(2) For tensile shear samples, different spot welded materials exhibited different fatigue crack paths. Under high loads, fatigue cracks in DP600 GI samples propagated along the workpieces interface and into the spot nugget for a short distance and then propagated perpendicular to the workpieces interface until complete fracture, while cracks in HSLA340Y GI samples propagate perpendicularly in the HAZ area. Under

low fatigue loads, cracks in DP600 GI samples directly propagate perpendicular to the workpieces interface from the HAZ area of spot nugget, while cracks in HSLA340Y GI samples propagate perpendicularly in the base material adjacent to HAZ area. In TRIP-steels, for both high and low load conditions, the cracks propagate from the tongue area perpendicular to the workpieces interface.

(3) For coach peel samples made of all three materials under high loads, crack propagates along the workpieces interface into the spot nugget for a short distance, and then propagates perpendicular to the workpieces interface until complete fracture. Under low loads, the cracks propagate along to the workpieces interface into the spot nugget for a relatively long distance.

(4) Microhardness tests showed that DP600 GI spot weld has the highest hardness, about 420 HV in weld nugget and 250 HV in base metal, followed by TRIP600, about 400 HV in weld nugget and 220 HV in base metal, and HSLA340Y GI, about 320 HV in weld nugget and 160 HV in base metal. It was also observed that both DP600 GI and HSLA340Y GI show some softening during high load and short cycles fatigue testing.

(5) Random loading fatigue tests show that DP600 GI has lower fatigue strength compared to HSLA340Y GI with both tensile shear and coach peel samples.

6.5 Acknowledgement

The partial financial support of Ford Motor Co. is gratefully acknowledged. John Bonnen, Ford Motor Co. is appreciated by supplying cycle reduced files.

6.6 References

1. Kelkar, A., Roth, R., and Clarl, J.,"Can aluminum be an economical alternative to steel", JOM 53(8), pp 28-32, 2001.

2. Internal materials from Inland co.

3. El-Sayed, M. E., Stawiarski, T. and Frutiger, R., Fatigue Analysis of Spot-Welded Joints under Variable Amplitude Load History, Engineering Fracture Mechanics, Vol.55, No.3, pp.363-369, 1996.

4. Stephens, R. I., Fatemi, A., Stephens, R.R. and Fuchs, H. O., Metal Fatigue in Engineering, second edition, A Wiley-Interscience Publication, John Wiley & Sons, Inc., 2001.

5. Sakuma, Y., Kimura, N., Itami, A. and et al: "Next-Generation High-Strength Sheet Steel Utilizing Transformation-Induced Plasticity (TRIP) Effect", Nippon Steel Technical Report, No.64, March, pp.20-25, 1995.

6. Fredriksson, K., Melander, A. and Hedman, M., "Influence of Prestraining and Ageing on Fatigue Properties of High-Strength Sheet Steel", International Journal of Fatigue, Vol.10, No.3, 1988, pp139-151.

7. Lindgren, C., Sperle, J. O. and Jonsson, M., "Fatigue Strength of Spot Welded Beams in High Strength Steels", Welding in the World, Vol.37, No.1, pp.90-104, 1996.

8. "Cycle Counting for Fatigue Analysis," ASTM Standard E-1049, Annual Book of ASTM Standards, Vol.03.01, ASTM, West Conshohocken, PA, 1998, p.693.

CHAPTER 7

SUMMARY AND FUTURE WORK

7.1 Summary

All the research conducted in the previous chapters has been summarized and briefly presented here for a quick reference.

(1) *Finite Element Simulation of Residual Stress in Spot Welded Low Carbon Steel.*

A two dimensional axisymmetric incremental and thermal-electro-mechanical coupled finite element model with temperature dependent materials properties has been used for simulating residual stresses distribution and the spot nugget size in a spot welded steel and aluminum alloy joints. The simulated results show good qualitative agreement with the experimental results. It has been found that in the spot nugget, a highest tensile residual stress occurs at the center of the nugget and the residual stress decreases significantly at the edge of the nugget.

(2) *Experimental Measurement of Thermal-mechanical and Thermal-physical Properties of 5754 and 6111 Grade Aluminum Alloys.*

The physical and mechanical properties of two aluminum alloys, 5754 and 6111, were experimentally determined between 20°C and 500°C. It was found that these aluminum alloys have similar thermo-physical properties, such as specific heat, thermal conductivity and thermal expansion. The thermo-mechanical properties, however, are quite different. 6111 aluminum alloy has a significantly higher yield strength and elastic modulus than that of 5754 alloy.

(3) *Finite Element Simulation of Residual Stress in Spot Welded 5754 and 6111 Aluminum Alloys.*

A two-dimensional axisymmetric finite element model was developed to determine the temperature distribution, internal stress development history and the welding

residual stress distribution in 5754 aluminum alloy spot welded joints. A coupled thermo-electrical-mechanical finite element model with temperature dependent physical and mechanical material properties was employed. All material properties used were measured by experiments. The temperature and internal stress development history in the spot welded joint provides a fundamental understanding of the deformation produced and the internal stresses generated in the welded region. Quantitative determination of these quantities should provide important data for safer and more durable design of thin sheet aluminum structures for automotive structures.

(4) *Experimental Investigation of Microscopic Deformation Mechanisms during Fatigue Loading of Spot Welded Steel.*

The investigation of the microstructure evolution and residual stress as well as their relations to fatigue behavior of spot welded steel sheets suggests that under high fatigue load, dislocation density in spot nugget edge is much higher than that in nugget center area, which indicates significant plastic deformation occurred in the edge of spot nugget during fatigue testing. Under low fatigue load, dislocation density is quite lower in both edge and center area in spot nugget. The effect of post-heating on the microstructure (mainly dislocation morphology) is more dislocations could be generated during fatigue test for both high and low loading. Post-heating results in strength decrease of spot welded joint while it releases the residual stress in it, which makes the fatigue life of welded sheet decrease under low fatigue loading condition.

(5) *Investigation of Fatigue Behavior in Advanced High Strength Steel Sheets.*

An experimental investigation of the fatigue properties of DP600 GI, TRIP600 and HSLA340Y GI spot welded samples has been conducted. It was found that fatigue

strength of spot welded DP600 GI samples is very similar to that of HSLA340Y GI samples under constant amplitude sinusoidal fatigue loading, and both of them are slightly higher than that of TRIP600 samples under high fatigue loads for both tensile shear and coach peel samples. Under low fatigue loads, all the three materials show very similar fatigue strength for both tensile shear and coach peel specimens. Under high loads, fatigue cracks in DP600 GI tensile samples propagated along the workpieces interface and into the spot nugget for a short distance and then propagated perpendicular to the workpieces interface until complete fracture, while cracks in HSLA340Y GI samples propagate perpendicularly in the HAZ area. Under low fatigue loads, cracks in DP600 GI samples directly propagate perpendicular to the workpieces interface from the HAZ area of spot nugget, while cracks in HSLA340Y GI samples propagate perpendicularly in the base material adjacent to HAZ. In TRIP-steels, for both high and low load conditions, the cracks in tensile shear samples propagate from the tongue area perpendicular to the workpieces interface.For coach peel samples made of all three materials under high loads, crack propagates along the workpieces interface into the spot nugget for a short distance, and then propagates perpendicular to the workpieces interface until complete fracture. Under low loads, the cracks propagate along to the workpieces interface into the spot nugget for a relatively long distance. Random loading fatigue tests show that DP600 GI has lower fatigue strength compared to HSLA340Y GI with both tensile shear and coach peel samples.

7.2 Future Work

A key feature of the modern durability design process is the use of computer aided finite element method to predict durability at an early stage in the design cycle. Calculation based on fatigue life and realistic loading histories permit structures and components to be optimized for durability without the need for expensive and time-consuming testing of a series of prototypes. Therefore, to establish a fatigue life prediction model for spot welded structure is very important in industries such as the automotive industry.

Although a vast amount of fatigue related research on spot welds have been carried out over the last 40 years, general models which don't need specific fatigue test parameters (such as specimen geometry, R-ratio) have been only proposed in the last decade. A number of techniques have been established so far for estimating fatigue life in spot welded joints. Among them, local strain based and structural stress based life prediction techniques are of more interest, which will be discussed in following sections. Since very little work has considered residual stress in the spot welded joint, our future work will be on how to implement the residual stress obtained our finite element analysis of the fatigue life prediction models. The near future work should focus on modifying the strain based spot weld fatigue life prediction by considering residual stress. We should quantitatively study the influence of residual stress on the fatigue life of a spot welded joint and focus on the fatigue crack initiation and early stage of propagation. Based on the proposed analysis, some residual stress affect factor maybe obtained in order to input into the simplified finite element analysis in the structural stress based fatigue life prediction for general design and analysis application in the future.

VITA

Xin Long was born on July 25, 1971 in Yingshan, Sichuan, People's Republic of China. He got his B.S. degree in Mechanical Engineering from Xi'an Petroleum Institute (China) in 1993. After that, he studied at Southwest Jiaotong University (China) where he got his M.S. degree in Materials Science and Engineering in 1996. In 1999, he got his first Ph.D degree in Materials Science and Engineering (China) from Chinese Academy of Sciences, Institute of Metal Research. Then he spent two years at Shanghai Jiaotong University for doing post-doc research fellow at Welding CAD/CAM/CAE Lab. He came to University of Missouri –Columbia as a visiting scholar in 2001. Then he studied his second Ph.D degree in Mechanical Engineering at University of Missouri-Columbia. He is married to Xiaonan Guo, who is studying her M.S. degree in Statistics at University of Missouri-Columbia. They have one boy born in 2002.